Carrier Frequency Offset Estimation for Orthogonal Frequency Division Multiplexing Systems

Xiang Nian Zeng

A Thesis

in

The Department

of

Electrical and Computer Engineering

Presented in Partial Fulfillment of the Requirements

for the Degree of Doctor of Philosophy at

Concordia University

Montreal, Quebec, Canada

August 2008

Your file Votre référence
ISBN: 978-0-494-45685-9
Our file Notre référence
ISBN: 978-0-494-45685-9

Abstract

Carrier Frequency Offset Estimation for Orthogonal Frequency Division Multiplexing Systems

Xiang Nian Zeng, Ph.D.

Concordia University, 2008

Orthogonal frequency division multiplexing (OFDM) is an attractive modulation scheme used in wideband communications because it essentially transforms the frequency selective channel into a flat fading channel. Furthermore, the combination of multiple-input multiple-output (MIMO) signal processing and OFDM seems to be an ideal solution for supporting reliable high data rate transmission for future wireless communication systems. However, despite the great advantages OFDM systems offer, such systems present challenges of their own. One of the most important challenges is carrier frequency offset (CFO) estimation, which is crucial in building reliable wireless communication systems.

In this thesis, we consider CFO estimation for the downlink and uplink OFDM systems. For the downlink channel, we focus on blind schemes where the cost functions are designed such that they exploit implicit properties associated with the transmitted signal where no training signal is required. By taking the unconditional maximum likelihood approach, we propose a virtual subcarrier based blind scheme for MIMO-OFDM systems in the presence of spatial correlation. We conclude that the presence of spatial correlation does not impact the CFO estimation significantly. We also propose a CFO estimator for OFDM systems with constant modulus signaling and extend it to MIMO-OFDM systems employing orthogonal space-time block coding. The curve fitting method is used which gives a closed-form expression for CFO estimation. Therefore, the proposed scheme provides an excellent trade-off between

complexity and performance as compared to prominent existing estimation schemes. Furthermore, we design a blind CFO estimation scheme for differentially modulated OFDM systems based on the finite alphabet constraint. It can achieve better performance at high signal-to-noise ratios (SNRs) at the expense of some additional computational complexity as compared to the schemes based on the constant modulus constraint. The constrained Cramer-Rao lower bound (CRLB) is also derived for the blind estimation scheme.

As for the uplink channel, which is a more challenging problem, we propose two training aided schemes. One is based on a scalar extended Kalman filter (EKF) and the other one is on the variable projection (VP) algorithm. For both schemes, we assume that the system uses an arbitrary subcarrier assignment scheme, which is more involved than the other two schemes, namely block and interleaved subcarrier assignment scheme.

In the first scheme, to apply the scalar EKF algorithm, we represent the measurement equation as a function of a scalar state, i.e., each user's CFO, in lieu of a state vector which consists of both CFO and channel coefficients by replacing the unknown channel coefficients with a nonlinear function of CFO. This proposed scheme can achieve the CRLB at high SNR for two users with a complexity lower than that of the alternating-projection method. In the second scheme, the VP algorithm is used for CFO estimation which is followed with a robust minimum mean square error (MMSE) estimator for channel estimation. In the VP algorithm, the nonlinear least square cost function is optimized numerically by updating the CFOs and channel coefficients separately at each iteration. We demonstrate that this proposed scheme is superior to the existing methods in terms of convergence speed, computational complexity and estimation performance.

This dissertation is dedicated to

my dearest mother, father for their love, trust and encouragement,

and my sister's families who bring lots of happiness into my life.

Acknowledgments

First of all, my sincere appreciation goes to my academic supervisor Dr. Ali Ghrayeb who has offered me invaluable support, constructive guidance and helpful discussion throughout my thesis research. I am grateful for his patience and kindness in answering my questions and revising my submitted reports. Without his continuous encouragement and stimulating suggestions I would not have completed my thesis.

I would like to thank the committee members Dr. M. R. Soleymani, Dr. W. Hamouda, Dr. X. Zhou and Dr. I. Psaromiligkos. Their comments make the presentation of this thesis more clear.

I would also like to thank May Gomaa and Jeyadeepan Jeganathan in our research group. It is because of their help that I overcame some technical problems when my knowledge to solve some problem had been exhausted. I want to thank all the people who help me throughout my study at Concordia University.

Finally, I would like to thank my parents for their love, trust and encouragement throughout all the four years. Without their support, it would have been impossible for me to accomplish what I have accomplished.

Contents

List of Figures

List of Tables

List of Symbols

f_0	carrier frequency offset [Hz]
f_d	Doppler frequency [Hz]
$\mathbf{I}_m$	$m \times m$ identity matrix
K	number of users
L	number of the multipath components of the fading channel
L_{CP}	length of cyclic prefix
N	number of subcarriers
N_t	number of transmit antennas
N_r	number of receive antennas
u	candidate CFO
u_k	the kth user's timing offset
σ_τ^2	channel delay spread
σ_n^2	noise power
E_s	symbol energy
ε	normalized CFO
ε_k	the kth user's normalized CFO
$\odot$	element-wise Hadamard product
$\otimes$	Kronecker product
^{H}	matrix hermitian transpose operation
^{T}	matrix tanspose operation
*	conjugate operation

$\delta\{\cdot\}$	Dirac delta impulse function
$\det\{\cdot\}$	determinant of matrix
$\mathrm{diag}\{\cdot\}$	diagonalization operation
$E\{\cdot\}$	expectation operation
$\mathrm{tr}\{\cdot\}$	trace operation
$((x))_N$	x modulo N

List of Acronyms

4G	fourth generation
APFE	alternating-projection frequency estimation
APSK	amplitude-phase shift keying
AWGN	additive white Gaussian noise
BER	bit error rate
CAS	carrier assignment scheme
CC	convolutional code
CCRLB	conditional Cramér-Rao lower bound
CFO	carrier frequency offset
CM	constant modulus
CML	conditional ML
CP	cyclic prefix
CRLB	Cramér-Rao lower bound
DAB	digital audio broadcasting
DFT	discrete Fourier transform
DLST	diagonal layered space-time
DOFDM	differentially modulated OFDM
DVB	terrestrial digital video broadcasting
EKF	extended Kalman filter
EM	expectation maximization
ESPRIT	estimation of signal parameters by rotational invariance technique
EVD	eigenvalue decomposition

FA	finite alphabet
FDM	frequency division multiplexing
FFO	fractional part of the normalized frequency offset
GF	Galois field
HLST	horizontal layered space-time
ICI	inter-carrier-interference
IDFT	inverse discrete Fourier transform
IFO	integer part of the normalized frequency offset
ISI	inter-symbol-interference
LAN	local area networks
LLS	linear least-square
LPF	low pass filter
LS	least-square
LST	layered space-time
MAI	multiple-access interference
MAN	metropolitan area networks
MIMO	multiple-input multiple-output
ML	maximum likelihood
MLST	multilayered space-time
MMSE	minimum mean square error
M-PSK	M-ary phase shift keying
M-QAM	M-order quadrature amplitude modulation
MSAGE	modified SAGE
MSE	mean square error
MUI	multiuser interference
MUSIC	multiple signal classification
NLLS	nonlinear LS
NMSE	normalized mean square error
OFDM	orthogonal frequency division multiplexing

OSTBC	orthogonal space-time block code
pdf	probability density function
QPSK	quaternary phase shift keying
RS	Reed-Solomon
SAGE	space-alternating generalized expectation-maximization
SISO	single-input single-output
SNLLS	separable NLLS
SNR	signal-to-noise ratio
STBCs	space-time block codes
STTCs	space-time trellis codes
TLST	threaded layered space-time
VP	variable projection
UCRLB	unconditional Cramér-Rao lower bound
UML	unconditional ML
VSC	virtual subcarrier
W-CDMA	wideband code division multiple access

Chapter 1

Introduction

1.1 Motivation

Over the last decade or so, we have witnessed a drastic increase in the demand for providing reliable high-speed wireless communication links to support applications such as voice, video, e-mail, web browsing, to name a few. This is a challenging task, however, since transmission through a wireless link is prone to a number of impairments of which the most important is fading and interference. In addition, in wideband communications (i.e., at high data rates), the signal bandwidth is normally larger than the channel bandwidth and this gives rise to frequency selective fading (or multipath fading). Orthogonal frequency division multiplexing (OFDM) has been a very popular method for wideband transmission because it essentially transforms the frequency selective fading channel into a flat fading channel. This is accomplished by transmitting the data symbols in a parallel fashion over a set of orthogonal subcarriers. As such the channel is seen by each subcarrier as a flat fading channel. Consequently, OFDM dramatically simplifies the receiver design in multipath fading. Inspired by these advantages, OFDM has been adopted in several standards, including the European digital audio broadcasting (DAB) [1], terrestrial digital video broadcasting (DVB) [2], wireless local area networks (LANs) (802.11 [3], [4], HiperLAN [5]), and wireless metropolitan area network (MAN) (802.16 [6]). It

is also considered as a strong candidate for the fourth generation (4G) air interface technology [7].

When some of the subcarriers experience deep fading, the data symbols transmitted on these subcarriers cannot be recovered without further protection. An effective approach to achieve this protection is to introduce diversity, which comes in different forms, including time, frequency and spatial. Spatial diversity, which is the only scheme that requires no additional bandwidth, can be achieved by employing multiple antenna elements at the transmitter and/or receiver. Such systems are normally referred to as multiple-input multiple-output (MIMO) systems. Multiple transmit antennas can be exploited to enhance the spatial diversity of the system by using space-time coding. Another way of exploiting these transmit antennas is to increase the link throughput through spatial multiplexing and this can be achieved by using layered space time coding. A compromise between spatial diversity and spatial rate can also be achieved by using multi-layered or threaded space-time coding. Using multiple antennas has already been adopted in several standards, including wideband code-division multiple access (W-CDMA) [8], 802.11 [3], [4], and 802.16 [6].

The combination of MIMO signal processing and OFDM seems to be an ideal solution for supporting high data rate transmission for future wireless communication systems where bandwidth efficiencies on the order of 10 b/s/Hz are feasible for LAN/MAN environments. However, despite the great advantages OFDM systems offer, such systems present challenges of their own. One of the most important challenges is carrier frequency offset (CFO) estimation, which is very crucial in building a reliable wireless communication system. CFO estimation involves finding an estimate of the difference in the frequencies between the transmit and receive local oscillators. CFO estimation is very important because any CFO results in losing the orthogonality between subchannels, which in turn leads to serious performance degradation.

1.2 Contributions

The contributions of this thesis can be summarized as follows.

- We propose maximum likelihood (ML) CFO estimation based on virtual subcarriers (VSCs) for MIMO-OFDM systems. In our ML approach, the channel and data are treated as random variables, unlike existing ML approaches in which the channel and data are treated as unknown constants. This in turn enables us to incorporate the spatial correlation into the analysis. In particular, we derive a cost function which can be used to accurately estimate the CFO. We also derive the Cramér-Rao lower bound (CRLB). We show that, as compared to the CML estimator, the UML estimator can exploit the knowledge of receive spatial correlation as well as the existence of VSCs to make additional contribution for CFO estimation. But, this additional contribution is marginal as compared to the CML estimator. The implication of this result is that one need not take spatial correlation into account in developing VSC-based CFO estimation scheme for MIMO-OFDM systems. This should simplify such development process.

- We propose a new blind CFO estimation scheme for OFDM systems with constant modulus (CM) signaling. Both single-input single-output (SISO) systems and MIMO systems with orthogonal space-time block coding (OSTBC) are considered. The proposed scheme is based on the reasonable assumption that the channel frequency response changes slowly in the frequency domain, which implies that the channel frequency response on two consecutive subcarriers is approximately the same. Based on this assumption, cost functions are derived in closed-form, which minimize the difference between the signal power of two neighboring subcarriers. The identifiability of the proposed scheme is mathematically proved, which implies that minimizing the derived cost function gives an approximate estimate of the CFO. We demonstrate that the proposed scheme provides an excellent trade-off between complexity and performance as

compared to prominent existing estimation schemes.

- We propose a blind CFO estimation scheme for differentially modulated OFDM (DOFDM) systems. The proposed scheme estimates the fractional part of the CFO (FFO) with only two consecutive OFDM symbols. The proposed cost function exploits two implicit properties associated with the differentially modulated DOFDM systems, i.e., the channel keeps constant over two consecutive OFDM symbols, and the employed M-ary phase-shift keying (M-PSK) constellation has a finite alphabet size. The proposed cost function can exploit more side information about the M-PSK constellation as compared to the cost functions based on the CM constraint. As a result, it can achieve better performance at high signal-to-noise ratios (SNRs) at the expense of some additional computational complexity. To reduce the complexity, we employ the modified Newton method where the number of cost function evaluations is reduced significantly as compared to the case when the grid search method is used to minimize the proposed cost function. The constrained CRLB is also derived, which we use to verify the correctness of the proposed scheme.

- We propose an extended Kalman filter (EKF)-based and training symbol aided CFO estimation scheme for the uplink channel of OFDM systems. Typically, in EKF-based estimation schemes, the measurement equation is a function of the CFO and channel coefficients. Therefore, a vector EKF has to be employed to estimate all the unknowns, which may sometime result in convergence problems. To avoid these problems, the proposed scheme uses a scalar EKF. The user signals are first separated by using multiple-access interference (MAI) cancellation. Then, the unknown channel coefficients in the measurement equation are replaced with a non-linear function of the CFO so that the scalar EKF can be employed. The observation noise power is analyzed and its approximation is used in the EKF algorithm. It is shown that the proposed scheme can achieve the CRLB when the number of users is small, whereas it degrades when the

number of users increases. We also compare its computational complexity with several existing schemes.

- We propose a joint CFO and channel estimation method for the uplink channel of OFDM systems. The well known *variable projection* (VP) method based on the least-squares (LS) criterion is used for CFO estimation. In each iteration of the VP method, the CFOs and channel coefficients are updated separately, which distinguishes the VP method from an existing non-separated minimum mean square error (MMSE) method in which the CFOs and channel coefficients are treated together as a whole. We demonstrate that by performing the estimation separately, we achieve significant improvement in the CFO estimation. However, the resulting channel estimation is not as good. To achieve better channel estimation, we employ the robust MMSE method, which comes after CFO estimation (via the VP method). We present several numerical examples through which we demonstrate the superiority of the proposed scheme in terms of convergence speed and estimation performance. The computational complexity of the proposed scheme is also lower than that of the non-separated MMSE method for large number of users at high SNRs. We also examine the performance of the proposed scheme in the presence of the near-far problem, which is what we normally encounter in real-life applications, where similar favorable results are obtained.

1.3 Organization

The rest of the thesis is organized as follows.

In Chapter 2, we introduce the fundamentals of MIMO-OFDM systems. We begin by introducing MIMO systems where we briefly discuss the capacity of such systems. We also mention the various space-time coding schemes used in such MIMO systems. We then introduce the basics of OFDM systems. This is followed by describing analytically the impact of CFO on inter-carrier-interference (ICI) and show how this

degrades the bit error rate (BER) performance of such systems.

In Chapter 3, we provide a broad review and classification of the recently proposed CFO estimation schemes for the downlink and uplink channels of OFDM systems. The CFO estimation for the downlink channel of OFDM systems has been investigated in the literature for many years, and thus we only review those bandwidth efficient non-data-aided schemes. For the CFO estimation of uplink channel of OFDM systems, we review both the data-aided and non-data-aided schemes available in the literature.

Chapters $4-6$ are devoted to blind CFO estimation for the downlink channel of OFDM systems.

In Chapter 4, we investigate the VSC-based CFO estimation for MIMO-OFDM systems with spatial correlation. We derive the unconditional ML estimator and unconditional CRLB. Then the impact of receive spatial correlation is studied in particular. Finally, we present simulation results.

In Chapter 5, we investigate the CM-based CFO estimation for OFDM systems. We present the proposed scheme for SISO-OFDM systems, and relate it with the kurtosis-type scheme. Then we extend the proposed scheme to MIMO-OFDM systems with OSTBCs. Simulation results are presented after that.

In Chapter 6, we investigate the finite alphabet (FA) based CFO estimation for DOFDM systems. Firstly, the FA based cost function is proposed for DOFDM systems with or without VSCs for FFO estimation. Then, the modified Newton method is presented to minimize the proposed cost function. The constrained CRLB for blind CFO estimation is also derived. Simulation results are presented finally.

Chapters 7 and 8 are devoted to training aided CFO estimation for the uplink channel of OFDM systems.

In Chapter 7, we investigate the EKF based CFO estimation. Firstly, we analyze each user's observed signal obtained from MAI cancellation and represent it as a function of CFO only. Then the observation noise power is derived and its approximation is used in the EKF algorithm. Computational complexity of the proposed scheme is also analyzed. Simulation results are shown to compare the proposed scheme with

two existing schemes after that.

In Chapter 8, we investigate CFO estimation based on the VP algorithm. Firstly, we present the proposed method in which the VP algorithm is used for CFO estimation and the channel estimation is obtained by using the robust MMSE method. Then the computational complexity is analyzed. Finally, we compare the proposed method with the non-separated MMSE method in terms of convergence speed, complexity and estimation performance by using simulations.

In Chapter 9, we make conclusions and propose topics for future research.

Chapter 2

Background

2.1 MIMO Systems

Channel capacity of multiple-input multiple-output (MIMO) systems has been studied in [9] and [10]. It has been shown that MIMO systems have the potential to provide enormous capacity compared to single-input single-output (SISO) systems. To elaborate, consider a MIMO system with N_t transmit antennas and N_r receive antennas. Let $h_{j,i}$ denote the flat fading coefficient between the ith transmit and jth receive antenna. The channel capacity in bits/sec/Hz is shown to be [10]

$$C = E\left\{\log_2 \det\left[\mathbf{I}_m + \frac{P}{N_t\sigma_n^2}\mathbf{Q}\right]\right\}, \tag{2.1}$$

where

$$\mathbf{Q} = \begin{cases} \bar{\mathbf{H}}\bar{\mathbf{H}}^H, & N_r < N_t \\ \bar{\mathbf{H}}^H\bar{\mathbf{H}}, & N_r \geq N_t \end{cases} \quad \text{and} \quad m = \min(N_r, N_t),$$

P is the total transmit power from all the transmit antennas, σ_n^2 is the noise power seen by each receive antenna and $E\{\cdot\}$ is the expectation operation with respect to the channel coefficients. $\bar{\mathbf{H}}$ is a $N_r \times N_t$ matrix with the element on its jth row and

ith column defined as $h_{j,i}$. Further analysis and numerical results show that in independent Rayleigh fading channel, when the number of the transmit antennas is the same or lower than the number of receive antennas, the capacity grows linearly with the number of transmit antennas. Otherwise the capacity grows only logarithmically with the number of transmit antennas.

To approach such capacity highlighted by information theory, various space-time codes have been designed. By efficiently exploiting the resources of multiple antennas, space-time codes are designed on one hand to combat the effect of fading by providing spatial diversity and on the other hand to increase system throughput by using spatial multiplexing. Space-time block codes (STBCs) [11] are designed to achieve full spatial diversity with a simple decoding scheme at the receive side. Space-time trellis codes (STTCs) [12] are designed to achieve both diversity and coding gains. However, its decoding complexity grows exponentially with the number of transmit antennas. Both STBCs and STTCs attempt to maximize transmit diversity by introducing redundancy across the spatial domain. But they do not provide any flexibility in increasing the transmission rate when high throughputs are needed for broadband communications. This motivates the use of layered space-time (LST) coding.

The idea behind the LST architecture is to multiplex the data stream into N_t substreams, and then encode each substream individually by using a traditional coding scheme before they are transmitted simultaneously from the N_t antennas. Each encoded substream is called a layer. As such, one-dimensional (in space) decoding can be used instead of the complex N_t-dimensional decoding used for STTCs. Furthermore, this architecture has the flexibility of providing trade-off between spatial diversity and spatial multiplexing. The horizontal layered space-time (HLST) architecture [13] is designed to assign each layer to one transmit antenna so no transmit diversity can be achieved. To achieve some transmit diversity, diagonal layered space-time (DLST) architecture [13] and threaded layered space-time (TLST) architecture [14] are designed to distribute each layer among the N_t transmit antennas. Another LST is the multilayered space-time (MLST) architecture presented in [15]. This scheme can

be thought of as a combination of space-time coding and layered space-time coding, where N_t transmit antennas are divided into subgroups and each subgroup is assigned to transmit a space-time coded stream.

2.2 OFDM Systems

OFDM is a bandwidth efficient modulation scheme designed for high speed transmission. The information bit stream is first modulated using M-ary phase shift keying (M-PSK) or M-order quadrature amplitude modulation (M-QAM). Then the constellation symbols are multiplexed into N parallel streams and transmitted simultaneously through N orthogonal subcarriers. Therefore, on each subcarrier, the transmission rate is relatively low which results in flat fading seen by each subcarrier. We notice that the OFDM system looks something like frequency division multiplexing (FDM). However, different from FDM, the spectrum of subcarriers in OFDM overlaps with each other which makes it very bandwidth efficient. Furthermore, the subcarriers are orthogonal to each other, so no inter-carrier-interference (ICI) exists in the ideal situation. To achieve orthogonality, the subcarrier interval Δf should be equal to $1/T$, where T is the OFDM symbol duration.

The OFDM transmitter and receiver is shown in Fig. 2.1. The inverse discrete Fourier transform (IDFT) and discrete Fourier transform (DFT) pair are used for OFDM modulation and demodulation in digital domain implementation. At the transmit side, the N output points of IDFT are actually N time domain samples of one OFDM symbol. They are converted into a serial stream and then concatenated with cyclic prefix (CP). Then these time domain samples are passed through a low pass filter (LPF) to reconstruct the continuous time signal and at last up converted to the radio frequency and transmitted from the transmit antenna.

The OFDM receiver design is very simple due to the orthogonality in ideal situations. The received signal is first down converted to baseband, and then sampled. The time domain samples are passed to the DFT followed by a one-tap channel equalizer

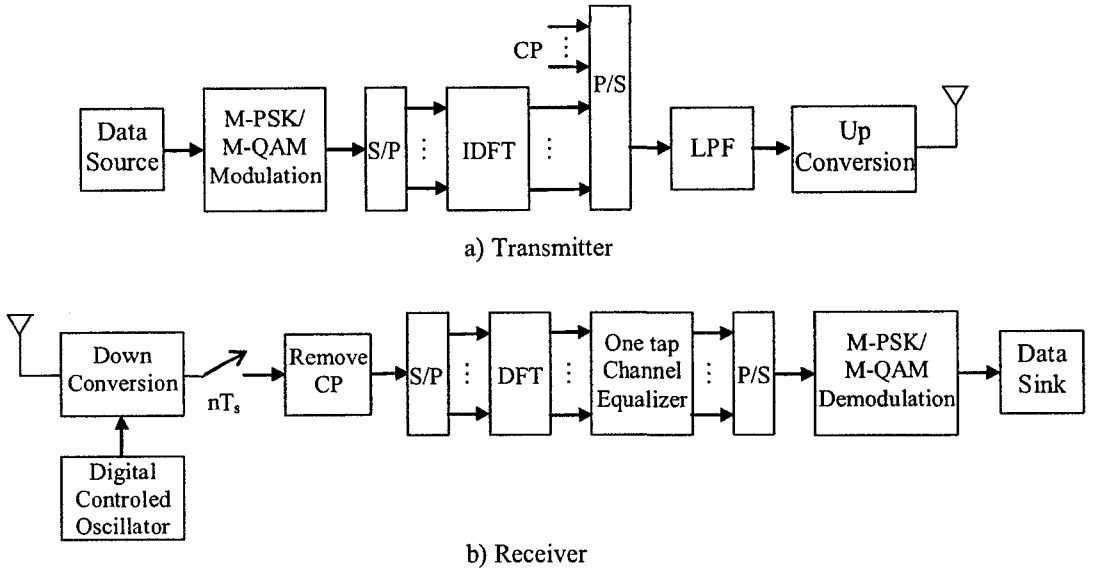

Figure 2.1: OFDM transmitter and receiver.

and a M-PSK or M-QAM detector.

CP insertion is done by adding the tail end part of the OFDM symbol to the front of it. The motivation of adding CP is twofold. First, by making sure that the length of CP is greater than the maximum delay spread, the inter-symbol-interference (ISI) can be completely eliminated. Second, the cyclic extension of the transmitted signal transforms a linear convolution of channel impulse response and signal to a circular convolution which intrinsically transforms a multipath fading channel into a flat fading channel on each subcarrier as will be shown next.

The baseband equivalent discrete-time channel impulse response can be represented as $h(n) = \sum_{l=0}^{L-1} h_l \delta(n-l)$, where L is the number of multipath components, and h_l is the fading coefficient on path l. Let us define the column vectors

$$\mathbf{d} = [d_0 \; d_1 \; \ldots \; d_{N-1}]^T,$$

and

$$\mathbf{y} = [Y_0\ Y_1\ \ldots\ Y_{N-1}]^T,$$

where d_k, $k = 0, 1, \ldots, N-1$ represents the symbol transmitted on subcarrier k, and Y_k, $k = 0, 1, \ldots, N-1$ represents the post-DFT signal on subcarrier k. Then the post-DFT signal $\mathbf{y}$ can be expressed by

$$\mathbf{y} = \mathbf{W}_N^H \mathbf{H}_{circ} \mathbf{W}_N \mathbf{d} + \mathbf{v},$$

where $\mathbf{H}_{circ}$ is an $N \times N$ circulant matrix with the first column defined as $\mathbf{h} = [h_0\ h_1\ \ldots\ h_{L-1}\ 0\ \ldots\ 0]^T$, $\mathbf{W}_N$ is the IDFT matrix with the element on the kth row and lth column defined as $\mathbf{W}_N^{k,l} = \frac{1}{\sqrt{N}} e^{j2\pi \frac{kl}{N}}$ and $\mathbf{v} = [v_0\ v_1\ \ldots\ v_{N-1}]^T$ is an $N \times 1$ vector of white Gaussian noise samples at the post-DFT stage.

Since $\mathbf{H}_{circ}$ is a circulant matrix, $\mathbf{W}_N^H \mathbf{H}_{circ} \mathbf{W}_N$ is a diagonal matrix with the channel frequency response on the diagonal, i.e.,

$$\mathbf{y} = \mathrm{diag}(\sqrt{N}\mathbf{W}_N^H \mathbf{h})\mathbf{d} + \mathbf{v}.$$

By defining H_k, $k = 0, 1, \ldots, N-1$ as the channel frequency response on subcarrier k, the post-DFT signal can be represented as

$$Y_k = H_k d_k + v_k, \qquad k = 0, 1, \ldots, N-1. \tag{2.2}$$

It is shown in the above expression that in an ideal situation, the multipath fading channel has been transferred to a multiplicative distortion on each subcarrier. Consequently, a one-tap equalizer can be used to compensate for this distortion where the output of equalizer would be $\hat{d}_k = Y_k / H_k$. This dramatically simplifies the channel equalizer design for multipath fading channels.

2.3 Effect of CFO

In real life applications, CFO always exists. It can be introduced by the difference between the transmit and receive oscillators and/or the Doppler spread. Let f_0 denote the CFO in Hz. The normalized CFO with respect to the subcarrier interval Δf can be decomposed into two parts, i.e., $f_0 T = k_0 + \varepsilon$, where k_0 is the integer part of the normalized frequency offset (IFO), and $\varepsilon \in [-\frac{1}{2}, \frac{1}{2})$ denotes the fractional part of the frequency offset (FFO). With this notation, the discrete-time receive signal in the presence of CFO can be expressed by

$$x_n = e^{j2\pi\frac{(k_0+\varepsilon)n}{N}} \frac{1}{\sqrt{N}} \sum_{k=0}^{N-1} H_k d_k e^{j2\pi\frac{nk}{N}} + z_n, \qquad n = 0, 1, \ldots, N-1, \tag{2.3}$$

where z_n is the zero mean white Gaussian noise sample at sampling instance n. From the above expression, we observe that CFO results in a phase shift evolving with time. Furthermore, the two parts of the normalized CFO, namely, k_0 and ε have different impact on the post-DFT signals.

Assume that $k_0 \neq 0$, and $\varepsilon = 0$. The post-DFT signals can then be represented as

$$\begin{aligned}
Y_k &= \frac{1}{\sqrt{N}} \sum_{n=0}^{N-1} x_n e^{-j2\pi\frac{nk}{N}} \\
&= \frac{1}{\sqrt{N}} \sum_{n=0}^{N-1} e^{j2\pi\frac{k_0 n}{N}} \frac{1}{\sqrt{N}} \sum_{k'=0}^{N-1} H_{k'} d_{k'} e^{j2\pi\frac{nk'}{N}} e^{-j2\pi\frac{nk}{N}} + v_k \\
&= \frac{1}{N} \sum_{k'=0}^{N-1} H_{k'} d_{k'} \sum_{n=0}^{N-1} e^{j2\pi\frac{(k'+k_0-k)n}{N}} + v_k \\
&= \sum_{k'=0}^{N-1} H_{k'} d_{k'} \delta(k' + k_0 - k) + v_k \\
&= H_{k-k_0} d_{k-k_0} + v_k.
\end{aligned} \tag{2.4}$$

By comparing (2.2) and (2.4), we observe that if CFO is an integer multiple of the subcarrier interval, it results in a cyclic rotation of the post-DFT signals, i.e., symbols are assigned to different subcarriers while preserving the order. This implies that the

demodulated symbols are still orthogonal to each other without interference. The BER performance is 0.5 in this case.

When $k_0 = 0$, and $\varepsilon \neq 0$, the post-DFT signals can be represented as

$$\begin{aligned}
Y_k &= \frac{1}{\sqrt{N}} \sum_{n=0}^{N-1} x_n e^{-j2\pi \frac{nk}{N}} \\
&= \frac{1}{\sqrt{N}} \sum_{n=0}^{N-1} e^{j2\pi \frac{\varepsilon n}{N}} \frac{1}{\sqrt{N}} \sum_{k'=0}^{N-1} H_{k'} d_{k'} e^{j2\pi \frac{nk'}{N}} e^{-j2\pi \frac{nk}{N}} + v_k \\
&= \sum_{k'=0}^{N-1} H_{k'} d_{k'} \frac{1}{N} \sum_{n=0}^{N-1} e^{j2\pi \frac{(\varepsilon + k' - k)n}{N}} + v_k \\
&= H_k d_k \frac{1}{N} \sum_{n=0}^{N-1} e^{j2\pi \frac{\varepsilon n}{N}} + \sum_{\substack{k'=0 \\ k' \neq k}}^{N-1} H_{k'} d_{k'} \frac{1}{N} \sum_{n=0}^{N-1} e^{j2\pi \frac{(\varepsilon + k' - k)n}{N}} + v_k \\
&= H_k d_k \frac{1}{N} \frac{\sin \pi\varepsilon}{\sin \frac{\pi\varepsilon}{N}} e^{j\pi \frac{\varepsilon(N-1)}{N}} + \sum_{\substack{k'=0 \\ k' \neq k}}^{N-1} H_{k'} d_{k'} \frac{1}{N} \sum_{n=0}^{N-1} e^{j2\pi \frac{(\varepsilon + k' - k)n}{N}} + v_k. \qquad (2.5)
\end{aligned}$$

We observe that the first term in the last line of the above expression represents the desired signal on the kth subcarrier with a scale and phase shift. We denote the second term as I_k, which represents the interference contributed from the signal transmitted on the other subcarriers. By comparing (2.2) and (2.5), we observe that if CFO is a fraction of the subcarrier interval, the post-DFT signals are not orthogonal to each other, resulting in ICI.

To elaborate more on this, the frequency spectrum of a 3-subcarrier OFDM signal is shown in Fig. 2.2. When $\varepsilon = 0$, the DFT outputs on the three subcarriers are represented by dotted lines. It is shown that the DFT output only consists of the signal transmitted on the corresponding subcarrier. When $\varepsilon = 0.3$, the DFT outputs on the three subcarriers are represented by dotted lines with marks. We observe that the DFT output consists both of the signal transmitted on the corresponding subcarrier and the signals transmitted on the neighboring subcarriers.

Fig. 2.3 illustrates the amplitude of the interference from subcarriers $1, \ldots, N-1$ on the 0th subcarrier for a 16-subcarrier OFDM signal in the presence of different

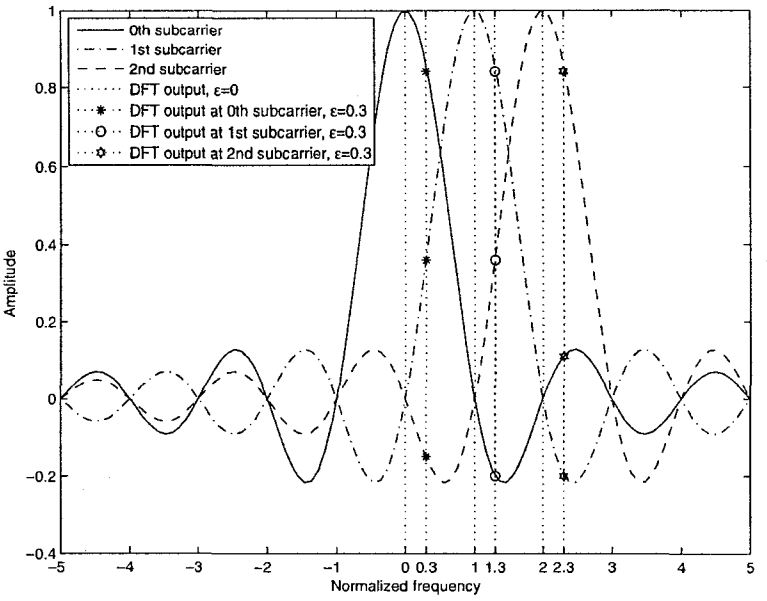

Figure 2.2: Illustration of ICI introduced by FFO ε by using frequency domain signal of an OFDM system with 3 subcarriers.

values of CFO. We observe that for the case of $\varepsilon = 0$ and $k_0 = 5$, the orthogonality of subcarriers is maintained. But the post-DFT on the 0th subcarrier takes the value of the signal on the 5th subcarrier. Therefore, in this case, the post-DFT signal requires to be reordered and this is usually called *coarse* CFO estimation and synchronization. For $k_0 = 0$ and $\varepsilon = 0.1$ or $\varepsilon = 0.4$, the orthogonality between subcarriers is lost. We can observe that by increasing FFO, the desired signal on the 0th subcarrier gets more severe deterioration and the interference from neighboring subcarriers becomes stronger. To eliminate the ICI, the received signal needs to be compensated at the pre-DFT stage. This is usually called *fine* CFO estimation and synchronization. Some CFO estimation/synchronization schemes are achieved by these two steps, namely, *coarse* and *fine* CFO estimation/synchronization.

In Fig. 2.4, the BER performance of a 4-PSK 64-subcarrier OFDM system in additive white Gaussian noise (AWGN) channel is shown. It can be observed that even small values of CFO can degrade the BER performance greatly.

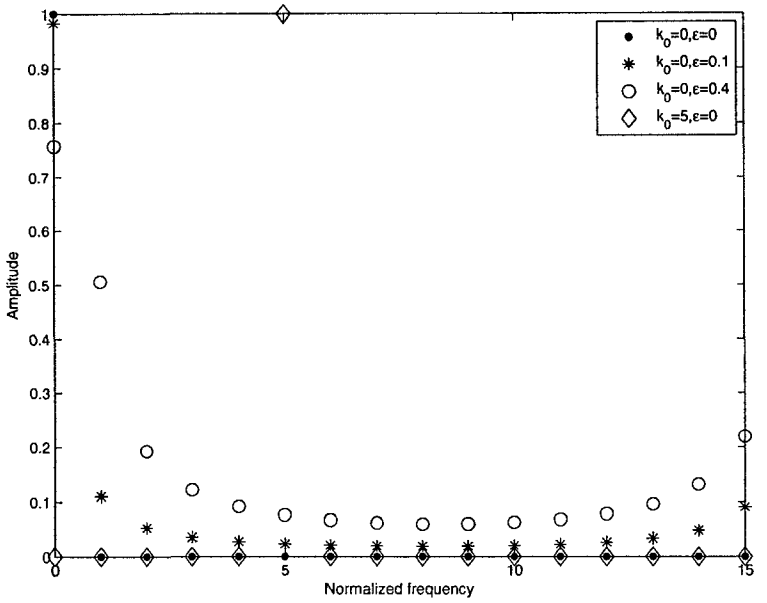

Figure 2.3: ICI amplitude of a 16-subcarrier OFDM signal in the presence of CFO

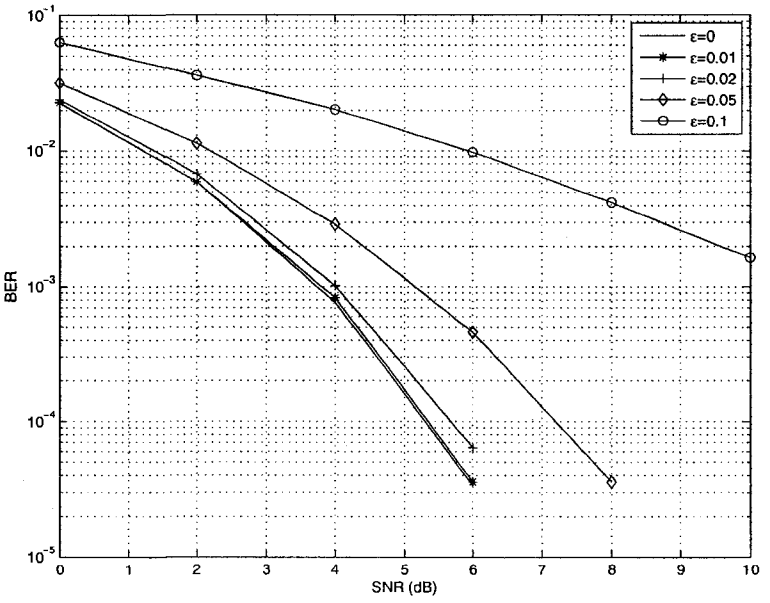

Figure 2.4: BER performance of a 64-subcarrier OFDM system in AWGN in the presence of CFO.

The above analysis is for SISO-OFDM systems. The impact of CFO on MIMO-OFDM systems has been studied in [16] and [17] for STBC and vertical LST (VLST) respectively. It is shown that using multiple antennas increases ICI compared to that of SISO-OFDM systems. Furthermore, for MIMO-OFDM systems employing VLST, ICI has significant impact on the error propagation across the successive interference cancellation process. To improve the performance, many ICI cancellation schemes have been proposed. However, most of them require the knowledge of the CFO. Thus, accurate CFO estimation is also essential for MIMO-OFDM systems.

Chapter 3

Literature Review

From previous discussion, we demonstrated that in order to detect symbols correctly, CFO needs to be estimated and compensated at the pre-DFT stage. Usually, the CFO estimation accuracy is required to be $1\% - 2\%$ of the subcarrier interval. Many CFO estimation schemes have been proposed in the literature. They can be divided into data-aided and non-data-aided (also known as blind estimation scheme). The data-aided schemes exploit the training sequence known to the receiver for CFO estimation. An advantage of this type of schemes is that they can improve the estimation performance and/or reduce the complexity of the estimation process through training sequence design. The blind schemes estimate the CFO from the receiver input without using any training sequences or pilot symbols. Instead, they exploit certain intrinsic properties of the information bearing signal itself for estimation, e.g., the cyclostationarity of the receive signal, the constant modulus property of the transmitted symbols, etc.. The immediate advantage of blind schemes is that they are bandwidth efficient and the cooperation between transmitter and receiver can be relaxed. In this chapter, the existing CFO estimation methods are reviewed for the downlink channel and uplink channel of OFDM systems respectively.

3.1 OFDM Downlink

CFO estimation for the downlink channel has been researched for many years. Therefore, we only review those recently proposed blind methods. They are classified based on the implicit properties that are exploited for estimation.

3.1.1 CP-Based Algorithms

One class of CFO estimation is designed based on CP. In [18], a joint maximum likelihood (ML) timing and CFO estimation is proposed for OFDM in AWGN channels by exploiting the correlation of the CP and the last part of the useful OFDM symbol. In [19], the authors improve the algorithm in [18] by deriving a new ML function which can globally characterize the estimation problem. The CP-based algorithms provide a closed form expression for CFO estimation and perform well with only one OFDM symbol. But they are prone to channel time spreading because these algorithms rely on the repetition structure in the time domain signal to extract CFO information. However, after undergoing the multipath fading channels, CP is contaminated by the preceding symbol which unfortunately destroys the repetition structure.

3.1.2 Real-Valued Constellation Constraint Based Algorithm

The real-valued constellation constraint can also be exploited for CFO estimation. The author in [20] notices that the algorithm in [18] models the OFDM signals as a proper complex Gaussian process and then derives a ML estimation based on the probability density function (pdf) of the multivariate proper complex Gaussian process. However, when data symbols belong to a real-valued constellation, the time domain OFDM signal is actually an improper complex Gaussian process. Therefore, the estimation in [18] is not a ML estimation under this constraint. In [20], a joint timing and CFO estimator is designed particularly for OFDM systems with real-valued constellation. The algorithm exploits the conjugate-symmetry property exhibited by the

time domain signal and estimates the CFO based on a minimum mean square error (MMSE) criterion. It performs better than the CP-based estimation over AWGN channels. However, like CP-based algorithms, it is also prone to multipath fading which destroys the conjugate-symmetry property of the received signals.

3.1.3 VSC-Based Algorithms

Another class of CFO estimation is based on virtual subcarriers (VSCs). The estimation can be accomplished by using only one OFDM symbol. Unlike the above two classes of schemes, it is robust to unknown multipath fading channels. VSCs are used in OFDM systems in order to avoid aliasing, help shaping the spectrum and prevent interfering with the adjacent OFDM channels. They are usually placed consecutively at both ends of the frequency spectrum. VSCs can be thought of as pilots since they transmit null symbols known to the receiver. However the main difference between VSCs and pilots is that VSCs do not waste any power.

The novel idea of VSC-based CFO estimation was first proposed in [21]. It is a subspace based estimation scheme, where a low rank signal model is introduced by the VSCs. This algorithm exploits the orthogonality between the virtual subcarriers and information bearing subcarriers. The idea behind it is that in the absence of noise, the received OFDM signals should be orthogonal to the VSCs after CFO being completely compensated. Based on this, a cost function is constructed to minimize the power of the received signal on the VSCs by adjusting the candidate CFO. There are two approaches in minimizing the cost function. The first approach uses one-dimensional grid search along the unit circle which is known as the multiple signal classification (MUSIC) searching algorithm in array signal processing [21]. The second approach is root finding, which is proposed in [22]. In this approach, the cost function is first approximated by Taylor expansion using a limited number of terms. Then derivative of the approximated cost function is computed and set to zero to find its roots. The root with the smallest value of cost function then gives the estimated CFO. The implementation complexity of root finding is much less than that of the grid search.

In [23], the authors derive the ML estimator for OFDM system with VSCs, and at last arrive at the same cost function given in [21].

In [24], another VSC-based subspace estimation is proposed. It uses the estimation of signal parameters by rotational invariance technique (ESPRIT) [25]. ESPRIT is a technique used for the problem of frequencies estimation of sinusoids embedded in noise. Unlike the above VSC-based subspace approach in [21], this approach gives a closed-form expression for CFO estimation in terms of the eigenvectors of the correlation matrix of the received OFDM signal in time domain. However, to estimate the correlation matrix, a sequence of OFDM symbols are required.

The difference between the subspace approaches in [21] and [24] is that in the latter approach the signal subspace of the observed signal is obtained from the estimated correlation matrix by taking the eigenvalue decomposition (EVD) and then CFO information is retrieved from the eigenvectors. Thus a sequence of observations is required. While, in the former approach, the noise subspace of the received signal in the absence of CFO is retrieved from the signal model. CFO is then estimated by adjusting the candidate CFO to minimize the projection of the compensated signal onto the noise subspace. Thus, it is possible to estimate the CFO by using only one OFDM symbol.

The authors in [26] point out that when VSCs are placed consecutively in the spectrum, the two VSC-based algorithms in [21] and [24] might not be able to uniquely determine the CFO in the presence of a channel frequency null on the DFT grid. In order to identify CFO without any ambiguity, they have designed three alternative VSCs placement schemes. In [27], the authors generalize the scheme in [26] to MIMO-OFDM systems and find that the estimation performance does not depend on the number of transmit antennas, but can be improved by increasing the number of symbols and receive antennas.

3.1.4 Oversampling-Based Algorithm

Oversampling the time domain signal by a factor of two at the receiver side can also introduce a low rank signal model and actually create the same effect as that of VSCs. In [28], an oversampling-based ML estimation is proposed, where the oversampled data is utilized to exploit the intrinsic phase shift among neighboring samples caused by CFO. This scheme is robust to channel frequency nulls and covers the entire acquisition range. The estimated CFO can be obtained by grid search in minimizing the cost function or root finding approach.

3.1.5 Constant Modulus Constraint Based (CM-Based) Algorithms

The constant modulus (CM) property of M-PSK modulation can also be exploited for CFO estimation. In [29], the authors derive a cost function by using the ML approach, and based on that a modified cost function is proposed to jointly exploit the existence of VSCs and the CM constraint. In [30], the CM property is exploited to decouple the squared amplitude of the channel frequency response from the received signal. Under the assumption that the length of the channel spread is always less than half of the length of one OFDM symbol duration, the vector of the squared amplitude of the channel frequency response is shown to be in a rank deficient subspace. Then a subspace approach is applied to estimate the CFO.

3.1.6 Correlation-Based Algorithms

The presence of the CFO impacts the correlation of the received signal, so the knowledge of the correlation in turn can help with the CFO estimation. This class of schemes requires the channel to keep constant over a sequence of OFDM symbols so that this sequence of symbols can be used to estimate the correlation.

In [31], the correlation of the pre-DFT signal is exploited. CFO is estimated by minimizing the Euclidean distance between the correlation estimated from the

observed signal and the analytical correlation obtained from the system model. It requires channel knowledge for CFO estimation.

In [32], the pseudo-correlation of the post-DFT signal is exploited for real-valued constellation. The pseudo-correlation instead of common correlation is used because it vanishes for the proper complex random variable, e.g., noise, but it is retained for the real-valued constellation symbol. It is shown that if CFO has been completely compensated, pseudo-correlation matrix becomes a diagonal matrix independent of channel. So, minimizing the total off-diagonal power of the estimated pseudo-correlation matrix by adjusting the candidate CFO gives the CFO estimation. Unlike the scheme in [31], it does not require the channel knowledge. Furthermore the cost function can be manipulated into a sinusoidal form such that curve fitting can be used in minimizing the cost function instead of grid search.

3.1.7 Cyclostationarity-Based Algorithms

Cyclostationarity of the time domain signal can also be exploited for CFO estimation. This class of schemes can give the CFO estimation in a closed-form expression. Like the above correlation-based algorithms, it also requires a sequence of symbols and requires the channel to be constant across this sequence of symbols.

In [33], a joint timing and CFO estimation scheme is proposed based on the second-order cyclostationarity of the time domain OFDM signal. The cyclostationarity of the OFDM signal can be introduced in different ways by CP, pulse shaping, power weighting or precoding. The existence of VSCs can be thought as a kind of power weighting scheme since the weights on VSCs are set to zeros. However, this scheme requires the channel knowledge. In [34], the authors modify the scheme in [33]. The modified scheme does not require the channel knowledge, and it performs as well as that in [33].

3.1.8 Fourth-order Statistics of Post-DFT Signal Based Algorithms

CFO can also be estimated from the information appearing in the higher-order statistic of the post-DFT signal. Compared to the second-order statistics based algorithms, a shortcoming of the higher-order statistic based algorithms is its high variance of the estimation especially at low signal-to-noise ratio (SNR).

In [35], the oversampled post-DFT signal is exploited. Because of the second-order stationarity of the post-DFT signal resulted from the "sinc" pulse shaping function, the second-order statistic does not contain any CFO information. Therefore, the author resorts to the fourth-order cyclostationarity which contains spectral line at CFO. The algorithm stems from recognizing that CFO impacts the frequency domain OFDM signal in the same way that timing offset impacts a M-QAM modulated signal in the time domain. Therefore, the authors adopt a blind clock recovery algorithm designed for linear modulation scheme to the CFO estimation. However, this scheme is prone to multipath fading channels.

In [36], a cost function based on the forth-order accumulation is proposed based on the criterion to minimize ICI terms. In [37], a kurtosis-type cost function is proposed based on the Gaussianity of the post-DFT signals. As we know, in the presence of CFO, the post-DFT signal is the linear combination of the signal transmitted on all the subcarriers. Without the CFO, only the desired signal appears on each subcarrier and ICI disappears. By exploiting the fact that the distribution of the linear combination of independent random variables is closer to Gaussian than that of the original variables, the kurtosis-type cost function which measures the Gaussianity of the signal is proposed. Furthermore, curve fitting is used in minimizing the cost function instead of grid search. The authors have also applied this scheme to the MIMO-OFDM systems. It is shown that the estimation performance improves with the increasing number of receive antennas due to the receive diversity. Unfortunately, it degrades in the scenario with multiple transmit antennas. The reason is that in such

scenario the received signal is the combination of the signals from all the transmit antennas which brings the signal distribution closer to Gaussian even in the absence of CFO.

3.1.9 Phase Rotation Based Algorithm

CFO also impacts the phase rotation between two consecutive symbols transmitted on the same subcarriers. This property has been exploited by [38]. The scheme proposed in [38] is based on two assumptions: 1) M-PSK or amplitude-phase shift keying (A-PSK) modulation scheme is used; 2) the channel keeps constant over two consecutive OFDM symbols. Therefore, by taking the M-th power method, the phase difference over two consecutive symbols introduced by modulation can be removed and only the phase rotation introduced by CFO is retained which gives a closed-form expression for CFO estimation. But this scheme performs worse for large CFO than small CFO because large CFO results in more severe ICI. Therefore, the authors have also proposed a scheme by iterating the estimation and correction steps several times to increase the CFO estimation accuracy.

3.2 OFDM Uplink

For the uplink channel of OFDM systems, CFO estimation is much more complicated. This is because different users suffer from distinctive CFOs. As such, the CFO of each user has to be estimated, which increases the number of unknowns. Furthermore, the received signal suffers not only ICI but also multiuser interference (MUI). Synchronizing one user with the base station means misalignment with the other users which results in MUI. Therefore, CFO compensation is usually not performed at base station. The CFO estimated by the base station is usually fedback to the mobile unit through a control channel so that the oscillator at the mobile unit can be adjusted accordingly.

Uplink CFO estimation schemes are designed based on how users are multiplexed

in the frequency domain. There are three carrier assignment schemes (CASs), namely, block, interleaved, and arbitrary. For the block assignment, the total subcarriers are divided into several blocks of adjacent subcarriers. Each user is assigned one block of adjacent subcarriers. A guard band is used between blocks to eliminate MUI. This assignment scheme is not optimum with regard to frequency diversity for each user, but it maximizes the spectrum distance between users which in turn decreases the impact of MUI. For the interleaved assignment scheme, the subcarriers assigned to each user are interleaved over the whole bandwidth such that a large frequency diversity can be achieved for each user. However, this scheme is more susceptible to MUI compared to the block assignment scheme. For the arbitrary assignment scheme, the subcarrier is allocated dynamically according to the current channel condition of each user. Therefore, it can provide more flexibility than the block and interleaved assignment schemes.

3.2.1 Block Assignment Scheme

In the block assignment scheme, with sufficient guard bands, CFO can be estimated by running for each user an individual estimator after separating their signals. Some of the estimators designed for the downlink channel in the previous section could be used as an individual estimator directly.

In [39], a user's signal is first separated by using a bank of bandpass filters and then the CP-based estimator presented in [18] is applied for each user individually. Using a filter bank to separate the different signals is possible for the block assignment scheme. Furthermore this way keeps the CP which would otherwise be removed if DFT is used to separate these signals. However, using a filter bank can not separate user signals perfectly because the user spectra actually overlap with each other. Therefore, a sufficient guard band is required to mitigate the effects of MUI. The estimation performance of this scheme is shown to degrade with the increasing number of users or with the decreasing number of subcarriers assigned to each user. This is because if each user is assigned with only a small portion of the total available subcarriers,

their time domain samples are not uncorrelated as it is modeled in [18]. In [40], the user signal is also separated by using a filter bank and then a VSC-based estimator [21] is used for each user. The guard band between users acts as VSCs to facilitate estimation. The simulation result shows that the estimation performance exhibits floor at high SNR. This reflects the imperfect user signal separation by using filter bank. The simulation result also shows that the CFO estimation performance is different from user to user. This is because each user has its distinctive CFO which results in different interference on the other users. In [41], a fourth-order statistic-based CFO estimator [35] is used for each user after user signals have been separated by using a filter bank.

In [37], the kurtosis-type CFO estimation has been extended to the uplink channel of OFDM systems. The user signal is separated by DFT operation at the receiver. Compared with the schemes in [40], this scheme performs better even with small guard bands.

By noticing that the estimation error in [40], which separates the user signals with a filter bank, is still high due to the MUI on VSCs, the authors in [42] propose an iterative VSC-based CFO estimation. The scheme separates user signals neither with a filter bank nor with DFT operation. Instead, to estimate the CFO of a particular user at each iteration, the signals from undesired users are suppressed from the received signal one by one based on CFO estimation obtained from the last iteration. The suppression operation is intended to lower the MUI on VSCs. The initial CFO estimation is obtained without any MUI suppression at all so it is not accurate. However, the estimation accuracy could be improved with the iterations. The simulation results show that this scheme performs much better than the one in [40]. In the suppression operation, a linear approximation is used. This results in a small estimation bias or a floor in terms of mean-square error at high SNR.

3.2.2 Arbitrary Assignment Scheme

For the interleaved and arbitrary assignment schemes, user signals cannot be separated easily at the base station by using a filter bank. Therefore, most of the CFO estimation algorithms designed for the downlink channel can not be applied here.

In [43], the cyclostationarity-based estimation in [33] is extended for the uplink channel of OFDM systems. It assumes that each user is assigned one subcarrier. In [44], the cyclostationarity-based estimation scheme is extended to the arbitrary assignment scheme. The cyclostationarity-based schemes require a sequence of OFDM symbols to obtain the estimated correlation. It is shown that the Fourier transform of the correlation function is in the form of the summation of complex sinusoids with the CFO associated with each user as parameters. Hence the CFO estimation problem is changed to the estimation of the parameters of sinusoids with noise which can be solved with the ESPRIT algorithm. The simulation results show that the estimation performance is more or less independent of SNR.

In [45], a CFO estimation based on the phase shift of consecutive repeated training symbols is designed for the arbitrary assignment scheme. However, it is applied only to the situation when one new user entering the network with all the other users having already been synchronized with the base station.

In [46] and [47], ML estimators are proposed to jointly estimate the CFO and channel for all the users simultaneously by using one OFDM training symbol. It is a multi-dimensional optimization problem. In [46], to solve the multi-dimensional optimization problem, an expectation maximization (EM) algorithm is used which essentially transforms a multi-dimensional maximization problem into a number of separate one-dimensional maximization problem. The CFO of each user is estimated by using grid search and the CFO estimation is then exploited to recover the channel response by using the least-square (LS) method. In [47], the alternating-projection method is used to estimate each user's CFO iteratively which also reduces the complexity of the multi-dimensional maximization problem. Compared with the EM scheme, the alternating projection method has a faster convergence rate.

In [48], the extended Kalman filter (EKF) is employed in time domain for CFO estimation by using one training symbol. Instead of using a multi-dimensional EKF to jointly estimate the CFO of all the users, a one-dimensional EKF is used for each user. In each recursion, each user's signal is separated from the received signal by cancelling the signal from the other users based on the CFO estimation obtained from the previous recursion. However, the disadvantage of this scheme is its requirement for channel knowledge.

3.2.3 Interleaved Assignment Scheme

In [49], a novel structure-based estimation method is proposed for the interleaved assignment scheme. The inner periodic structure of the received signal is exploited to arrange the received signal into a matrix form. A low rank signal model is introduced by assuming that the number of active users is less than the maximum number of the users that could be supported or by extending the length of CP. Then a subspace based method is used to build the cost function. The user CFOs are estimated by finding the local minima of the cost function and are mapped to users according to the ranges of CFO distribution. The algorithm uses only one OFDM symbol. Its performance can be improved by using receive diversity and/or decreasing system load. It outperforms the cyclostationarity-based estimation in [43].

In [50], by noticing that the scheme in [49] has a problem with mapping the estimated CFOs with users at low SNR, the authors propose to combine the structure-based estimation and the ML mapping method to solve the problem of mismatch.

Chapter 4

CFO Estimation in Correlated MIMO-OFDM Systems

4.1 Introduction

In this chapter, we propose a virtual subcarriers (VSCs) based CFO estimation scheme for correlated MIMO-OFDM systems [51]. The idea of exploiting VSCs for CFO estimation was first proposed in [21]. This approach is based on the fact that the received OFDM signals in the absence of noise should be orthogonal to the VSCs after CFO being properly compensated. In [23], the authors take the conditional maximum likelihood (CML) approach, in which the likelihood function is conditioned on the nuisance parameters, e.g., channel and data, to derive the estimation scheme and at last arrive at the same cost function as the one in [21]. In [26], the authors point out that the cost function in [21] might not be able to uniquely determine the CFO in the presence of channel frequency null on the DFT grid. In order to solve the problem of identifiability, they propose an improved estimation scheme by using several OFDM symbols and hopping the virtual subcarrier location from symbol to symbol. In [27], the authors generalize the scheme in [26] to MIMO-OFDM systems and find that the estimation performance does not depend on the number of transmit antennas, but can be improved with an increased number of OFDM symbols and receive antennas.

In practical MIMO-OFDM systems, it may be the case that the transmit (and/or receive) antennas are placed close to each other. This gives rise to spatial correlation where the corresponding subchannels are no longer independent. The existing CML CFO estimation techniques do not take this correlation into consideration. Therefore, the impact of the presence of such correlation on the CFO estimation remains unknown. This motivates us to consider ML CFO estimation in the presence of spatial correlation. To be able to do so, we treat the channel and data as random variables with known statistics. This approach is normally referred to as unconditional ML (UML), where the nuisance parameters are averaged out from the conditional likelihood function. We also notice that the data symbols transmitted on different antennas and subcarriers may also be correlated as data is normally coded by an error correcting coding scheme, e.g., a convolutional code, a turbo code, etc., as well as a space-time coding scheme. However, in our underlying analysis, we only consider uncorrelated symbols as we believe that symbol correlation introduced by coding is very weak and can be ignored. It should be pointed out that the authors in [52] consider the UML CFO estimation (with some approximations) on additive white Gaussian noise (AWGN) channels (with no fading or MIMO). In contrast, the analysis presented in this chapter is exact, i.e., no approximations assumed, and is developed for MIMO frequency selective fading channels.

We derive the UML estimator that can be used to accurately estimate the CFO in the presence of spatial correlation. We also derive the unconditional Cramér-Rao lower bound (UCRLB). The derived UCRLB depends on the second order statistics of data, channel and channel noise, unlike the existing conditional Cramér-Rao lower bound (CCRLB) which depends on the channel and data realizations [23]. We show from an analytical point of view that the UML estimator can additionally exploit the knowledge of receive spatial correlation together with VSCs to contribute to the CFO estimation. However, this contribution is relatively weak. The simulation results show that in the presence of spatial correlation, by using UML estimator, there is not much performance improvement as compared to the CML estimator. The significance

of this result is that one may develop VSC-based CFO estimation scheme without considering spatial correlation which would make this task a lot easier.

The organization of the rest of this chapter is as follows. In Section 4.2, we present the system model of the MIMO-OFDM system under consideration. In Section 4.3, the UML estimator and UCRLB are derived for MIMO-OFDM systems in the presence of spatial correlation. In Section 4.4, we disclose how the receive spatial correlation can contribute to the CFO estimation by inspecting a system with only two receive antennas. In Section 4.5, we present simulation results. Finally, Section 4.6 concludes this chapter.

4.2 System Model

Let us consider a MIMO-OFDM system with N_t transmit antennas, N_r receive antennas and N orthogonal subcarriers. Without loss of generality, we assume that the first M subcarriers are used for information data transmission, and the last $N - M$ subcarriers are reserved for VSCs. In each OFDM symbol duration, let $d_{i,k}$ denote the symbol transmitted from the ith antenna on the kth subcarrier. At the transmitter, a vector of M symbols $\mathbf{d}_i = [d_{i,0}, d_{i,1}, \ldots, d_{i,M-1}]^T$ are passed through the IDFT transformation. The IDFT outputs are then converted into a serial stream and added with CP before the signal is transmitted from the ith antenna.

Let us denote the discrete time channel impulse response between the ith transmit and jth receive antenna as $h_{i,j}(n) = \sum_{l=0}^{L-1} h_{i,j,l}\delta(n-l)$, where L is the length of channel spread and $h_{i,j,l}$ denotes the multipath fading coefficient which is modeled as complex Gaussian random variable with zero mean and variance $\sigma_{h_l}^2$. The multipath fading coefficients associated with different delays are assumed to be independent. The channel power is normalized, i.e., $\sum_{l=0}^{L-1} \sigma_{h_l}^2 = 1$. The channel frequency response between the ith transmit and jth receive antenna at the DFT grids can be represented as $\mathbf{H}_{i,j}$ =diag($[H_{i,j,0}, H_{i,j,1}, \ldots, H_{i,j,M-1}]^T$), where $H_{i,j,k} = \sum_{l=0}^{L-1} h_{i,j,l} e^{-j2\pi\frac{kl}{N}}$.

Let ε denote the normalized CFO with respect to the subcarrier interval. Then,

at the jth receive antenna, the N time domain samples of the received signal in one OFDM symbol duration, i.e., $\mathbf{x}_j = [x_{j,0}, x_{j,1}, \ldots, x_{j,N-1}]^T$, can be represented as

$$\mathbf{x}_j(n) = \sum_{i=1}^{N_t} \mathbf{P}(\varepsilon)\mathbf{W}\mathbf{H}_{i,j}\mathbf{d}_i + \mathbf{z}_j, \quad j = 1, 2, \ldots, N_r, \tag{4.1}$$

where $\mathbf{P}(\varepsilon)$ =diag($[1\ e^{j\frac{2\pi\varepsilon}{N}}\ \ldots\ e^{j\frac{2\pi(N-1)\varepsilon}{N}}]^T$) represents phase shift introduced by CFO and $\mathbf{z}_j = [z_{j,0}, z_{j,1}, \ldots, z_{j,N-1}]^T$ is a vector of independent white Gaussian noise samples with variance σ_n^2. The matrix $\mathbf{W}$ is defined as $\mathbf{W} = \mathbf{W}_N\mathbf{J}$, where $\mathbf{W}_N$ is the normalized $N \times N$ IDFT matrix with its element on the kth row and lth column defined as $\frac{1}{\sqrt{N}}e^{j2\pi\frac{kl}{N}}$, $\mathbf{J}$ is an $N \times M$ matrix which consists of the first M columns of $\mathbf{I}_N$ and $\mathbf{I}_m$ denotes the $m \times m$ identity matrix. CFO estimation is then computed from the signals received across all the receive antennas in one OFDM symbol duration.

When spatial correlation is present, it is normally assumed that the spatial correlation at the transmit side is independent of that at the receive side. This means that the spatial correlation between the fading of two distinct antenna pairs is the product of the corresponding transmit spatial correlation and receive spatial correlation [53]. We denote the transmit spatial correlation between the (i_1)th and (i_2)th transmit antenna as $\rho^t_{i_1,i_2} = E\{h_{i_1,j,l}h^*_{i_2,j,l}\}/\sigma^2_{h_l}$, and the receive spatial correlation between the (j_1)th and (j_2)th receive antenna as $\rho^r_{j_1,j_2} = E\{h_{i,j_1,l}h^*_{i,j_2,l}\}/\sigma^2_{h_l}$, where $E\{\cdot\}$ denotes expectation. We consider the case of uncorrelated symbols such that $E\left\{\mathbf{d}_{i_1}\mathbf{d}^H_{i_2}\right\} = E_s\mathbf{I}_M\delta(i_1 - i_2)$, where E_s is the symbol energy per transmit antenna.

4.3 UML CFO Estimation with Spatial Correlation

In this section, we derive the UML CFO estimation for a MIMO-OFDM system in the presence of spatial correlation. Let us define the observed vector $\mathbf{x} \triangleq [\mathbf{x}_1^T, \mathbf{x}_2^T, \ldots, \mathbf{x}_{N_r}^T]^T$. As per the system model in (4.1), $\mathbf{x}$ is multivariate Gaussian distributed as long as

the number of subcarriers N is large enough, according to the central limit theorem. Then, the likelihood function of $\mathbf{x}$ conditioned on ε can be represented as

$$f(\mathbf{x}|\varepsilon) = \frac{1}{\pi^{N_r N} \det(\mathbf{R}_{\mathbf{xx}})} \exp(-\mathbf{x}^H \mathbf{R}_{\mathbf{xx}}^{-1} \mathbf{x}), \tag{4.2}$$

where $\mathbf{R}_{\mathbf{xx}} = E\left\{\mathbf{x}\mathbf{x}^H\right\}$.

Let us define Define $\mathcal{H}_{i,j} \triangleq [H_{i,j,0}\ H_{i,j,1}\ \ldots\ H_{i,j,M-1}]^T$, then we have

$$\begin{aligned}
& E\left\{\mathbf{x}_{j_1}\mathbf{x}_{j_2}^H\right\} \\
= \ & \mathbf{P}(\varepsilon)\mathbf{W} \sum_{i_1=1}^{N_t} \sum_{i_2=1}^{N_t} \left[E\{\mathcal{H}_{i_1,j_1}\mathcal{H}_{i_2,j_2}^H\} \odot E\left\{\mathbf{d}_{i_1}\mathbf{d}_{i_2}^H\right\}\right] \mathbf{W}^H \mathbf{P}(\varepsilon)^H + \sigma_n^2 \mathbf{I}_N \delta\left(j_1 - j_2\right) \\
= \ & \mathbf{P}(\varepsilon)\mathbf{W} \sum_{i=1}^{N_t} \left[E\{\mathcal{H}_{i,j_1}\mathcal{H}_{i,j_2}^H\} \odot E_s \mathbf{I}_M\right] \mathbf{W}^H \mathbf{P}(\varepsilon)^H + \sigma_n^2 \mathbf{I}_N \delta\left(j_1 - j_2\right), \\
= \ & N_t \rho_{j_1,j_2}^r E_s \mathbf{P}(\varepsilon)\mathbf{W}\mathbf{W}^H \mathbf{P}(\varepsilon)^H + \sigma_n^2 \mathbf{I}_N \delta\left(j_1 - j_2\right)
\end{aligned} \tag{4.3}$$

where $\odot$ denotes element-wise Hadamard product. The last line of the above expression comes from the fact that $E\{H_{i,j_1,k}H_{i,j_2,k}^*\} = \rho_{j_1,j_2}^r$.

Let $\mathbf{R}^r$ denote the $N_r \times N_r$ receive spatial correlation matrix with the element on the (j_1)th row and (j_2)th column defined as ρ_{j_1,j_2}^r. We then have

$$\mathbf{R}_{\mathbf{xx}} = [\mathbf{I}_{N_r} \otimes (\mathbf{P}(\varepsilon)\mathbf{W}_N)]\, \mathbf{R} [\mathbf{I}_{N_r} \otimes (\mathbf{W}_N^H \mathbf{P}(\varepsilon)^H)], \tag{4.4}$$

where $\otimes$ is Kronecker product, and

$$\mathbf{R} \triangleq \mathbf{R}^r \otimes \left(N_t E_s \mathbf{J}\mathbf{J}^H\right) + \sigma_n^2 \mathbf{I}_{NN_r}, \tag{4.5}$$

which could be computed offline if the receive spatial correlation and noise power are known.

By plugging (4.4) into (4.2), and noting that $\det(\mathbf{R}_{\mathbf{xx}})$ is not a function of ε, we

arrive at the UML CFO estimation, which is given by

$$\hat{\varepsilon}_{UML_1} = \arg\min_{\tilde{\varepsilon}} \left\{ \mathbf{x}^H \left[\mathbf{I}_{N_r} \otimes (\mathbf{P}(\tilde{\varepsilon})\mathbf{W}_N) \right] \mathbf{R}^{-1} [\mathbf{I}_{N_r} \otimes (\mathbf{W}_N^H \mathbf{P}(\tilde{\varepsilon})^H)] \mathbf{x} \right\}. \tag{4.6}$$

We can use the formula of Cramér-Rao lower bound (CRLB) for the general Gaussian case in [54] to obtain the CRLB for the mean square error (MSE) of the estimated ε. The formula is

$$\text{CRLB} = 1/\,\text{Re}\left[\text{tr}\left(\mathbf{R}_{\mathbf{xx}}^{-1} \frac{d\mathbf{R}_{\mathbf{xx}}}{d\varepsilon} \mathbf{R}_{\mathbf{xx}}^{-1} \frac{d\mathbf{R}_{\mathbf{xx}}}{d\varepsilon} \right) \right]. \tag{4.7}$$

According to (4.4), we have

$$\begin{aligned} \frac{d\mathbf{R}_{\mathbf{xx}}}{d\varepsilon} &= j \left[\mathbf{I}_{N_r} \otimes (\mathbf{P}(\varepsilon)\mathbf{A}\mathbf{W}_N) \right] \mathbf{R} [\mathbf{I}_{N_r} \otimes (\mathbf{W}_N^H \mathbf{P}(\varepsilon)^H)] \\ &\quad -j \left[\mathbf{I}_{N_r} \otimes (\mathbf{P}(\varepsilon)\mathbf{W}_N) \right] \mathbf{R} [\mathbf{I}_{N_r} \otimes (\mathbf{W}_N^H \mathbf{A}\mathbf{P}(\varepsilon)^H)], \end{aligned} \tag{4.8}$$

where $\mathbf{A} = \frac{2\pi}{N}\text{diag}([0, 1, \ldots, N-1]^T)$. By plugging (4.8) into (4.7), we obtain

$$\text{UCRLB} = 1/\,\text{Re}(2a), \tag{4.9}$$

where $a = \text{tr}\left\{ \mathbf{R}^{-1} \left[\mathbf{I}_{N_r} \otimes \left(\mathbf{W}_N^H \mathbf{A} \mathbf{W}_N \right) \right] \mathbf{R} \left[\mathbf{I}_{N_r} \otimes \left(\mathbf{W}_N^H \mathbf{A} \mathbf{W}_N \right) \right] \right\} - N_r \text{tr}\{\mathbf{A}^2\}$.

In light of the above, we make the following remarks.

1. We note that the UML estimator in (4.6) is different from the CML estimator in [23]. In the UML approach, the channel and data are treated as random variables, hence the spatial correlations can be incorporated into the estimation process naturally. However, we notice that the transmit spatial correlation does not impact the UML estimator at all due to the assumption of uncorrelated symbols.

2. The UML cost function in (4.6) degenerates to the CML cost function in [23] in the absence of spatial correlation. To elaborate on this, let us assume $\mathbf{R}^r = \mathbf{I}_{N_r}$.

Then, we have

$$\mathbf{R}^{-1} = \frac{1}{\sigma_n^2}\mathbf{I}_{Nr} \otimes (\mathbf{I}_N - \frac{\gamma}{1+\gamma}\mathbf{J}\mathbf{J}^H). \tag{4.10}$$

where $\gamma \triangleq N_t E_s/\sigma_n^2$ denotes the SNR observed at each receive antenna. Therefore, the UML estimator in (4.6) can be simplified as

$$\begin{aligned}\hat{\varepsilon}_{UML_2} &= \arg\min_{\tilde{\varepsilon}} \mathbf{x}^H \left[\mathbf{I}_{N_r} \otimes \left(\mathbf{I}_N - \frac{\gamma}{1+\gamma}\mathbf{P}(\tilde{\varepsilon})\mathbf{W}\mathbf{W}^H\mathbf{P}(\tilde{\varepsilon})^H\right)\right]\mathbf{x} \\ &= \arg\min_{\tilde{\varepsilon}} \sum_{j=1}^{N_r} \mathbf{x}_j^H(\mathbf{I}_N - \mathbf{P}(\tilde{\varepsilon})\mathbf{W}\mathbf{W}^H\mathbf{P}(\tilde{\varepsilon})^H)\mathbf{x}_j. \end{aligned} \tag{4.11}$$

where, the last line comes from the fact that $\mathbf{x}_j^H\mathbf{x}_j$ is not a function of $\tilde{\varepsilon}$. By comparing (4.11) and (9) in [23], we see that they are equivalent, as expected.

3. The CCRLB can be shown as [1]

$$\text{CCRLB} = \frac{\sigma_n^2/2}{\sum_{j=1}^{N_r}(|\mathbf{A}\mathbf{W}\sum_{i=1}^{N_t}\mathbf{H}_{i,j}\mathbf{d}_i|^2 - |\mathbf{W}^H\mathbf{A}\mathbf{W}\sum_{i=1}^{N_t}\mathbf{H}_{i,j}\mathbf{d}_i|^2)}.$$

It will be shown in the simulation results that the CCRLB is tighter than the UCRLB. This is because the signals received in only one OFDM symbol duration are used for estimation. If a large number of symbols, however, are used for estimation, the two CRLBs would be equivalent. The advantage of the UCRLB is that it depends only on the channel and data statistics, while the CCRLB depends on the channel and data realizations.

[1]The CCRLB has been provided in [23] but only for single-input single-output OFDM systems using multiple OFDM symbols for CFO estimation.

4.4 UML CFO Estimation with Two Receive Antennas

To gain more insight into the principle behind the UML estimation, let us consider a MIMO-OFDM system employing only two receive antennas with receive spatial correlation matrix denoted by

$$\mathbf{R}^r = \begin{bmatrix} 1 & \rho \\ \rho^* & 1 \end{bmatrix}.$$

As such, we have $\mathbf{x} = [\mathbf{x}_1^T, \mathbf{x}_2^T]^T$. Based on the expressions in (4.4) and (4.5), we have

$$\mathbf{R}_{\mathbf{xx}} = \sigma_n^2 \begin{bmatrix} \gamma\mathbf{P}(\varepsilon)\mathbf{W}\mathbf{W}^H\mathbf{P}(\varepsilon)^H + \mathbf{I}_N & \rho\gamma\mathbf{P}(\varepsilon)\mathbf{W}\mathbf{W}^H\mathbf{P}(\varepsilon)^H \\ \rho^*\gamma\mathbf{P}(\varepsilon)\mathbf{W}\mathbf{W}^H\mathbf{P}(\varepsilon)^H & \gamma\mathbf{P}(\varepsilon)\mathbf{W}\mathbf{W}^H\mathbf{P}(\varepsilon)^H + \mathbf{I}_N \end{bmatrix}. \tag{4.12}$$

Furthermore, by using the inversion property of block matrices, we obtain

$$\mathbf{R}_{\mathbf{xx}}^{-1} = \frac{1}{\sigma_n^2} \begin{bmatrix} a\mathbf{P}(\varepsilon)\mathbf{W}\mathbf{W}^H\mathbf{P}(\varepsilon)^H + \mathbf{I}_N & b\rho\mathbf{P}(\varepsilon)\mathbf{W}\mathbf{W}^H\mathbf{P}(\varepsilon)^H \\ b\rho^*\mathbf{P}(\varepsilon)\mathbf{W}\mathbf{W}^H\mathbf{P}(\varepsilon)^H & a\mathbf{P}(\varepsilon)\mathbf{W}\mathbf{W}^H\mathbf{P}(\varepsilon)^H + \mathbf{I}_N \end{bmatrix}, \tag{4.13}$$

where $a = -\frac{(1-|\rho|^2)\gamma^2+\gamma}{(1+\gamma)^2-|\rho|^2\gamma^2}$ and $b = -\frac{\gamma}{(1+\gamma)^2-|\rho|^2\gamma^2}$.

Thus the UML CFO estimation can be obtained by

$$\begin{aligned} &\hat{\varepsilon}_{UML_3} \\ = \ &\arg\min_{\tilde{\varepsilon}} \mathbf{x}_1^H\mathbf{P}(\tilde{\varepsilon})\left(\mathbf{I}_N - \mathbf{W}\mathbf{W}^H\right)\mathbf{P}(\tilde{\varepsilon})^H\mathbf{x}_1 + \mathbf{x}_2^H\mathbf{P}(\tilde{\varepsilon})\left(\mathbf{I}_N - \mathbf{W}\mathbf{W}^H\right)\mathbf{P}(\tilde{\varepsilon})^H\mathbf{x}_2 \\ &+c[\rho\mathbf{x}_1^H\mathbf{P}(\tilde{\varepsilon})\left(\mathbf{I}_N - \mathbf{W}\mathbf{W}^H\right)\mathbf{P}(\tilde{\varepsilon})^H\mathbf{x}_2 + \rho^*\mathbf{x}_2^H\mathbf{P}(\tilde{\varepsilon})\left(\mathbf{I}_N - \mathbf{W}\mathbf{W}^H\right)\mathbf{P}(\tilde{\varepsilon})^H\mathbf{x}_1]. \end{aligned} \tag{4.14}$$

where $c = \frac{1}{1+(1-|\rho|^2)\gamma}$. By comparing the UML estimator in (4.14) and the CML estimator in (4.11) with $N_r = 2$, we notice that the first two terms in (4.14) contribute

to the CFO estimation by minimizing the power of the received signal on the VSCs as what the CML estimator does. In addition, the third term in (4.14) also contributes to CFO estimation by exploiting the knowledge of receive spatial correlation as well as the existence of VSCs as we will explain next.

The expression $\mathbf{x}_2^H \mathbf{P}(\tilde{\varepsilon}) \left(\mathbf{I}_N - \mathbf{W}\mathbf{W}^H\right) \mathbf{P}(\tilde{\varepsilon})^H \mathbf{x}_1$ in the third term of (4.14) actually gives an estimation of the cross-correlation of the received signal from the two receive antennas on those VSCs. If the CFO is completely compensated, the received signals on the VSCs are just noise. Thus, the estimated cross-correlation is zero. On the other hand, if the CFO is not completely compensated, the received signal on the VSCs is noise together with the signals leaked from the information bearing subcarriers. Consequently, the estimated cross-correlation can be represented as $C\rho$, where $C > 0$ and its value depends on the mismatch between the true CFO and the CFO candidate. Therefore, we observe that minimizing the third term of expression (4.14) also contributes to the CFO estimation. So, from this analytical point of view, the knowledge of receive spatial correlation as well as the presence of VSCs can make additional contribution to CFO estimation. However, simulation results show that the contribution from the third term of (4.14) is marginal as compared to the contribution from its first two terms.

4.5 Simulation Results

We consider a MIMO-OFDM system with $N = 64$, $N - M = 12$, $N_t = 2$ and $N_r = 2$. The quaternary phase shift keying (QPSK) modulation scheme is applied and no any coding scheme is used at the transmit side. The length of the fading channel spread is set to $L = 8$, which is assumed to be shorter than the length of the CP. The channel has uniform power delay profile. The normalized frequency offset is set to $\varepsilon = 0.2$. The grid search method is used to minimize the cost function where $1,000$ equally spaced CFO candidates in the range of $[-0.5, 0.5]$ are used to achieve a precision of 10^{-3}. The performance of estimation schemes is measured by MSE, which is defined

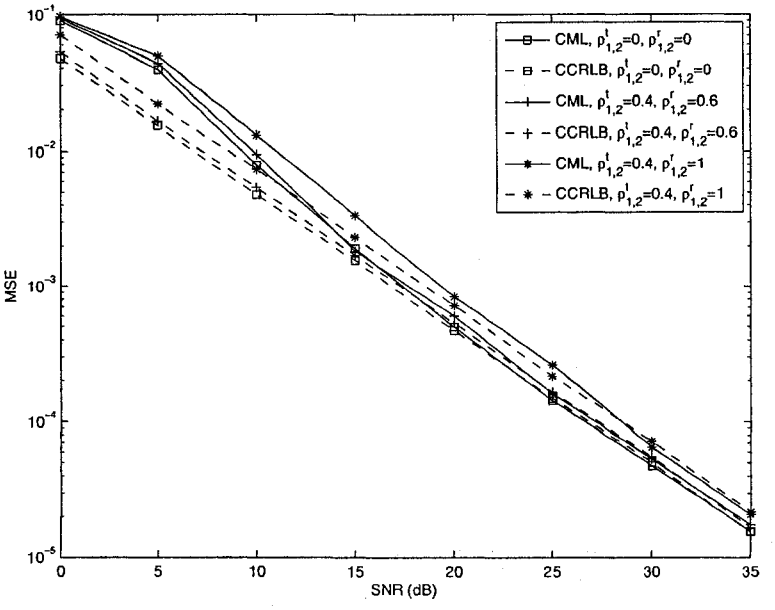

Figure 4.1: Comaprison of the perforamnce of the CML estimator for a MIMO-OFDM system with or without spatial correlaion.

as MSE= $E\{(\hat{\varepsilon} - \varepsilon)^2\}$.

In Fig. 4.1, we show the performance of the CML estimator in the presence of spatial correlation. We compare three cases, i.e., 1) $\rho^t_{1,2} = \rho^r_{1,2} = 0$, 2) $\rho^t_{1,2} = 0.4$, $\rho^r_{1,2} = 0.6$ and 3) $\rho^t_{1,2} = 0.4$, $\rho^r_{1,2} = 1$. We observe that the presence of spatial correlation degrades the performance of the CML estimator.

In Fig. 4.2, we compare the performance of the UML CFO estimator and the CML estimator in the presence of receive spatial correlation, i.e., $\rho^t_{1,2} = 0$ and $\rho^r_{1,2} = 0.6$. We first plot the simulation results by using one OFDM symbol for the estimation process. We observe that the performances of the two estimators almost overlap with each other. It shows that although the UML estimator can exploit the knowledge of receive spatial correlation as well as the existence of VSCs to make additional contribution for CFO estimation, this contribution does not provide any noticeable performance improvement in comparison with the CML estimator. The CCRLB and UCRLB are also plotted. We notice that when only one OFDM symbol is used for

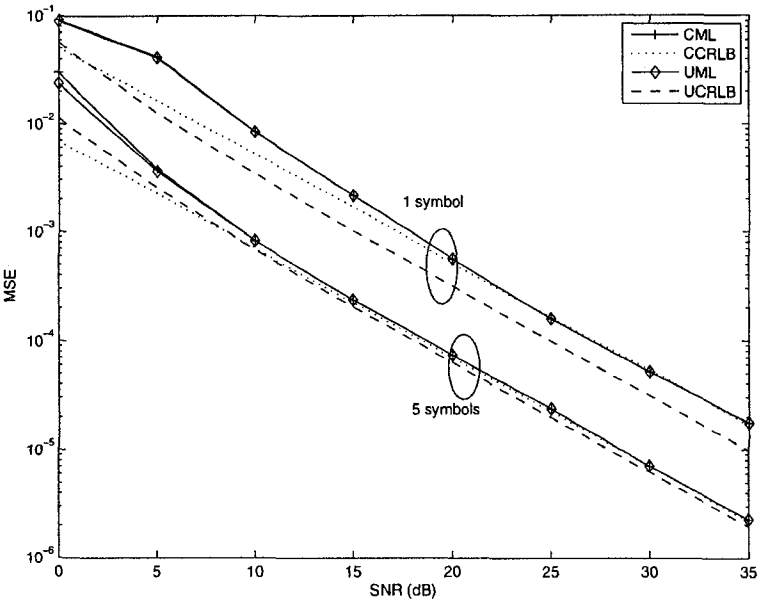

Figure 4.2: Comparison of UML and CML estimator for an MIMO-OFDM system with receive spatial correaltion.

estimation, there is a gap between CCRLB and UCRLB. In this figure, we also plot the simulation results when five symbols are used for estimation. We observe that when the number of OFDM symbols used for estimation increases, the gap between CCRLB and UCRLB diminishes.

4.6 Conclusion

In this chapter we discussed the UML CFO estimation scheme based on VSCs for MIMO-OFDM systems in the presence of spatial correlation. In our derivation, we treated the channel and data as random variables with known second order statistics. We derived UML CFO estimator and UCRLB. We also disclosed from an analytical point of view that, as compared to the CML estimator, the UML estimator can exploit the knowledge of receive spatial correlation as well as the existence of VSCs to make additional contribution for CFO estimation. However, as this additional

contribution is very small, the simulation results showed that in the presence of spatial correlation, there is no significant difference between the performance of UML estimator and the CML estimator. The implication of this result is that one need not take spatial correlation into account in developing VSC-based CFO estimation scheme for MIMO-OFDM systems. This should simplify such development process.

Chapter 5

A Blind CFO Estimation Scheme for OFDM Systems with Constant Modulus Signaling

5.1 Introduction

Blind CFO estimation for OFDM systems has been studied in [21], [26], [28], [29], [30], [32], [33], [35], [37], and references therein. A virtual subcarriers (VSCs)-based scheme is proposed in [26] for MIMO-OFDM systems. This scheme provides a large acquisition range, but the computational complexity is high since the grid search method has to be used in minimizing the cost function. In [37], the kurtosis metric, which measures the Gaussianity of a random sequence, is exploited to construct a kurtosis-type cost function for fine CFO estimation. Although this scheme has the advantage of giving a closed-form CFO estimation by using curve fitting, its estimation accuracy requires a large number of OFDM symbols which introduces processing delay. A constant modulus (CM)-based subspace scheme is proposed in [30]. This scheme exploits the correlation of the squared amplitude spectrum of the channels under the reasonable assumption that the channel delay spread is always less than half the number of subcarriers. The squared amplitude spectrum of the channel is

shown to be a low rank signal such that a subspace scheme is applied to accomplish the CFO estimation with only one OFDM symbol. However, in minimizing the cost function, it requires using the gradient descent method, which makes it complex. Furthermore, this scheme is developed for OFDM systems with only a single transmit antenna. This motivates us to find an estimation scheme which can accomplish the CFO estimation for MIMO systems with only a small number of OFDM symbols and at the same time provide estimation in an explicit form.

In this chapter, we present a novel CFO estimation scheme for OFDM systems with CM signaling [55]. We consider both SISO-OFDM systems and MIMO-OFDM systems that employ orthogonal space-time block codes (OSTBCs). The proposed scheme assumes that the channel frequency response changes slowly in the frequency domain. The implication of this assumption is that the channel frequency response on two neighboring subcarriers is about the same. We exploit this assumption to derive cost functions in closed form that are based on minimizing the difference of the signal power between two neighboring subcarriers. It is mathematically shown that minimizing these cost functions yields an unique estimate of the CFO, as desired. This process is normally referred to in the literature by the *identifiability*.

In terms of performance, it is shown that the proposed scheme substantially outperforms the kurtosis-type scheme, but it is a little worse than the CM-based subspace scheme. On the other hand, in terms of complexity, the proposed scheme has a computational complexity similar to that of the kurtosis-type scheme, but it has a much lower complexity as compared to the CM-based subspace scheme. This clearly suggests that the proposed scheme offers an excellent trade-off between performance and complexity.

The organization of the rest of this chapter is as follows. In Section 5.2, we present the system model for the SISO-OFDM system under consideration. In Section 5.3, we present the proposed scheme for SISO-OFDM systems, and relate it with the kurtosis-type scheme given in [37]. In Section 5.4, we extend the proposed scheme to MIMO-OFDM systems with OSTBCs. Simulation results are presented in Section

5.5. Finally, Section 5.6 concludes this chapter.

5.2 System Model

Let us consider a SISO-OFDM system with N orthogonal subcarriers. In the mth OFDM symbol duration, a vector of N symbols, namely, $\mathbf{d}_m = [d_{m,0}\ d_{m,1}\ \dots\ d_{m,N-1}]^T$, with each symbol drawn uniformly from a CM constellation, are transmitted simultaneously on N orthogonal subcarriers. By assuming that the multipath fading channel keeps constant in one OFDM symbol duration, we can denote the channel frequency response at the DFT grid in the mth OFDM symbol duration as $\mathbf{H}_m$ =diag($[H_{m,0}$ $H_{m,1}\ \dots\ H_{m,N-1}]^T$). Let f_0 denote the CFO, which is introduced by the mismatch between the local and transmit oscillators and define the normalized CFO over the subcarrier interval as ε. We assume that the coarse CFO will be handled in the next stage. We also assume that CFO keeps constant while the estimation is performed, i.e., M OFDM symbols. Then, the N time-domain samples in the mth received OFDM symbol duration, namely, $\mathbf{x}_m = [x_{m,0}\ x_{m,1}\ \dots\ x_{m,N-1}]^T$ can be represented as

$$\mathbf{x}_m = e^{\frac{j2\pi\epsilon}{N}[(m-1)N+mL_{CP}]}\mathbf{C}(\varepsilon)\mathbf{W}\mathbf{H}_m\mathbf{d}_m + \mathbf{z}_m, \tag{5.1}$$

where $m = 1, 2, \dots, M$, L_{CP} denotes the length of CP which is assumed to be longer than the maximum channel delay spread, $\mathbf{W}$ is the $N \times N$ normalized IDFT matrix with the element on the kth row and lth column being defined as $\mathbf{W}^{k,l} = \frac{1}{\sqrt{N}}e^{j2\pi\frac{kl}{N}}$, and $\mathbf{z}_m = [z_{m,0}\ z_{m,1}\ \dots\ z_{m,N-1}]^T$ is a vector of independent zero mean white Gaussian noise samples with variance σ_n^2. The effects of accumulated phase shift resulting from the CFO on the time-domain samples of OFDM signals are represented by $\mathbf{C}(\varepsilon)$ =diag($[1$ $e^{\frac{j2\pi\epsilon}{N}}$ $\cdots$ $e^{\frac{j2\pi(N-1)\epsilon}{N}}]^T$) and $e^{\frac{j2\pi\epsilon}{N}[(m-1)N+mL_{CP}]}$ where the latter expression represents the common phase shift resulting from the CFO.

At the receive side, the CFO is first estimated and then the signal is compensated in the time domain by using this estimated CFO denoted by u. After compensation, the outputs from the DFT stage for the mth OFDM symbol, namely, $\mathbf{y}_m(u)$ =

$[y_{m,0}(u)\ y_{m,1}(u)\ \cdots\ y_{m,N-1}(u)]^T$ can be represented as

$$\mathbf{y}_m(u) = \mathbf{W}^H \mathbf{C}^*(u)\mathbf{x}_m. \tag{5.2}$$

5.3 SISO-OFDM Systems

5.3.1 Proposed Scheme

In this section, we present the proposed scheme for SISO-OFDM systems; we will extend it to MIMO-OFDM systems in the next section.

If CFO has been completely compensated in the pre DFT stage, i.e., $u = \varepsilon$, the DFT outputs would be without ICI. So in the noise-free case, the DFT outputs would be $\mathbf{y}_m(u|u=\varepsilon) = \mathbf{H}_m\mathbf{d}_m$. As such, the squared amplitude of the DFT outputs would be the squared amplitude of the channel frequency response, i.e., $|y_{m,n}(u|u=\varepsilon)|^2 = |H_{m,n}|^2$. This is true because the square amplitude operation essentially removes the data symbols when CM signaling is used.

When the channel frequency response changes slowly in the frequency domain, the channel frequency response on two consecutive subcarriers is approximately the same. Consequently, we would have

$$|y_{m,n}(u|u=\varepsilon)|^2 \approx \left|y_{m,((n+1))_N}(u|u=\varepsilon)\right|^2, \tag{5.3}$$

where $((x))_N$ denotes x modulo N. Based on this, for SISO-OFDM systems with CM constellations, we propose a cost function which minimizes the difference of the signal power for each pair of consecutive subcarriers as $\hat{\varepsilon} = \arg \min_{u\in[-0.5\ 0.5)} J_1(u)$, where

$$J_1(u) = \sum_{m=0}^{M-1}\sum_{n=0}^{N-1}\left(|y_{m,n}(u)|^2 - |y_{m,((n+1))_N}(u)|^2\right)^2. \tag{5.4}$$

Since we have $\sum_{m=0}^{M-1}\sum_{n=0}^{N-1}|y_{m,n}(u)|^4 = \sum_{m=0}^{M-1}\sum_{n=0}^{N-1}|y_{m,((n+1))_N}(u)|^4$, the above cost

function can be simplified as

$$J_1(u) = 2\sum_{m=0}^{M-1}\sum_{n=0}^{N-1}\left[|y_{m,n}(u)|^4 - |y_{m,n}(u)|^2\,|y_{m,((n+1))_N}(u)|^2\right]. \tag{5.5}$$

Lemma 1 *Under the assumption in (5.3), the cost function in (5.5) can be well approximated as*

$$J_1(u) \approx A\cos[2\pi(\varepsilon - u)] + C, \tag{5.6}$$

where A and C are not functions of u but constants that depend on the channel and symbol realization with $A < 0$. (See Appendix 5.A for the proof.)

Lemma 1 shows that the proposed cost function does achieve its minimum at $u = \varepsilon$. Furthermore, instead of using the grid search [26] or the gradient descent method [30] for minimization, curve fitting [37] can be used to obtain the CFO estimation, which makes the proposed scheme simpler than those in [26] and [30]. We point out that Lemma 1 is derived based on the assumption that all the subcarriers are used for information carrying. In real life applications, a number of VSCs always exist in OFDM systems for various purposes. Let us assume that the first Q subcarriers, i.e., from the 0th to the $(Q-1)$th subcarrier, are used for data carrying, and the last $N-Q$ subcarriers are VSCs. Then the cost function in (5.4) should be modified as

$$J_1(u) = \sum_{m=0}^{M-1}\sum_{n=0}^{Q-2}\left(|y_{m,n}(u)|^2 - |y_{m,((n+1))_N}(u)|^2\right)^2, \tag{5.7}$$

such that the estimation scheme minimizes the difference of the signal power only over each pair of the two consecutive data carrying subcarriers. In such cases, the cost function is not an exact cos function even under the noise-free assumption. So the estimation result obtained from curve fitting would be suboptimal as compared to that obtained from grid search. However, we will demonstrate later via simulations that curve fitting degrades the performance only by little even in the presence of a

large number of VSCs.

5.3.2 Relation with the Kurtosis-type Scheme

Among the existing CFO estimation schemes, the one that is most related to our proposed scheme is the one presented in [37], which is a kurtosis-type scheme. This scheme was shown in [37] to be superior to several schemes that were developed before. Motivated by this, we will next compare this estimation scheme with our proposed one.

The key idea behind the kurtosis-type scheme is that if CFO has not been completely compensated, the distribution of the post DFT signals is closer to Gaussian than that when CFO has been completely removed. Consequently, the normalized kurtosis is used as the cost function to measure the non-Gaussianity of the post DFT signals. However, factors such as increased channel frequency selectivity and employing non-CM signaling make the distribution of the post DFT signal closer to Gaussian even if the CFO has been completely compensated, which can consequently degrade the accuracy of kurtosis-type estimation. To show the advantage of our proposed scheme over the kurtosis-type scheme in a frequency selective channel, we expand the kurtosis-type cost function and obtain the following Lemma.

Lemma 2 *If CM signaling is used, the kurtosis-type cost function* $J_2(u) = \sum_{m=0}^{M-1} \sum_{n=0}^{N-1} |y_{m,n}(u)|^4$ *given by [37] can be written as*

$$\begin{aligned} J_2(u) &= A' \cos[2\pi(\varepsilon - u)] + B' \sin[2\pi(\varepsilon - u)] + C' \\ &= A'' \cos[2\pi(\varepsilon - u + \phi)] + C', \end{aligned} \tag{5.8}$$

where A', B', C', A'' *and* ϕ *are constants that depend on the channel and data realization and are not functions of* u. *(See Appendix 5.B for the proof.)*

We observe from the above Lemma that the kurtosis-type cost function does not really achieve its minimum at $u = \varepsilon$. Actually the minimum can be achieved at

$u = \varepsilon$ only when M is very large such that B' in the first line of (5.8) can be approximated by zero as shown in the proof in [37]. Unfortunately, when M takes on small values, B' may be significant which shifts the minimum of the cost function from the true CFO. In contrast, our proposed cost function defined by (5.5) is in the form of the subtraction of two terms, which intrinsically can alleviate the amplitude of $\sin[2\pi(\varepsilon - u)]$ so that it can be ignored from the expanded cost function in (5.6) for any value of M as long as the assumption in (5.3) is satisfied.

5.4 MIMO-OFDM Systems

In this section, we extend the proposed scheme to MIMO-OFDM systems. Consider a MIMO-OFDM system with N_t transmit and N_r receive antennas employing an OSTBC with T symbol durations in each block. We assume that subchannels keep constant over the duration of each block. Let us define the row vector $\mathbf{h}_{m,n,j} = [H_{m,n,j,1}\ H_{m,n,j,2}\ \ldots\ H_{m,n,j,N_t}]$, with $m = 1, 2, \ldots, M$, $n = 0, 1, \ldots, N-1$, and $j = 1, 2, \ldots, N_r$, which represents the channel frequency response between the N_t transmit antennas and the jth receive antenna on the nth DFT grid over the mth block duration. Let the $N_t \times T$ matrix $\mathbf{D}_{m,n}$ represent the space-time block coded sequence transmitted over the N_t transmit antennas simultaneously in the mth block duration on the nth subcarrier. The element on its ith row and tth column refers to the symbol transmitted from the ith transmit antenna during the tth symbol slot. Due to the orthogonality of the OSTBC [11] and the CM signaling under consideration, we have $\mathbf{D}_{m,n}\mathbf{D}_{m,n}^H = c\mathbf{I}$, where c is a positive constant. Define the row vector $\mathbf{y}_{m,n,j}(u) \triangleq [y_{m,n,j,1}(u)\ y_{m,n,j,2}(u)\ \ldots\ y_{m,n,j,T}(u)]$, as the DFT outputs on the nth DFT grid of the jth receive antenna over the mth block duration. If CFO has been completely compensated and in the noise-free case we have $\mathbf{y}_{m,n,j}(u|u = \varepsilon) = \mathbf{h}_{m,n,j}\mathbf{D}_{m,n}$.

By taking the norm of $\mathbf{y}_{m,n,j}(u|u=\varepsilon)$, we obtain

$$\begin{aligned}\left\|\mathbf{y}_{m,n,j}(u|u=\varepsilon)\right\|^2 &= \mathbf{y}_{m,n,j}(u|u=\varepsilon)\,\mathbf{y}^H_{m,n,j}(u|u=\varepsilon) \\ &= c\mathbf{h}_{m,n,j}\mathbf{h}^H_{m,n,j} = c\sum_{i=1}^{N_t}\left|H_{m,n,j,i}\right|^2,\end{aligned}$$

where the summation of the squared amplitude of the channel frequency response has been decoupled from the received signal. Consequently, the proposed estimation scheme for MIMO-OFDM systems employing orthogonal space-time coding is

$$\hat{\varepsilon} = \arg\min_{u\in[-0.5\ 0.5)}\sum_{j=1}^{N_r}\sum_{m=0}^{M-1}\sum_{n=0}^{N-1}\left(\left\|\mathbf{y}_{m,n,j}(u)\right\|^2 - \left\|\mathbf{y}_{m,((n+1))_N,j}(u)\right\|^2\right)^2. \tag{5.9}$$

By comparing the cost function in (5.9) with that for the SISO-OFDM in (5.4), we observe that the former cost function is simply the summation of the cost functions corresponding to each single receive antenna. Furthermore, for MIMO systems with multiple transmit antennas using OSTBCs, the squared amplitude of the DFT outputs in the duration of one block of the OSTBC are summed together, as shown in (5.9).

5.5 Simulation Results

In our simulations, we assume CFO ε is uniformly distributed in the range $[-0.5\ 0.5)$. The multipath fading channels and ε are assumed to remain constant during M consecutive OFDM symbols for SISO-OFDM systems, and M consecutive space-time block coded OFDM blocks for MIMO-OFDM systems. Let $h_{\mathrm{PDP}}(D)$ be a polynomial (in D) representing the power delay profile of the discrete-time multipath fading channel. Several frequency selective fading channels with different power delay profiles and delay spreads σ_τ^2 [56] are used in the simulations to illustrate the efficacy of the proposed scheme. They are $h_{\mathrm{PDP}_1}(D) = 0.35 + 0.25D + 0.18D^2 + 0.13D^3 + 0.09D^4$, $h_{\mathrm{PDP}_2}(D) = 0.34+0.28D+0.23D^2+0.11D^6+0.04D^{11}$, and $h_{\mathrm{PDP}_3}(D) = 0.25+0.25D^4+$

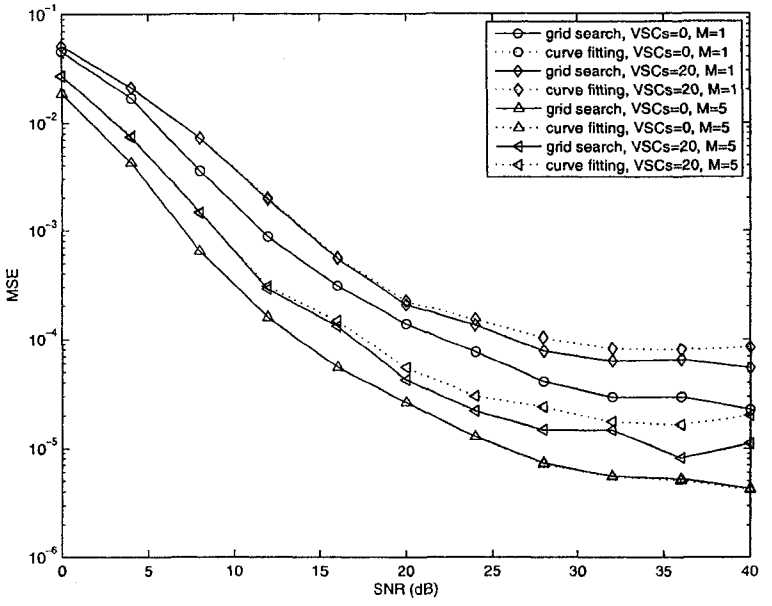

Figure 5.1: Comparison of curve fitting and grid search of the proposed scheme for a 4-PSK SISO-OFDM system with the number of VSCs equal to 0 and 20 respectively.

$0.25D^8 + 0.25D^{12}$, with channel delay spreads $\sigma_\tau^2 = 1.74$, 6.37, and 20 respectively. In calculating σ_τ^2, the path delay has been normalized with respect to the sampling interval. The number of subcarriers is $N = 64$, and the length of CP is $L_{CP} = 16$. The CM signaling used in the simulation is 4-phase-shift keying (4-PSK). The MSE of the CFO estimation is obtained by running 1000 independent Monte-Carlo simulations.

5.5.1 SISO-OFDM Systems

As mentioned above, in the presence of VSCs, the curve fitting approach becomes suboptimal, while using the grid search approach increases the complexity of the scheme. As such, we examine in Fig. 5.1 the degradation suffered by using curve fitting as opposed to grid search. For both cases, the cost function minimized is the one defined by (5.7) where the number of VSCs is set to 0 and 20. The frequency selective channel has $\sigma_\tau^2 = 6.37$. We give the estimation performance for the cases $M = 1$, and 5. We observe from the figure that curve fitting performs as well as

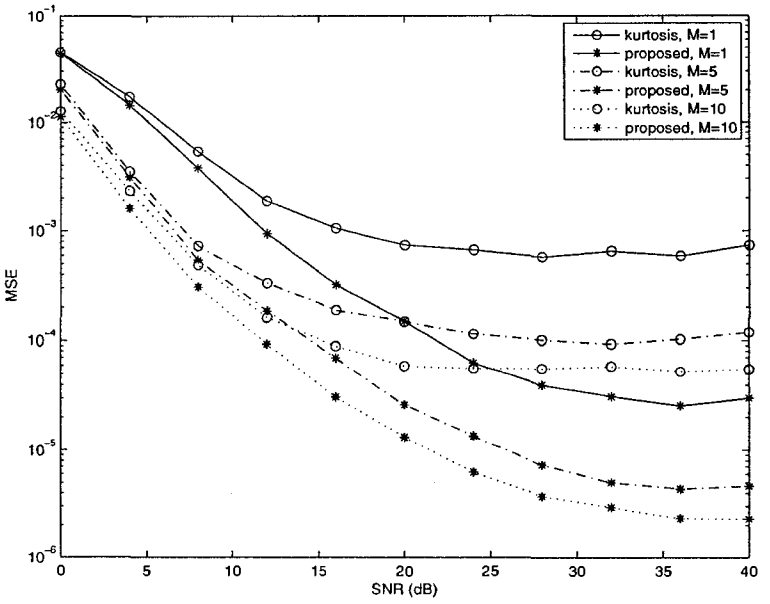

Figure 5.2: Comparison between the proposed scheme and the kurtosis-type scheme for 4-PSK SISO-OFDM with $\sigma_\tau^2 = 6.37$; $M = 1, 5, 10$ symbols.

grid search with a slight degradation in the presence of a large number of VSCs. Therefore, we use curve fitting and assume the fully loaded OFDM systems without the presence of the VSCs for the rest of the simulations when the proposed scheme is used.

In Fig. 5.2, we compare the proposed scheme with the kurtosis-type scheme over a frequency selective fading channel with $\sigma_\tau^2 = 6.37$. The two schemes are compared for $M = 1$, 5, and 10 symbols. We observe from the figure that the proposed scheme significantly outperforms the kurtosis-type scheme. In terms of complexity, both schemes have somewhat the same complexity.

In Fig. 5.3, we compare the performance of the proposed scheme with that of the kurtosis-type scheme and the CM-based subspace scheme over three types of frequency selective fading channels, namely, $\sigma_\tau^2 = 1.74$, 6.37 and 20. We use $M = 5$ symbols for the estimation. We observe that the proposed scheme performs better than the kurtosis-type scheme even over severe frequency selective fading channels.

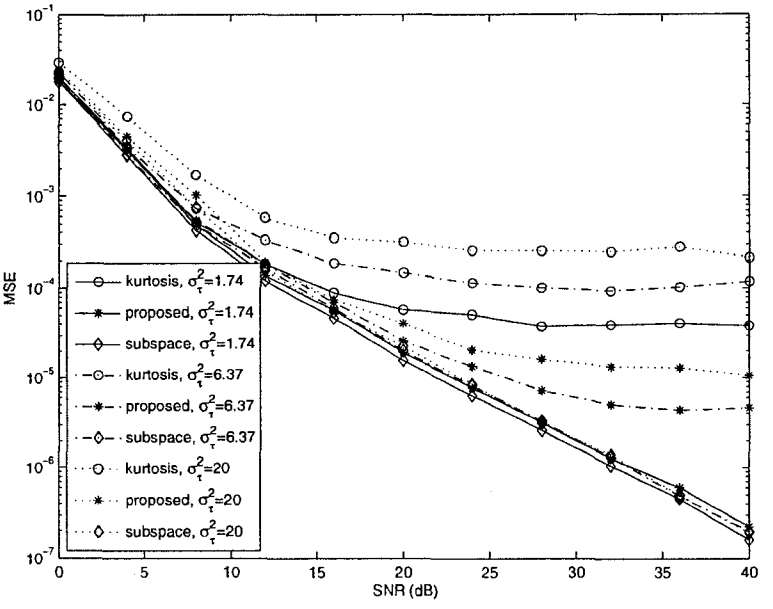

Figure 5.3: Comparison between the proposed scheme, the kurtosis-type scheme and the CM-based subspace scheme for 4-PSK SISO-OFDM with $\sigma_\tau^2 = 1.74$, 6.37, and 20; $M = 5$ symbols.

But it performs a little worse than the CM-based subspace scheme for large values of σ_τ^2, which is attributed to the fact that with the increased channel frequency selectivity the assumption in (5.3) is slightly violated. As far as complexity is concerned, by comparing the proposed scheme to the CM-based subspace scheme, the proposed estimation scheme is much simpler because the curve fitting involves evaluating the cost function at only three candidate CFOs, whereas the CM-based subspace scheme requires the gradient descent method in which the number of iterations depends on the channel and data realization. Furthermore, in evaluating the cost function at each candidate CFO, an $N \times N$ projection matrix has to be multiplied with the squared amplitude of the post DFT signals for the CM-based subspace scheme. However, for the proposed scheme shown in (5.4), the computational complexity is obviously much less than that.

In Fig. 5.4, we plot the BER performance of a SISO-OFDM system with $\sigma_\tau^2 = 6.37$

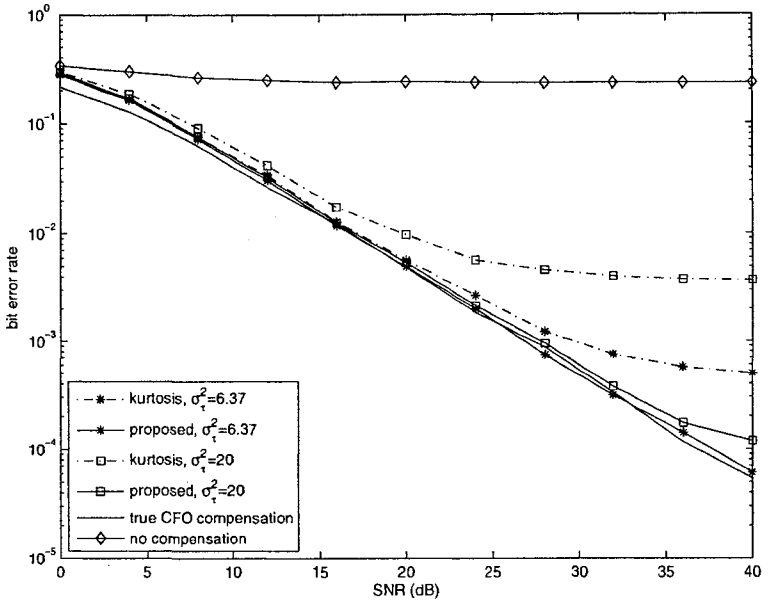

Figure 5.4: Comparison of bit error rate performance of 4-PSK SISO-OFDM by using the proposed scheme and the kurtosis-type scheme for CFO estimation respectively with $M = 1$.

and 20 and with CFO ε that is uniformly distributed in the range $[-0.5\ 0.5)$. The received signal is first compensated with the CFO estimated by using the kurtosis-type scheme and the proposed scheme respectively at the fine CFO estimation and compensation stage. For both schemes, one OFDM symbol is used for the CFO estimation. We assume that the integer part of the CFO (introduced by the CFO estimation error at the fine CFO estimation stage) can be completely compensated at the following coarse CFO estimation and compensation stage. We also assume that the receiver has perfect knowledge of the channel fading coefficients for symbol detection. The BER performance obtained with no CFO compensation and with the true CFO compensation are also included in the figure for comparison. We can see from the figure the superiority of the proposed scheme over the kurtosis-type scheme, which suggests that improvements in the CFO estimation translate to improvements in the BER performance.

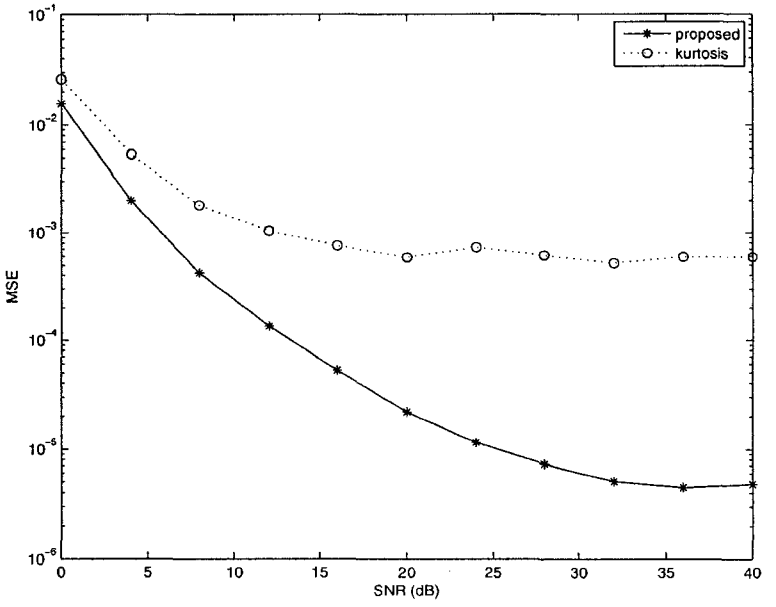

Figure 5.5: Comparison between the proposed scheme and the kurtosis-type scheme for 4-PSK MIMO-OFDM system with Alamouti scheme, $N_r = 1$, $\sigma_\tau^2 = 6.37$, $M = 5$ blocks.

5.5.2 MIMO-OFDM Systems

In Fig. 5.5, we compare the proposed scheme with the kurtosis-type scheme for a MIMO-OFDM system employing Alamouti scheme with one receive antenna over a frequency selective fading channel with $\sigma_\tau^2 = 6.37$. The number of space-time block coded OFDM blocks used in estimation is set to $M = 5$ blocks (i.e., 10 OFDM symbols). We observe from the figure that the proposed scheme performs much better than the kurtosis-type scheme since it has the capability of exploiting the orthogonal structure of the OSTBC. We remark that the performance of the kurtosis-type scheme can be improved by modifying it to exploit the orthogonality of the OSTBC. However, the resulting performance is still much inferior to that of the proposed one.

5.6 Conclusions

In this chapter, we have proposed a low-complexity blind CFO estimation scheme for SISO- and MIMO-OFDM systems with CM signaling. We proved the identifiability of the proposed scheme. We have shown that the proposed scheme offers an excellent performance-complexity trade-off as compared to existing estimation schemes.

5.A Proof of Lemma 1

We shall now prove Lemma 1. In the development of this proof, we consider the noise-free case in (5.1). We also consider the case $M = 1$. As such, we remove the index of m from the notation, i.e., d_k denotes $d_{m,k}$. The proof for the case $M > 1$ follows immediately from the proof for the $M = 1$ case. We also remove the parameter u for simplicity, i.e., y_n denotes $y_{m,n}(u)$.

From (5.2), we have $y_n = \frac{1}{N}\sum_{k=0}^{N-1}\tilde{y}_k \sum_{p=0}^{N-1} e^{j2\pi\frac{(\tilde{\varepsilon}+k-n)p}{N}}$, where $\tilde{y}_k \triangleq H_k d_k$ and $\tilde{\varepsilon} \triangleq \varepsilon - u$. Then it is easy to show that

$$\sum_{n=0}^{N-1}|y_n|^4 = \frac{2}{N^3}\mathrm{Re}\left\{e^{-j2\pi\tilde{\varepsilon}}\sum_{k_1,k_2,l_1,l_2=0}^{N-1}\tilde{y}_{k_1}\tilde{y}^*_{k_2}\tilde{y}_{l_1}\tilde{y}^*_{l_2} \times\sum_{p_1=0}^{N-1}\sum_{p_2=p_1+1}^{N-1}\sum_{q_1=0}^{p_2-p_1-1} e^{j2\pi\frac{(k_1-l_2)p_1}{N}}e^{-j2\pi\frac{(k_2-l_2)p_2}{N}}e^{j2\pi\frac{(l_1-l_2)q_1}{N}}\right\}+C_1, \tag{5.10}$$

where C_1 is a real constant which is not a function of $\tilde{\varepsilon}$.

Now define $\Omega \triangleq \{k_1,k_2,l_1,l_2\}$, $\Omega_1 \triangleq \{k_1,k_2,l_1,l_2\,|k_1=k_2 \text{ or } l_1=l_2\}$, and $\Omega_2 \triangleq \{k_1, k_2, l_1, l_2 \mid k_1 \neq k_2 \text{ and } l_1 \neq l_2\}$, with $k_1,k_2,l_1,l_2 \in \{0,1,\ldots,N-1\}$. We have $\Omega = \Omega_1 \cup \Omega_2$ and $\Omega_1 \cap \Omega_2 = \varnothing$. Then (5.10) can be represented as

$$\sum_{n=0}^{N-1}|y_n|^4 = \frac{2}{N^3}\mathrm{Re}\left\{e^{-j2\pi\tilde{\varepsilon}}B_{\Omega_1}\right\}+\frac{2}{N^3}\mathrm{Re}\left\{e^{-j2\pi\tilde{\varepsilon}}B_{\Omega_2}\right\}+C_1, \tag{5.11}$$

where B_Ψ, with $\Psi = \Omega_1$ or Ω_2, is defined as

$$B_\Psi \triangleq \sum_{\substack{k_1,k_2,l_1,l_2=0 \\ k_1,k_2,l_1,l_2\in\Psi}}^{N-1} \tilde{y}_{k_1}\tilde{y}^*_{k_2}\tilde{y}_{l_1}\tilde{y}^*_{l_2} \sum_{p_1=0}^{N-1}\sum_{p_2=p_1+1}^{N-1}\sum_{q_1=0}^{p_2-p_1-1} e^{j2\pi\frac{(k_1-l_2)p_1}{N}} e^{-j2\pi\frac{(k_2-l_2)p_2}{N}} e^{j2\pi\frac{(l_1-l_2)q_1}{N}}. \tag{5.12}$$

Similarly, we can obtain

$$\sum_{n=0}^{N-1} |y_n|^2 \left|y_{((n+1))_N}\right|^2 = \frac{2}{N^3}\mathrm{Re}\left\{e^{-j2\pi\tilde{\varepsilon}}D_{\Omega_1}\right\} + \frac{2}{N^3}\mathrm{Re}\left\{e^{-j2\pi\tilde{\varepsilon}}D_{\Omega_2}\right\} + C_2,$$

where C_2 is a real constant which is not a function of $\tilde{\varepsilon}$, and D_Ψ, with $\Psi = \Omega_1$ or Ω_2, is defined as

$$D_\Psi \triangleq \sum_{\substack{k_1,k_2,l_1,l_2=0 \\ k_1,k_2,l_1,l_2\in\Psi}}^{N-1} \tilde{y}_{k_1}\tilde{y}^*_{k_2}\tilde{y}_{l_1}\tilde{y}^*_{l_2} \sum_{p_1=0}^{N-1}\sum_{p_2=p_1+1}^{N-1}\sum_{q_1=0}^{p_2-p_1-1} e^{j2\pi\frac{(k_1-l_2+1)p_1}{N}} e^{-j2\pi\frac{(k_2-l_2+1)p_2}{N}} e^{j2\pi\frac{(l_1-l_2)q_1}{N}}. \tag{5.13}$$

Next we will show that $B_{\Omega_1} \approx D_{\Omega_1}$ under the reasonable assumption in (5.3). Let us define $\Omega_3 \triangleq \{k_1,k_2,l_1,l_2\,|k_1 \neq k_2 \text{ and } l_1 = l_2\}$, $\Omega_4 \triangleq \{k_1,k_2,l_1,l_2\,|k_1 = k_2 \text{ and } l_1 \neq l_2\}$, and $\Omega_5 \triangleq \{k_1,k_2,l_1,l_2|k_1 = k_2 \text{ and } l_1 = l_2\}$, where $\Omega_1 = \Omega_3 \cup \Omega_4 \cup \Omega_5$, $\Omega_3 \cap \Omega_4 = \varnothing$, $\Omega_4 \cap \Omega_5 = \varnothing$, and $\Omega_3 \cap \Omega_5 = \varnothing$. Then we have $B_{\Omega_1} = B_{\Omega_3} + B_{\Omega_4} + B_{\Omega_5}$ and $D_{\Omega_1} = D_{\Omega_3} + D_{\Omega_4} + D_{\Omega_5}$, where B_{Ω_3}, B_{Ω_4} and B_{Ω_5} are defined in (5.12), and D_{Ω_3}, D_{Ω_4} and D_{Ω_5} are defined in (5.13).

Denoting $v_1 = ((l_1-1))_N$ and $v_2 = ((l_2-1))_N$, we have

$$\begin{aligned}
& D_{\Omega_3} \\
= & \sum_{\substack{k_1,k_2,v_1,v_2=0 \\ k_1,k_2,((v_1+1))_N,((v_2+1))_N\in\Omega_3}}^{N-1} \tilde{y}_{k_1}\tilde{y}^*_{k_2}\tilde{y}_{((v_1+1))_N}\tilde{y}^*_{((v_2+1))_N} \\
& \sum_{p_1=0}^{N-1}\sum_{p_2=p_1+1}^{N-1}\sum_{q_1=0}^{p_2-p_1-1} e^{j2\pi\frac{(k_1-v_2)p_1}{N}} e^{-j2\pi\frac{(k_2-v_2)p_2}{N}} e^{j2\pi\frac{(v_1-v_2)q_1}{N}} \\
\approx & \sum_{\substack{k_1,k_2,v_1,v_2=0 \\ k_1,k_2,v_1,v_2\in\Omega_3}}^{N-1} \tilde{y}_{k_1}\tilde{y}^*_{k_2}\tilde{y}_{v_1}\tilde{y}^*_{v_2} \sum_{p_1=0}^{N-1}\sum_{p_2=p_1+1}^{N-1}\sum_{q_1=0}^{p_2-p_1-1} e^{j2\pi\frac{(k_1-v_2)p_1}{N}} e^{-j2\pi\frac{(k_2-v_2)p_2}{N}} e^{j2\pi\frac{(v_1-v_2)q_1}{N}},
\end{aligned}$$

where the last line is obtained from the fact that if $k_1, k_2, ((v_1+1))_N, ((v_2+1))_N \in \Omega_3$ then $k_1, k_2, v_1, v_2 \in \Omega_3$ and the approximation comes from the assumption in (5.3). So we have shown that $D_{\Omega_3} \approx B_{\Omega_3}$. Similarly, it is easy to show that $D_{\Omega_4} \approx B_{\Omega_4}$ and $D_{\Omega_5} \approx B_{\Omega_5}$ under the assumption in (5.3). Consequently, we have $\sum_{n=0}^{N-1} |y_n|^4 - \sum_{n=0}^{N-1} |y_n|^2 \left|y_{((n+1))_N}\right|^2 \approx \frac{2}{N^3} \mathrm{Re}\left\{e^{-j2\pi\tilde{\varepsilon}} (B_{\Omega_2} - D_{\Omega_2})\right\} + C$, where $C = C_1 - C_2$. It is straight forward to show that B_{Ω_2} and D_{Ω_2} take on real values, and $B_{\Omega_2} - D_{\Omega_2} < 0$. This proves Lemma 1.

5.B Proof of Lemma 2

Now we prove Lemma 2. As for the kurtosis-type cost function in (5.11), it is easy to show that B_{Ω_2} is a real negative value. However, B_{Ω_1} can be a complex value, which makes the kurtosis-type cost function in the form $\sum_{n=0}^{N-1} |y_n|^4 = A' \cos(2\pi\tilde{\varepsilon}) + B' \sin(2\pi\tilde{\varepsilon}) + C'$, where A', B' and C' are constants that depend on the channel and data realization and are not functions of u. This proves Lemma 2.

Chapter 6

A Finite Alphabet Based CFO Estimator for Differential OFDM Systems

6.1 Introduction

CFO estimation schemes can be classified into two groups. In the first group, the CFO estimation is accomplished in one stage while in the second group the CFO estimation is accomplished in two stages. Schemes in [21], [24], [28] and [29] belong to the first group. A problem associated with this group of schemes is that they have to minimize their cost functions over the entire CFO range. In the case when the CFO is expected to be in a large range, in minimizing their cost functions, the exhaustive grid search method could be very time consuming, or alternatively, the gradient descent method may end up with a local minimum instead of a global minimum as the cost functions are in general not convex over the entire range. To deal with the large estimation range at an affordable complexity, another group of CFO estimation schemes which consist of two stages are usually preferred. In the first stage, the fractional part of the CFO (FFO) is estimated and compensated [30], [37], [57], [58]. Then, in the second stage, the integer part of CFO (IFO) is estimated [60]−[62]. The focus of this chapter

is on the FFO estimation.

Like single-carrier systems, OFDM systems can also employ differential modulation, especially in situations where channel estimation becomes impossible. Consequently, symbols can be detected without channel knowledge and the receiver complexity can be reduced. A time domain differentially modulated OFDM (DOFDM) system is adopted by the European digital audio broadcasting (DAB) standard [1]. Like OFDM systems, DOFDM systems are also sensitive to CFO. Therefore, in [58] and [59], a novel blind FFO estimation scheme is proposed in particular for DOFDM systems by exploiting the finite alphabet (FA) property of the transmitted signal. We notice that in their data model the impact of the accumulated phase rotation introduced by CFO is excluded from consideration. However, as their proposed cost function relies on comparing the phase difference between the two consecutive OFDM symbols on the same subcarrier, the accumulated phase rotation should not be ignored. With this phase rotation included into the data model, their cost function actually does not give a minimum at the true FFO and in turn could not give an accurate estimation.

Therefore, in this chapter, like that in [58], by exploiting the two implicit properties associated with the DOFDM systems again, i.e., the channel keeps constant over two consecutive OFDM symbols, and the employed M-ary phase-shift keying (M-PSK) constellation has a finite alphabet size, we propose a blind FA based FFO estimator that relies on only two consecutive OFDM symbols [63]. Different from that in [58], we use a differentiation in the frequency domain to bypass the accumulated phase rotation introduced by CFO in designing the cost function.

The proposed FA based cost function is shown to be periodic even in systems having VSCs. Therefore, the proposed FA based scheme can be applied to both systems with and without VSCs, whereas some of the existing FFO estimators, e.g., the CM based subspace FFO estimator in [30] can not be applied to the former scenario. As the proposed FA based cost function is in a somewhat complicated form, to find the minimum of it via the grid search method is almost prohibited.

Therefore, we present the modified Newton method which can obtain the minimum of the cost function more efficiently. In [57], a CRLB for blind CFO estimation problem is derived. However, this CRLB is more suitable for blind CFO estimation based on a large number of OFDM symbols. Therefore, we derive the constrained CRLB [65] and use it as a bench mark in assessing the performance of the proposed FA based scheme.

The simulation results show that the modified Newton method works well with the FA based cost function. We compare the FA based scheme with a scheme that only exploits the CM constraint of the M-PSK constellation. The FA based scheme is more complicated but it can achieve a better performance at high SNRs by exploiting more side information of the M-PSK constellation. The FA based scheme also outperforms the CM based subspace scheme in [30] at high SNRs, which has been shown to have a superior performance over several other schemes.

We also note here that the proposed FA based scheme is designed for single transmit antenna systems. Its idea can not be applied to MIMO-OFDM systems employing differential space-time coding. It would be an interesting topic to design blind CFO estimation scheme for such systems in our future research work.

The rest of the chapter is organized as follows. In Section 6.2, we describe the system model. In Section 6.3, we propose a FA based cost function for FFO estimation. In Section 6.4, the modified Newton method is presented. In Section 6.5, the constrained CRLB for CFO estimation is derived. Section 6.6 shows the simulation results. Finally, conclusion is made in Section 6.7.

6.2 System Model

We consider a DOFDM system with N subcarriers. The information symbols are differentially modulated along the time direction on each subcarrier. The channel is assumed to keep constant over two consecutive OFDM symbols such that differential detection can be performed at the receiver with the channel information bypassed.

Let us denote the vector of differentially modulated symbols transmitted in the nth OFDM symbol as $\mathbf{s}(n) = [s_0(n), s_1(n), \ldots, s_{N-1}(n)]^T$, where $s_k(n)$ denotes the differentially modulated symbol transmitted on the kth subcarrier. Let $\mathbf{d}(n) = [d_0(n), d_1(n), \ldots, d_{N-1}(n)]^T$ denote the vector of information symbols carried in the nth OFDM symbol, where $d_k(n)$ denotes the information symbol on the kth subcarrier. The information symbol $d_k(n)$ belongs to a M-PSK constellation, i.e., $\mathcal{A} := \{\beta_0, \beta_1, \ldots, \beta_{M-1}\}$ with $\beta_i = e^{j2\pi\frac{i}{M}}$. Then, the differential modulation can be represented as

$$\mathbf{s}(n) = \mathbf{D}(n)\mathbf{s}(n-1),$$

where $\mathbf{D}(n)$ =diag($\mathbf{d}(n)$). In general, OFDM systems usually have a number of VSCs [21] to help with spectrum shaping. So, let us denote the number of VSCs as P and the number of information bearing subcarriers as $M = N - P$. The set of indices of the VSCs is denoted by φ. For any k in φ, we have $s_k(n) = 0$ and $d_k(n) = 0$ for all n.

At the transmitter, the differentially modulated signal is first passed through the IDFT, and then appended with a CP before it is propagated through the multipath fading channel. We denote the equivalent baseband discrete time channel impulse response over the nth OFDM symbol as $h(n,t) = \sum_{l=0}^{L-1} h_l(n)\delta(t-l)$, where L is the length of the channel impulse response in samples and $h_l(n)$ with $l = 0, \ldots, L-1$, are channel coefficients modeled as independent complex Gaussian random variables with zero mean and any normalized power delay profile. The channel frequency response on the kth subcarrier can then be represented as $H_k(n) = \sum_{l=0}^{L-1} h_l(n)e^{-j2\pi\frac{lk}{N}}$. The length of CP which is denoted by L_{CP}, is always assumed to be larger than L such that there is no inter-symbol-interference (ISI). Therefore, the total number of samples in an OFDM symbol including CP is $Q = L_{CP} + N$.

The received signal vector in the time domain with the CP removed can be represented as

$$\mathbf{r}(n) = e^{j\theta}e^{j2\pi\frac{\varepsilon(n-1)Q}{N}}\mathbf{C}(\varepsilon)\mathbf{F}^H\mathbf{H}(n)\mathbf{s}(n) + \mathbf{v}(n), n = 1, 2, \ldots \tag{6.1}$$

where θ denotes the initial phase offset of the first OFDM symbol, and ε is the normalized CFO with respect to the subcarrier interval. The CFO has two parts, i.e., $\varepsilon = \varepsilon_i + \varepsilon_f$. The integer part denoted by ε_i is an integer value, and the fractional part ε_f is within the range $[-0.5, 0.5)$. The diagonal matrix $\mathbf{C}(\varepsilon)$ and $\mathbf{H}(n)$ are defined as $\mathbf{C}(\varepsilon) = \text{diag}([1, e^{j2\pi\frac{\varepsilon}{N}}, \ldots, e^{j2\pi\frac{\varepsilon(N-1)}{N}}])$, and $\mathbf{H}(n) = \text{diag}([H_0(n), H_1(n), \ldots, H_{N-1}(n)])$, respectively. The $N \times N$ DFT matrix $\mathbf{F}$ has its element on the mth row and nth column defined as $\frac{1}{\sqrt{N}} e^{-j2\pi\frac{mn}{N}}$. The noise vector is defined as $\mathbf{v}(n) = [v_0(n), v_1(n), \ldots, v_{N-1}(n)]^T$, where $v_k(n)$ with $k = 0, \ldots, N-1$, are modeled as independent complex Gaussian random variables with zero mean and variance σ_n^2.

6.3 Proposed FFO Estimator

The proposed scheme is inspired by the scheme in [58] but developed for the data model in (6.1) which has a slight difference from that in [58]. We first propose a cost function based on a DOFDM system without VSCs, and then show that this cost function can also be applied directly to systems having VSCs.

As the proposed scheme involves only two consecutive OFDM symbols, i.e., $(n-1)$th and nth, in the rest of this chapter we denote $\mathbf{H}(n-1)$ and $\mathbf{H}(n)$ by $\mathbf{H}$ for simplicity of notation.[1] Let us assume that the received time domain signal $\mathbf{r}(n)$ is first compensated with a FFO candidate $\tilde{\varepsilon} \in [-0.5, 0.5)$. Then, its DFT output can be represented as

$$\begin{aligned} \mathbf{y}(n, \tilde{\varepsilon}) &= \mathbf{F}\mathbf{C}(\tilde{\varepsilon})^H \mathbf{r}(n) \\ &= e^{j\theta} e^{j2\pi\frac{\varepsilon(n-1)Q}{N}} \mathbf{F}\mathbf{C}(\breve{\varepsilon}_f)\mathbf{C}(\varepsilon_i)\mathbf{F}^H \mathbf{H}\mathbf{s}(n) + \mathbf{F}\mathbf{C}(\tilde{\varepsilon})^H \mathbf{v}(n), \end{aligned} \tag{6.2}$$

where $\breve{\varepsilon}_f = \varepsilon_f - \tilde{\varepsilon}$.

Let us denote $y_k(n, \tilde{\varepsilon})$ as the kth element of $\mathbf{y}(n, \tilde{\varepsilon})$. From (6.2), we have that, for

[1] We note that requiring the channel to remain constant at least over two consecutive OFDM symbols is a general requirement for all systems employing differential detection.

$\tilde{\varepsilon} = \varepsilon_f$,

$$y_k(n, \varepsilon_f) = e^{j\theta} e^{j2\pi \frac{\varepsilon(n-1)Q}{N}} H_{((k-\varepsilon_i))_N} s_{((k-\varepsilon_i))_N}(n) + w_k(n), \tag{6.3}$$

where $w_k(n)$ denotes the kth element of $\mathbf{FC}(\varepsilon_f)^H \mathbf{v}(n)$, and $((k-\varepsilon_i))_N$ represents $(k-\varepsilon_i)$ modulo N. It reveals that if ε_f is accurately compensated then DFT outputs do not have any ICI, and the transmitted symbols together with the channel frequency response are cyclically shifted among the DFT outputs due to the presence of the IFO.

We observe from (6.3) that, in the absence of noise,

$$y_{k_1}(n, \varepsilon_f) y^*_{k_2}(n, \varepsilon_f) = H_{((k_1-\varepsilon_i))_N} s_{((k_1-\varepsilon_i))_N}(n) H^*_{((k_2-\varepsilon_i))_N} s^*_{((k_2-\varepsilon_i))_N}(n).$$

Consequently, for $k_1 \neq k_2$, we have

$$y_{k_1}(n, \varepsilon_f) y^*_{k_2}(n, \varepsilon_f) = y_{k_1}(n-1, \varepsilon_f) y^*_{k_2}(n-1, \varepsilon_f) d_{((k_1-\varepsilon_i))_N}(n) d^*_{((k_2-\varepsilon_i))_N}(n).$$

As both $d_{((k_1-\varepsilon_i))_N}(n)$ and $d^*_{((k_2-\varepsilon_i))_N}(n)$ belong to the M-PSK constellation, so does their multiplication denoted by α_{k_1,k_2}. Therefore, heuristically, we can have a cost function for joint estimation of ε_f and detection of α_{k_1,k_2}, that is

$$J_{k_1,k_2}(\tilde{\varepsilon}, \tilde{\alpha}_{k_1,k_2}) = |y_{k_1}(n, \tilde{\varepsilon}) y^*_{k_2}(n, \tilde{\varepsilon}) - \tilde{\alpha}_{k_1,k_2} y_{k_1}(n-1, \tilde{\varepsilon}) y^*_{k_2}(n-1, \tilde{\varepsilon})|^2. \tag{6.4}$$

This is because in the absence of noise, we have $J_{k_1,k_2}(\tilde{\varepsilon}, \tilde{\alpha}_{k_1,k_2}) = 0$ at $\tilde{\varepsilon} = \varepsilon_f$ and $\tilde{\alpha}_{k_1,k_2} = \alpha_{k_1,k_2}$. Or, alternatively, we can have a FFO estimation represented by minimizing $J_{k_1,k_2}(\tilde{\varepsilon}, \hat{\alpha}_{k_1,k_2}(\tilde{\varepsilon}))$ over $\tilde{\varepsilon} \in [-0.5, 0.5)$, with

$$\hat{\alpha}_{k_1,k_2}(\tilde{\varepsilon}) = \arg \min_{\tilde{\alpha} \in \mathcal{A}} J_{k_1,k_2}(\tilde{\varepsilon}, \tilde{\alpha}). \tag{6.5}$$

By exploiting the frequency diversity of the OFDM system, finally we propose a

cost function for the FFO estimation as

$$J(\tilde{\varepsilon}) = \sum_{k_1=0}^{N-1} \sum_{k_2=k_1+1}^{N-1} J_{k_1,k_2}(\tilde{\varepsilon}, \hat{\alpha}_{k_1,k_2}(\tilde{\varepsilon})). \tag{6.6}$$

The FFO estimation is obtained by $\hat{\varepsilon}_f = \arg \min_{\tilde{\varepsilon} \in [-0.5, 0.5)} J(\tilde{\varepsilon})$.

In light of the above, we make the following remarks.

1) Above we derive a cost function based on a system without VSCs. Actually, the cost function in (6.6) can be applied directly to DOFDM systems having VSCs. This is supported by two facts. Firstly, in the absence of noise, all of the terms in the summation of (6.6) have a minimum at $\tilde{\varepsilon} = \varepsilon_f$. For example, by assuming $\tilde{\varepsilon} = \varepsilon_f$, let us consider those terms that have either $((k_1 - \varepsilon_i))_N$ or $((k_2 - \varepsilon_i))_N$ as a VSC, or have both of them as VSCs. For such terms, we have $J_{k_1,k_2}(\varepsilon_f, \hat{\alpha}_{k_1,k_2}(\varepsilon_f)) = 0$ where $\hat{\alpha}_{k_1,k_2}(\varepsilon_f)$ can take any value in $\mathcal{A}$.

Secondly, the cost function $J(\tilde{\varepsilon})$ in (6.6) is periodic with a period of 1, such that $J(\tilde{\varepsilon} + m) = J(\tilde{\varepsilon})$ holds for any integer $m \in [0, N)$ and $\tilde{\varepsilon} \in [-0.5, 0.5)$. This property also holds for DOFDM systems having VSCs and its proof is shown in Appendix 6.A.

The reason we emphasize the application of the proposed scheme as a FFO estimator to DOFDM systems having VSCs is that some of the existing blind FFO estimation methods are developed for systems without VSCs and can not be applied to systems having VSCs, e.g., the CM based subspace scheme in [30]. In general, VSCs are always present in OFDM systems as specified in several standards. Therefore, from this point of view, the proposed FA based FFO estimator has a wider application compared with those schemes.

2) From (6.3), we can also obtain a CM based cost function for FFO estimation by exploiting the fact that the channel keeps constant over two consecutive OFDM symbols. It is given by [55]

$$J_{CM}(\tilde{\varepsilon}) = \sum_{k=0}^{N-1} (|y_k(n, \tilde{\varepsilon})|^2 - |y_k(n-1, \tilde{\varepsilon})|^2)^2. \tag{6.7}$$

Compared to the above CM based cost function, we notice that the FA based cost function exploits more side information of the M-PSK constellation. Accordingly, the computation of the FA based cost function is more demanding than that of the CM based cost function due to two factors. Firstly, the FA based cost function consists of $\mathcal{O}(N^2)$ terms while the CM based cost function only has N terms. Secondly, a symbol detection process is actually carried out implicitly within the FA based FFO estimation which indicates that the complexity of the FA based scheme increases with the constellation size. However, we will show via simulations that, compared with this CM based scheme, the FA based scheme can achieve an additional performance improvement at high SNRs in exchange for the increased computational complexity.

3) The proposed scheme is designed for and limited to DOFDM systems. That is, it can not be applied to regular OFDM systems. Also, it is limited to M-PSK modulation. Furthermore, the proposed scheme uses two OFDM symbols for CFO estimation, whereas the schemes in [21] and [28]−[30] use only one OFDM symbol. We note here that the channel is expected to remain somewhat constant over two consecutive OFDM symbols, which is also a requirement for systems employing any of the schemes in [21] and [28]−[30] in conjunction with differential detection.

6.4 Newton Method

In minimizing the cost function in (6.6), we use the Newton method as an alternative to the grid search to reduce the computational complexity. The gradient and Hessian of the cost function can be obtained as

$$J'(\tilde{\varepsilon}) = \sum_{k_1=0}^{N-1} \sum_{k_2=k_1+1}^{N-1} \frac{d}{d\tilde{\varepsilon}} J_{k_1,k_2}(\tilde{\varepsilon}, \hat{\alpha}_{k_1,k_2}(\tilde{\varepsilon})),$$

and

$$J''(\tilde{\varepsilon}) = \sum_{k_1=0}^{N-1} \sum_{k_2=k_1+1}^{N-1} \frac{d^2}{d\tilde{\varepsilon}^2} J_{k_1,k_2}(\tilde{\varepsilon}, \hat{\alpha}_{k_1,k_2}(\tilde{\varepsilon})),$$

with $\frac{d}{d\tilde{\varepsilon}} J_{k_1,k_2}(\tilde{\varepsilon}, \hat{\alpha}_{k_1,k_2}(\tilde{\varepsilon}))$ and $\frac{d^2}{d\tilde{\varepsilon}^2} J_{k_1,k_2}(\tilde{\varepsilon}, \hat{\alpha}_{k_1,k_2}(\tilde{\varepsilon}))$ given in the Appendix 6.B. The modified Newton method [64, pp. 114] is repeated over here for completeness.

As the modified Newton method is efficient when the initial point is near the actual minimum, we select two points that are separated apart by 0.5, e.g., $\varepsilon^{(0)} = -0.25$ and 0.25, and evaluate the cost function at these two points respectively and choose the point with a smaller cost value as the initial. After setting the initial, the Newton iteration is repeated. Let $0 < \alpha < 1$ be a given constant. In our simulation, we set $\alpha = 0.5$. At the ith iteration, $i = 0, 1, 2, \ldots$, compute $J''(\varepsilon^{(i)})$. If $J''(\varepsilon^{(i)}) > 0$, proceed as in case I; otherwise, proceed as in case III.

Case I: Compute $\varepsilon^{(i+1)} = \varepsilon^{(i)} - J''(\varepsilon^{(i)})^{-1} J'(\varepsilon^{(i)})$. If $\varepsilon^{(i+1)} \notin [\varepsilon^{(i)} - 0.5, \varepsilon^{(i)} + 0.5)$ and/or $J(\varepsilon^{(i+1)}) > J(\varepsilon^{(i)}) - \frac{1}{2}\alpha J'(\varepsilon^{(i)})^2 J''(\varepsilon^{(i)})^{-1}$, then proceed as in case II; otherwise, check the stopping criterion.

Case II: Define $\varepsilon^{(i+1)}(m) = \varepsilon^{(i)} - J'(\varepsilon^{(i)}) 2^{-m}$. Find the smallest integer $m(i)$ from $m = 0, 1, \ldots$ such that $\varepsilon^{(i+1)}(m) \in [\varepsilon^{(i)} - 0.5, \varepsilon^{(i)} + 0.5)$ and $J(\varepsilon^{(i+1)}(m)) - J(\varepsilon^{(i)}) < -2^{-m}\alpha J'(\varepsilon^{(i)})^2$. Set $\varepsilon^{(i+1)} = \varepsilon^{(i+1)}(m(i))$ and check the stopping criterion.

Case III: Set $\delta^{(i)} = -1$ if $J'(\varepsilon^{(i)}) \geq 0$, and $\delta^{(i)} = +1$ if $J'(\varepsilon^{(i)}) < 0$. Define $\varepsilon^{(i+1)}(m) = \varepsilon^{(i)} - 2^{-m} J'(\varepsilon^{(i)}) + \delta^{(i)} 2^{-m/2}$. Find $m(i)$, the smallest integer from $m = 0, 1, \ldots$, such that $\varepsilon^{(i+1)}(m) \in [\varepsilon^{(i)} - 0.5, \varepsilon^{(i)} + 0.5)$ and $J(\varepsilon^{(i+1)}(m)) - J(\varepsilon^{(i)}) < \alpha[-2^{-m} J'(\varepsilon^{(i)})^2 + 2^{-m-1} J''(\varepsilon^{(i)})]$. Set $\varepsilon^{(i+1)} = \varepsilon^{(i+1)}(m(i))$ and check the stopping criterion.

We use a relative-change stopping criterion, that is if $|\varepsilon^{(i+1)} - \varepsilon^{(i)}| < 0.001$ is satisfied, then the iteration process is terminated and the fractional part of $\varepsilon^{(i+1)}$ is accepted as a FFO estimation; otherwise, continue to the next iteration.

6.5 Constrained CRLB Derivation

In our underlying estimation problem, the observation vectors are $\mathbf{r}(n-1)$ and $\mathbf{r}(n)$. By defining $\mathbf{x}(n-1) = e^{j\theta}e^{j2\pi\frac{\varepsilon(n-2)Q}{N}}\mathbf{H}\mathbf{s}(n-1)$, the observation vectors can be represented as

$$\mathbf{r}(n-1) = \mathbf{C}(\varepsilon)\breve{\mathbf{F}}^H\breve{\mathbf{x}}(n-1) + \mathbf{v}(n-1),$$

and

$$\mathbf{r}(n) = e^{j2\pi\frac{\varepsilon Q}{N}}\mathbf{C}(\varepsilon)\breve{\mathbf{F}}^H\breve{\mathbf{D}}(n)\breve{\mathbf{x}}(n-1) + \mathbf{v}(n),$$

where $\breve{\mathbf{x}}(n-1)$, $\breve{\mathbf{d}}(n)$, and $\breve{\mathbf{F}}$ are matrices obtained by removing those rows with the indices in the set φ from $\mathbf{x}(n-1)$, $\mathbf{d}(n)$, and $\mathbf{F}$, respectively, and $\breve{\mathbf{D}}(n)$ =diag($\breve{\mathbf{d}}(n)$).

The unknown deterministic parameters are ε, $\breve{\mathbf{x}}(n-1)$ and $\breve{\mathbf{d}}(n)$. As each element of $\breve{\mathbf{d}}(n)$ takes discrete value in a M-PSK constellation, the regular CRLB, which can only be applied to the estimation problem with continuous unknown parameters, does not make sense. So, we use the constrained CRLB formulation presented in [65]. The constrained CRLB with a FA constraint can be obtained by treating the symbols as if they were known prior [66]. Therefore, in the next, we derive the CRLB of ε, by assuming that $\breve{\mathbf{d}}(n)$ is known already.

Let us define the observation vector as $\mathbf{r} = [\mathbf{r}(n-1)^T\ \mathbf{r}(n)^T]^T$ and the vector of unknown deterministic parameters as $\Theta = [\varepsilon, \bar{\mathbf{x}}^T, \tilde{\mathbf{x}}^T]^T$, where $\bar{\mathbf{x}}$ and $\tilde{\mathbf{x}}$ denote the real and imaginary part of $\breve{\mathbf{x}}(n-1)$, respectively. Then, the likelihood function of $\mathbf{r}$ conditioned on Θ is given by

$$\begin{aligned} f(\mathbf{r}|\Theta) \;=\; & \frac{1}{(\pi\sigma_n^2)^{2N}}\exp\left[-\frac{1}{\sigma_n^2}\left(\|\mathbf{r}(n-1) - \mathbf{C}(\varepsilon)\breve{\mathbf{F}}^H\,\breve{\mathbf{x}}(n-1)\|^2\right.\right. \\ & \left.\left. + \|\mathbf{r}(n) - e^{j2\pi\frac{\varepsilon Q}{N}}\mathbf{C}(\varepsilon)\breve{\mathbf{F}}^H\breve{\mathbf{D}}(n)\,\breve{\mathbf{x}}(n-1)\|^2\right)\right]. \end{aligned}$$

Then the Fisher information matrix (FIM) can be obtained as

$$\begin{aligned}\text{FIM} &= E\left\{\left[\frac{\partial \ln f(\mathbf{r}|\Theta)}{\partial \Theta}\right]\left[\frac{\partial \ln f(\mathbf{r}|\Theta)}{\partial \Theta}\right]^T\right\} \\ &= \frac{2}{\sigma_n^2}\begin{bmatrix} \frac{4\pi^2}{N^2}a & \frac{2\pi}{N}\text{Im}\{\mathbf{b}^H\} & \frac{2\pi}{N}\text{Re}\{\mathbf{b}^H\} \\ \frac{2\pi}{N}\text{Im}\{\mathbf{b}^*\} & 2\mathbf{I}_M & \mathbf{0}_{M\times M} \\ \frac{2\pi}{N}\text{Re}\{\mathbf{b}^*\} & \mathbf{0}_{M\times M} & 2\mathbf{I}_M \end{bmatrix},\end{aligned}$$

where

$$a = \|\mathbf{E}_1 \breve{\mathbf{F}}^H \breve{\mathbf{x}}(n-1)\|^2 + \|\mathbf{E}_2 \breve{\mathbf{F}}^H \breve{\mathbf{D}}(n) \breve{\mathbf{x}}(n-1)\|^2,$$

$$\mathbf{b} = \breve{\mathbf{F}}\mathbf{E}_1\breve{\mathbf{F}}^H\breve{\mathbf{x}}(n-1) + \breve{\mathbf{D}}(n)^H\breve{\mathbf{F}}\mathbf{E}_2\breve{\mathbf{F}}^H\breve{\mathbf{D}}(n) \times \breve{\mathbf{x}}(n-1),$$

$\mathbf{E}_1$ =diag($[0, 1, \ldots, N-1]^T$), and $\mathbf{E}_2 = Q\mathbf{I}_N + \mathbf{E}_1$. By using the block matrix inversion lemma, we have

$$\text{CRLB}(\varepsilon) = (\text{FIM}^{-1})_{1,1} = \frac{N^2\sigma_n^2}{8\pi^2}[a - \frac{1}{2}\text{Re}(\mathbf{b}^H\mathbf{b})]^{-1}.$$

6.6 Simulation Results

We consider a DOFDM system with $N = 64$ and $L_{CP} = 16$. There are $P = 12$ VSCs. One VSC is on the direct current (DC) subcarrier. The others are located at the two edges of the spectrum with each side having 6 and 5 VSCs, respectively. The multipath fading channel has an exponential power delay profile with $L = 8$, i.e., $E\{|h_l(n)|^2\} = \frac{1}{\sum_{i=0}^{7}\exp(-i)}\exp(-l)$, $l = 0, 1, ..., 7$. The FFO is estimated by using two consecutive DOFDM symbols during which the fading channel is keeping constant. The MSE and the CRLB are obtained by averaging over 10,000 runs of simulation. The SNR is defined as E_s/σ_n^2 where E_s is the symbol energy on each information bearing subcarrier.

Unless stated otherwise, the CFO is uniformly distributed in the range $[-5, 5]$. Only the fractional part of the CFO is estimated by using our proposed methods.

Due to the periodicity of the cost functions for FFO estimation, we use the modified MSE as a performance measurement, in which the modified squared error is defined as $\mathrm{SE}_{\mathrm{modified}} = \min[(\hat{\varepsilon}_f - \varepsilon_f)^2, (\hat{\varepsilon}_f - \bar{\varepsilon}_f)^2]$, where $\bar{\varepsilon}_f$ is the complement of ε_f given by

$$\bar{\varepsilon}_f = \begin{cases} \varepsilon_f - 1, & \text{if } \varepsilon_f > 0 \\ \varepsilon_f, & \text{if } \varepsilon_f = 0 \\ \varepsilon_f + 1, & \text{if } \varepsilon_f < 0 \end{cases} .$$

The reason for not using regular MSE is that when CFO is in the neighborhood of $m + 0.5$, with integer m, the regular MSE may not be able to provide a correct measurement on the estimation performance. For example, let us assume that in one realization, the CFO is 0.48. The FFO estimation could be -0.49 because of noise. This is an acceptable FFO estimation as after the FFO compensation by using this estimation, not much ICI is left at the DFT outputs. However, the regular squared error is given by $(0.97)^2$, which indicates that it is a rather poor estimation on the contrary.

For the CM based scheme (6.7) and CM based subspace scheme [30] that are used for comparison, the grid search method is used in minimizing their cost functions. In the range $[-0.5, 0.5)$, $1,000$ equally spaced FFO candidates are used to achieve a precision of 10^{-3}

In Fig. 6.1, we compare the modified MSE performance of the FA based scheme with the CM based scheme (6.7) for 2-PSK, 4-PSK and 8-PSK, respectively. We observe that the FA based scheme performs better than the CM based scheme at high SNRs. This is more prominent for 4-PSK and 8-PSK, in which the SNR gain is about 4dB at high SNR.

We also examine the efficiency of the Newton method for the FA based scheme. In Table 6.1, we show the required number of iterations and the number of cost function evaluations at several SNRs. It shows that the complexity decreases as the SNR increases. This is because the cost function is better defined at high SNR, at which the modified Newton method can converge at around 3 or 4 iterations on average.

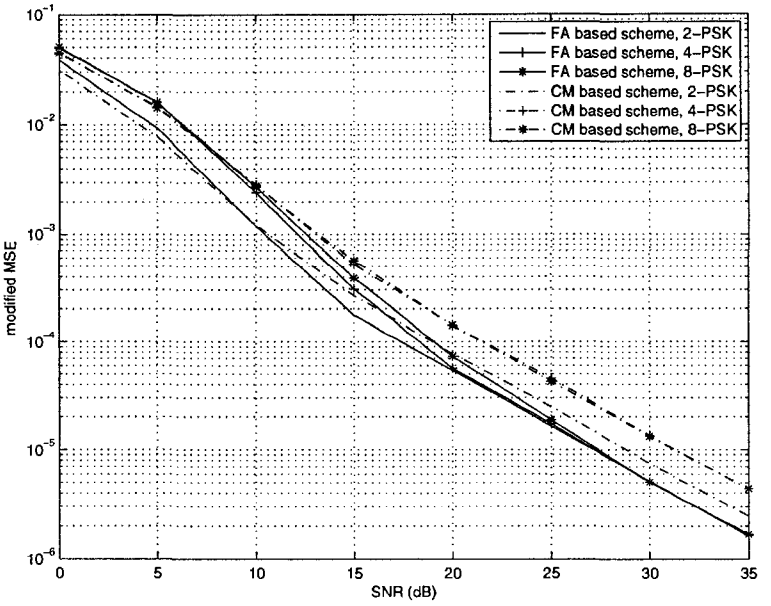

Figure 6.1: Comparison of the modified MSE of the FA based FFO estimator and the CM based FFO estimator for a system with VSCs and $\varepsilon \in$[-5,5].

Table 6.1: Efficiency of the Newton method for the FA based FFO estimator over a system with VSCs and $\varepsilon \in$[-5,5].

complexity	# of iterations		# of cost func. evaluations	
SNR	10dB	25dB	10dB	25dB
2-PSK	3.7	3.0	5.9	5.5
4-PSK	6.8	3.1	8.8	5.1
8-PSK	8.8	4.0	10.8	6.0

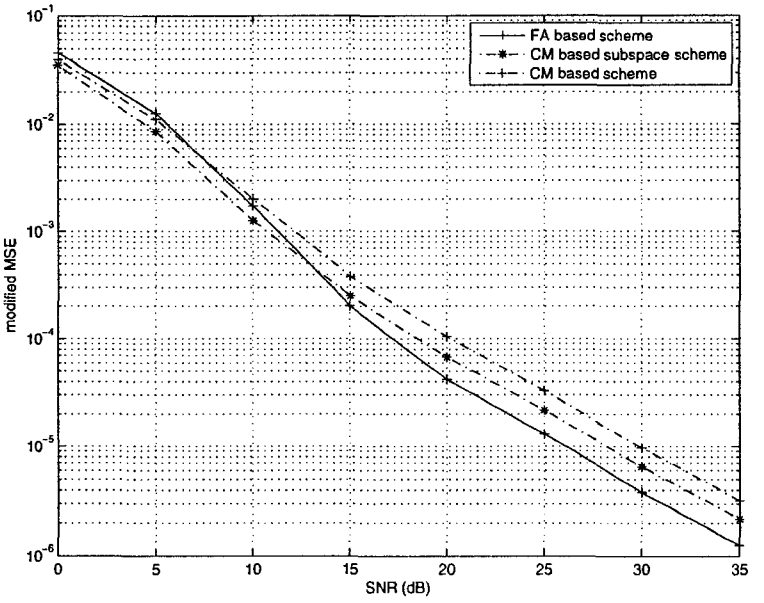

Figure 6.2: Comparison of the modified MSE of the FA based FFO estimator, the CM based FFO estimator and the CM based subspace FFO estimator for a 4-PSK DOFDM systems without VSCs and $\varepsilon \in$[-5,5].

In Fig. 6.2, we compare the modified MSE of the FA based scheme with the CM based scheme and the CM based subspace scheme[30] for a 4-PSK DOFDM system without VSCs. The CM based subspace scheme requires the knowledge of the channel length, which is usually unknown. So, the channel length is assumed to be equal to the length of CP in the estimation process. In [30], the CM based subspace scheme is shown to be superior to several other blind schemes, i.e., VSC method [24], CM method [29], and VSC+CM method [29]. In this figure, we show that the FA based scheme performs a little better than the CM based subspace scheme at high SNRs. However, at low SNRs, it performs a little worse than the CM based subspace scheme. This is because the cost function of the FA based scheme is in the form of comparing two noisy signals. We might say that there is twice as much noise associated with the FA based scheme compared with the CM based subspace scheme.

In Table 6.2, we consider the same system setup as that of Fig. 6.2 and compare

Table 6.2: Comparison of computational complexity of the FA based FFO estimator, CM based FFO estimator, and the CM based subspace FFO estimator for a system without VSCs.

Schemes	10dB	25dB
FA based scheme	1.05s	0.58s
CM based scheme	0.21s	
CM based subsapce scheme	0.27s	

the computational complexity of the three schemes. The complexity is measured by the average time in seconds used for each estimation process performed by computer simulation with Matlab. The proposed scheme uses the Newton method in minimizing its cost function. Its complexity decreases with SNR as shown in Table 6.2. The CM based scheme and the CM based subspace scheme use grid search in minimizing their cost functions. So, their complexity is almost the same at all SNRs. We also observe that, although the Newton method is very efficient, the computational burden of the proposed scheme is still higher than that of the other two schemes due to the complexity of its cost function.

In Fig. 6.3, we examine the regular MSE of the FA based scheme by setting $\varepsilon = 4.32$, and compare it with the constrained CRLB. The modulation scheme is 4-PSK. To show the robustness of the modified Newton method, in each run of the simulation, we randomly select two points that are separated apart by 0.5 in the range $[-0.5, 0.5)$ as the candidates for the initial estimate. As expected, the constrained CRLB is much better than the performance of the FA based scheme as it is actually derived by assuming that the information symbols are known. The performance of the FA based scheme is also compared for systems with or without VSCs. It shows that the presence of the VSCs only degrades the performance slightly.

In Fig. 6.4, we examine regular MSE performance of the FA based scheme and the CM based scheme for a 4-PSK DOFDM system in a time variant channel with $\varepsilon = 4.32$. It is assumed that the fading channel keeps constant within each OFDM symbol but changes slowly from one OFDM symbol to another according to the Jakes'

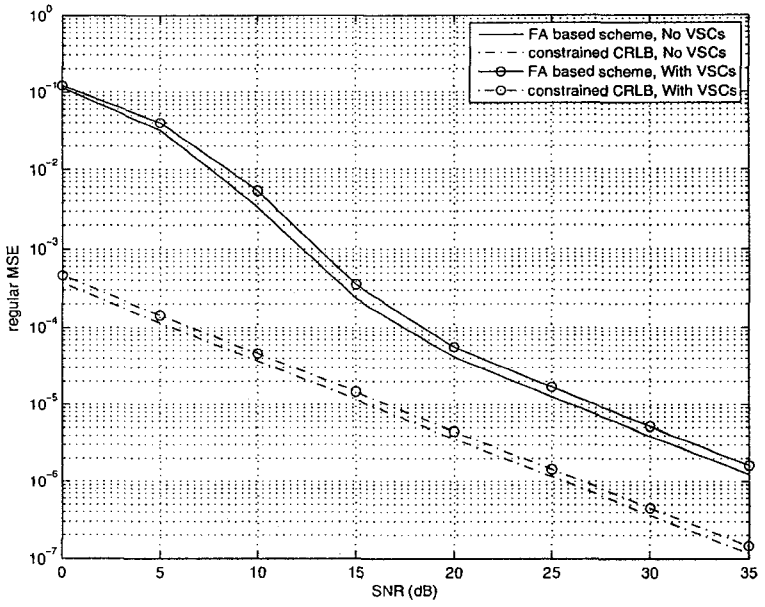

Figure 6.3: Regular MSE performance of the FA based FFO estimator for a 4-PSK DOFDM system with or without VSCs, and $\varepsilon = 4.32$.

fading model [67]. The underlying 64-carrier OFDM system operates at a central carrier frequency of 5GHz with a 1.25MHz total bandwidth. The corresponding time duration of one OFDM symbol including CP is $T = 64\mu s$. The normalized Doppler frequency $f_d T$ is set to 0.003, 0.009, 0.015 and 0.03, which correspond to mobile speeds of 10, 30, 50, and 100km/h, respectively. Comparing the two plots in Fig. 6.4, we observe that the FA based scheme is more sensitive to channel variation than the CM based scheme. The performance of the FA based scheme degrades a little at small Doppler frequencies but shows an error floor at high Doppler frequencies. We remark here that the CM based subspace scheme is insensitive to channel variations since it requires only one OFDM symbol for FFO estimation.

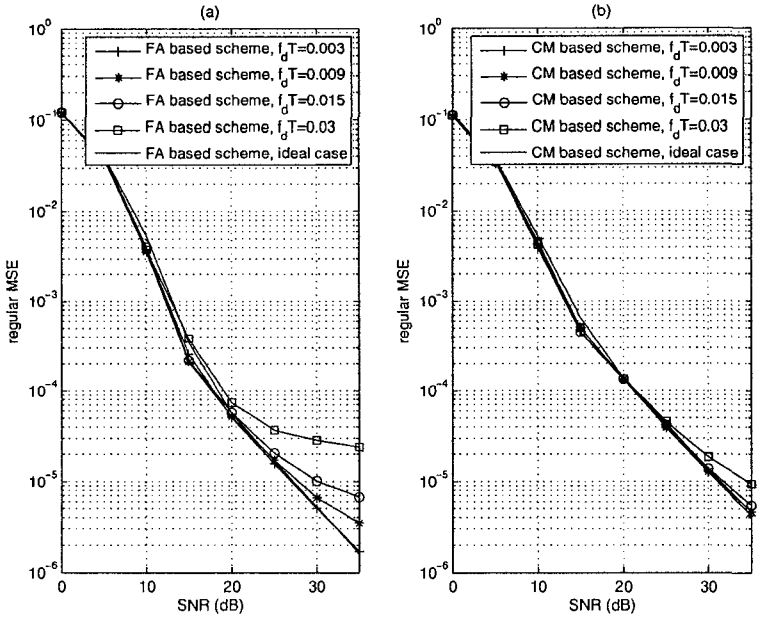

Figure 6.4: Regular MSE performance of (a) the FA based FFO estimator and (b) CM based FFO estimator in a time variant channel for a 4-PSK DOFDM system having VSCs and $\varepsilon = 4.32$.

6.7 Conclusions

In this chapter, we propose a FA based FFO estimator for DOFDM systems. The proposed scheme relies on two consecutive OFDM symbols and can be applied to systems with or without VSCs. The modified Newton method is presented in minimizing the cost function and is shown to be very efficient at high SNRs. The constrained CRLB is also derived. The proposed FA based scheme has a higher computational complexity than that of the CM based scheme and the CM based subspace scheme but it can achieve a better performance at high SNRs. Compared with the CM based subspace scheme, it also provides a wider application to systems with VSCs. However, it is sensitive to channel variations.

6.A Proof of the Periodicity

From (6.2), we notice that $\mathbf{y}(n, \tilde{\varepsilon} + m)$ can be obtained by circularly shifting $\mathbf{y}(n, \tilde{\varepsilon})$ upward by m elements. Therefore, we have $y_k(n, \tilde{\varepsilon} + m) = y_{((k+m))_N}(n, \tilde{\varepsilon})$. So, we have

$$\begin{aligned} J(\tilde{\varepsilon} + m) &= \sum_{k_1=0}^{N-1} \sum_{k_2=k_1+1}^{N-1} J_{k_1,k_2}(\tilde{\varepsilon} + m, \hat{\alpha}_{k_1,k_2}(\tilde{\varepsilon} + m)) \\ &= \sum_{k_1=0}^{N-1} \sum_{k_2=k_1+1}^{N-1} J_{k_1',k_2'}(\tilde{\varepsilon}, \hat{\alpha}_{k_1',k_2'}(\tilde{\varepsilon})), \end{aligned}$$

where $k_1' = ((k_1 + m))_N$ and $k_2' = ((k_2 + m))_N$. Then, we have

$$\begin{aligned} J(\tilde{\varepsilon} + m) &= \sum_{k_1'=m}^{N-1} \sum_{k_2'=k_1'+1}^{N-1} J_{k_1',k_2'}(\tilde{\varepsilon}, \hat{\alpha}_{k_1',k_2'}(\tilde{\varepsilon})) + \sum_{k_1'=0}^{m-1} \sum_{k_2'=k_1'+1}^{m-1} J_{k_1',k_2'}(\tilde{\varepsilon}, \hat{\alpha}_{k_1',k_2'}(\tilde{\varepsilon})) \\ &\quad + \sum_{k_1'=0}^{m-1} \sum_{k_2'=m}^{N-1} J_{k_2',k_1'}(\tilde{\varepsilon}, \hat{\alpha}_{k_2',k_1'}(\tilde{\varepsilon})). \end{aligned} \tag{6.8}$$

From (6.4), we also have that

$$J_{k_2',k_1'}(\tilde{\varepsilon}, \hat{\alpha}_{k_2',k_1'}(\tilde{\varepsilon})) = |[y_{k_1'}(n, \tilde{\varepsilon})][y_{k_2'}(n, \tilde{\varepsilon})]^* - \hat{\alpha}^*_{k_2',k_1'}(\tilde{\varepsilon}) y_{k_1'}(n-1, \tilde{\varepsilon})[y_{k_2'}(n-1, \tilde{\varepsilon})]^*|^2. \tag{6.9}$$

Furthermore, it can be easily shown that $\hat{\alpha}^*_{k_2',k_1'}(\tilde{\varepsilon}) = \hat{\alpha}_{k_1',k_2'}(\tilde{\varepsilon})$. Therefore, we have from (6.9) that

$$J_{k_2',k_1'}(\tilde{\varepsilon}, \hat{\alpha}_{k_2',k_1'}(\tilde{\varepsilon})) = J_{k_1',k_2'}(\tilde{\varepsilon}, \hat{\alpha}_{k_1',k_2'}(\tilde{\varepsilon})).$$

Finally, from (6.8), we arrive at

$$J(\tilde{\varepsilon} + m) = \sum_{k_1'=0}^{N-1} \sum_{k_2'=k_1'+1}^{N-1} J_{k_1',k_2'}(\tilde{\varepsilon}, \hat{\alpha}_{k_1',k_2'}(\tilde{\varepsilon})) = J(\tilde{\varepsilon}).$$

6.B Gradient and Hessian

Let us define

$$\mathbf{A}(\tilde{\varepsilon}, n) = [\mathbf{FC}(\tilde{\varepsilon})^H \mathbf{r}(n)][\mathbf{FC}(\tilde{\varepsilon})^H \mathbf{r}(n)]^H,$$

$$\bar{\mathbf{A}}(\tilde{\varepsilon}, n) = -\frac{4\pi}{N} \mathrm{Im}\{[\mathbf{FE}_1\mathbf{C}(\tilde{\varepsilon})^H \mathbf{r}(n)][\mathbf{FC}(\tilde{\varepsilon})^H \mathbf{r}(n)]^H\}$$

and

$$\begin{aligned}\breve{\mathbf{A}}(\tilde{\varepsilon}, n) &= -\frac{8\pi^2}{N^2}(\mathrm{Re}\{[\mathbf{FE}_1^2\mathbf{C}(\tilde{\varepsilon})^H \mathbf{r}(n)][\mathbf{FC}(\tilde{\varepsilon})^H \mathbf{r}(n)]^H\} \\ &\quad -[\mathbf{FE}_1\mathbf{C}(\tilde{\varepsilon})^H \mathbf{r}(n)][\mathbf{FE}_1\mathbf{C}(\tilde{\varepsilon})^H \mathbf{r}(n)]^H).\end{aligned}$$

For the proposed FA based cost function, the gradient and Hessian of $J_{k_1,k_2}(\tilde{\varepsilon}, \hat{\alpha}_{k_1,k_2}(\tilde{\varepsilon}))$ at $\tilde{\varepsilon} = \varepsilon^{(i)}$, are given by

$$\begin{aligned}&\frac{d}{d\tilde{\varepsilon}} J_{k_1,k_2}(\tilde{\varepsilon}, \bar{\alpha}_{k_1,k_2}(\tilde{\varepsilon}))\Big|_{\tilde{\varepsilon}=\varepsilon^{(i)}} \\ &= 2\,\mathrm{Re}\{\bar{a}_{k_1,k_2} a^*_{k_1,k_2} + \bar{b}_{k_1,k_2} b^*_{k_1,k_2} - \hat{\alpha}^*_{k_1,k_2}(\varepsilon^{(i)}) \bar{a}_{k_1,k_2} b^*_{k_1,k_2} - \hat{\alpha}^*_{k_1,k_2}(\varepsilon^{(i)}) a_{k_1,k_2} \bar{b}^*_{k_1,k_2}\},\end{aligned}$$

and

$$\begin{aligned}&\frac{d^2}{d\tilde{\varepsilon}^2} J_{k_1,k_2}(\tilde{\varepsilon}, \bar{\alpha}_{k_1,k_2}(\tilde{\varepsilon}))\Big|_{\tilde{\varepsilon}=\varepsilon^{(i)}} \\ &= 2\,\mathrm{Re}\{\breve{a}_{k_1,k_2} a^*_{k_1,k_2} + \bar{a}_{k_1,k_2} \bar{a}^*_{k_1,k_2} + \breve{b}_{k_1,k_2} b^*_{k_1,k_2} + \bar{b}_{k_1,k_2} \bar{b}^*_{k_1,k_2} - \hat{\alpha}^*_{k_1,k_2}(\varepsilon^{(i)}) \breve{a}_{k_1,k_2} b^*_{k_1,k_2} \\ &\quad -\hat{\alpha}^*_{k_1,k_2}(\varepsilon^{(i)}) \bar{a}_{k_1,k_2} \bar{b}^*_{k_1,k_2} - \hat{\alpha}^*_{k_1,k_2}(\varepsilon^{(i)}) \bar{a}_{k_1,k_2} \bar{b}^*_{k_1,k_2} - \hat{\alpha}^*_{k_1,k_2}(\varepsilon^{(i)}) a_{k_1,k_2} \breve{b}^*_{k_1,k_2}\},\end{aligned}$$

where a_{k_1,k_2}, $\bar{a}_{k_1,k_2}$, $\breve{a}_{k_1,k_2}$, b_{k_1,k_2}, $\bar{b}_{k_1,k_2}$, $\breve{b}_{k_1,k_2}$ are elements on the (k_1)th row and (k_2)th column of matrices $\mathbf{A}(\varepsilon^{(i)}, n)$, $\bar{\mathbf{A}}(\varepsilon^{(i)}, n)$, $\breve{\mathbf{A}}(\varepsilon^{(i)}, n)$, $\mathbf{A}(\varepsilon^{(i)}, n-1)$, $\bar{\mathbf{A}}(\varepsilon^{(i)}, n-1)$, $\breve{\mathbf{A}}(\varepsilon^{(i)}, n-1)$, respectively.

Chapter 7

A CFO Estimation Scheme Based on a Scalar Extended Kalman Filter for Uplink OFDM Systems

7.1 Introduction

CFO estimation for the uplink channel of OFDM systems is a much more challenging problem than that of the downlink channel. One factor that affects what estimation approach to use in this case is the carrier assignment scheme (CAS) employed. There are three main CASs, including block, interleaved and arbitrary [47]. The arbitrary CAS has more flexibility and advantages over the others, but its CFO estimation is much more challenging.

In [40] and [49], the authors propose CFO estimation schemes for the block and interleaved CASs, respectively. For arbitrary CAS, joint CFO and channel estimation algorithms based on one training symbol have been proposed in [46], [47], [68] and [69]. A common characteristic among these schemes is that they are iterative algorithms. In [46], the space-alternating generalized expectation-maximization (SAGE) algorithm is proposed. In [47], the alternating-projection frequency estimation (APFE) is proposed. It has faster convergence speed than SAGE and can achieve the CRLB. In

spite of its good performance, the APFE algorithm has high complexity because it still requires to perform grid search in maximizing the several one-dimensional objective functions. A modified SAGE (MSAGE) is proposed in [68]. It is based on using a cyclically equal-spaced, equal-energy, interleaved pilot preamble. A frequency-domain window is used in addition to the time-domain multiple-access interference (MAI) cancellation so that the interference is efficiently suppressed which leads to a faster convergence speed than SAGE. In [69], a line search based estimator is proposed. This scheme stands out among all the others as its computational complexity is dramatically reduced while it maintains a good estimation performance.

The algorithms in [46], [47], [68] and [69] approach the problem through an iterative method. In [48], a sequential method is proposed. An extended Kalman filter (EKF)-based CFO estimation is proposed for the uplink channel as a low complexity alternative to the multidimensional optimization problem. It works efficiently even with large values of CFO, but it is based on the assumption that the channel coefficients of all users are known which is a rather impractical assumption. This weakness motivates us to design a modified recursive method that can estimate CFO and channel jointly.

In this chapter, we propose a CFO estimation scheme for the uplink OFDM systems with arbitrary CAS [70]. The proposed scheme is based on using a scalar EKF algorithm. One important feature of the proposed scheme is that it does not require any prior knowledge of the channel coefficients unlike the scheme in [48]. The proposed scheme uses CFO and channel estimates obtained from a previous recursion to separate each user's measurement. Then the channel coefficients are replaced with a non-linear function of CFO. The observation noise power is analyzed and its approximation is used in the EKF algorithm. We compare the performance of the proposed scheme to the CRLB. We observe that the proposed scheme can achieve the CRLB for small number of users whereas its performance degrades with the increased number of users. In terms of the computational complexity, our proposed scheme is much more complex than MSAGE [68] and line-search scheme [69], but is a little lower than

APFE and close to SAGE at high SNR.

We also note here that the idea behind the proposed scheme is not suitable for OFDM systems employing multiple transmit antennas. As the performance of the proposed scheme degrades with the increased number of user, we would expect that it is prone to MIMO systems due to the increased number of unknown channel coefficients.

The rest of this chapter is organized as follows. In Section 7.2, the system model for the uplink channel is introduced. The proposed CFO estimation is presented in Section 7.3. Simulation results are shown in Section 7.4. Finally, Section 7.5 concludes this chapter.

7.2 System Model

We consider an uplink OFDM system with N subcarriers and K users. The subcarriers are assigned to users exclusively. Each user is assigned N/K subcarriers. Let $\mathbf{s}_k = [s_{k,0}, s_{k,1}, \ldots, s_{k,N-1}]^T$ denote the symbols transmitted in the frequency-domain by the kth user in the training symbol duration. The element $s_{k,i}$ is non-zero and takes its value from a constellation symbol if the ith subcarrier is assigned to user k, and is zero otherwise. Then the time-domain samples of the kth user's output signal denoted by $\mathbf{b}_k \triangleq [b_{k,0}, b_{k,1}, \ldots, b_{k,N-1}]^T$ can be represented as $\mathbf{b}_k = \mathbf{W}\mathbf{s}_k$, where $\mathbf{W}$ is the normalized IDFT matrix with the element on its mth row and nth column defined as $\frac{1}{\sqrt{N}} e^{j2\pi \frac{nm}{N}}$.

After appended with the CP, the kth user's training signal is then propagated through the multipath Rayleigh fading channel. Let us denote the number of the sample-spaced paths between the kth user and the base station as L_k, and denote the fading coefficients by $h_{k,0}, h_{k,1}, \ldots, h_{k,(L_k-1)}$. Assume the largest value of L_k among all the users as $L_{\max}$. Due to different distance to the base station, each user's signal also experiences an individual timing offset. The timing offset is normalized with respect to the sampling interval with the fractional part being absorbed into the

channel impulse response [47]. Let us denote the kth user's timing offset by u_k. It is modeled as a discrete random variable uniformly distributed in the range of $[0, u_{\max}]$, where $u_{\max}$ is determined by the cell radius [47]. Therefore, in order to avoid the ISI, the length of CP, denoted by L, is required to be equal to or larger than $u_{\max} + L_{\max}$. Then the multipath fading channel between the kth user and the base station can be effectively modeled as having L paths with the fading coefficients denoted by $\mathbf{h}_k = [\mathbf{0}_{u_k}^T, h_{k,0}, h_{k,1}, \ldots, h_{k,(L_k-1)}, \mathbf{0}_{L-u_k-L_k}^T]^T$.

At the receiver, the CP is first removed. In the training symbol duration, up to the nth sampling point, the vector of time-domain samples $\mathbf{y}(n) \triangleq [y(0), y(1), \ldots, y(n)]^T$ can be represented as

$$\mathbf{y}(n) = \sum_{k=1}^{K} \mathbf{x}_k(n) + \mathbf{v}(n), \text{ with } n = 0, 1, \ldots, N-1, \tag{7.1}$$

where $\mathbf{x}_k(n)$ is the user k's signal component. It is given by

$$\mathbf{x}_k(n) \triangleq \mathbf{C}_{\varepsilon_k}(n)\mathbf{D}_k(n)\mathbf{h}_k, \tag{7.2}$$

where ε_k denotes the kth user's CFO normalized with respect to the subcarrier interval and has a uniform distribution in the range of $[-\tau, \tau]$. The diagonal matrix $\mathbf{C}_{\varepsilon_k}(n) \triangleq \text{diag}([1, e^{j2\pi\frac{\varepsilon_k}{N}}, \ldots, e^{j2\pi\frac{n\varepsilon_k}{N}}])$ represents the phase shift introduced by the CFO. The matrix $\mathbf{D}_k(n)$ consists of the first $(n+1)$ rows of $\mathbf{D}_k$, where $\mathbf{D}_k$ is a $N \times L$ matrix with its element on the mth row and nth column defined as $b_{k,((m-n))_N}$. The channel noise vector is defined as $\mathbf{v}(n) = [v(0), v(1), \ldots, v(n)]^T$, where $v(n)$, $n = 0, 1, \ldots, N-1$, are noise samples modeled as independent complex Gaussian random variables with zero mean and variance σ_n^2.

Therefore, based on (7.2), (7.1) can be represented as

$$\mathbf{y}(n) = \Gamma(n)\mathbf{D}(n)\boldsymbol{\xi} + \mathbf{v}(n), \tag{7.3}$$

where $\Gamma(n) \triangleq [\mathbf{C}_{\varepsilon_1}(n), \mathbf{C}_{\varepsilon_2}(n), \ldots, \mathbf{C}_{\varepsilon_K}(n)]$ and $\boldsymbol{\xi} = [\mathbf{h}_1^T, \mathbf{h}_2^T, \ldots, \mathbf{h}_K^T]^T$. The matrix

$\mathbf{D}(n)$ is a $K \times K$ block diagonal matrix with $\mathbf{D}_k(n)$, $k = 1, 2, \ldots, K$ on its diagonal.

7.3 Proposed CFO Estimation

7.3.1 Development of the Proposed Estimator

We observe from (7.1) that the received signal vector $\mathbf{y}(n)$ is a superposition of the noisy signal components from all users. The idea behind our proposed scheme is, at each recursion, each user's signal is first separated, and then represented as a function of its CFO only such that scalar EKFs can be applied to the different users. In every recursion, CFO estimates obtained from the last recursion are used to separate the received signals for each user. Although the estimated CFOs used for signal separation are inaccurate at the beginning, they get updated and refined recursion by recursion.

Since the knowledge of channel coefficients is required to reconstruct the user signal components, let us first get their estimations. From (7.3), with the observation $\mathbf{y}(n)$, where $n \geq KL$, the maximum likelihood channel estimation is [47]

$$\hat{\boldsymbol{\xi}}(n) = \{[\Gamma(n)\mathbf{D}(n)]^H \Gamma(n)\mathbf{D}(n)\}^{-1} [\Gamma(n)\mathbf{D}(n)]^H \mathbf{y}(n), \tag{7.4}$$

when $\Gamma(n)\mathbf{D}(n)$ has a full column rank, where $\hat{\boldsymbol{\xi}}(n) \triangleq [\hat{\mathbf{h}}_1^T(n), \hat{\mathbf{h}}_2^T(n), \ldots, \hat{\mathbf{h}}_K^T(n)]^T$, with $\hat{\mathbf{h}}_k(n)$ representing the estimated channel coefficients of the kth user. Let us assume that we have obtained the CFO estimations $\hat{\varepsilon}_k(n-1)$ for $k = 1, 2, \ldots, K$ from the previous recursion. Since the true CFOs are unknown, we replace ε_k on the right hand side of (7.4) with $\hat{\varepsilon}_k(n-1)$, and obtain the channel estimation at the nth recursion as

$$\hat{\boldsymbol{\xi}}(n) = \{[\Psi(n)\mathbf{D}(n)]^H \Psi(n)\mathbf{D}(n)\}^{-1} [\Psi(n)\mathbf{D}(n)]^H \mathbf{y}(n), \tag{7.5}$$

where $\Psi(n) \triangleq \left[\mathbf{C}_{\hat{\varepsilon}_1(n-1)}(n), \mathbf{C}_{\hat{\varepsilon}_2(n-1)}(n), \ldots, \mathbf{C}_{\hat{\varepsilon}_K(n-1)}(n)\right]$.

Then, with the estimated CFOs and the channel coefficients, i.e., $\hat{\varepsilon}_k(n-1)$, $\hat{\mathbf{h}}_k(n)$,

we can approximately reconstruct each user's signal component $\hat{\mathbf{x}}_k(n)$ by

$$\hat{\mathbf{x}}_k(n) \triangleq \mathbf{C}_{\hat{\varepsilon}_k(n-1)}(n)\mathbf{D}_k(n)\hat{\mathbf{h}}_k(n). \tag{7.6}$$

Finally, we can use MAI cancellation to decouple the received signal for each user $\hat{\mathbf{y}}_k(n)$ by

$$\hat{\mathbf{y}}_k(n) \triangleq \mathbf{y}(n) - \textstyle\sum_{i=1,i\neq k}^{K} \hat{\mathbf{x}}_i(n). \tag{7.7}$$

In order to apply the EKF algorithm for CFO estimation, we need next to express the measurement $\hat{y}_k(n)$ as a function of the state ε_k. Let us define the channel estimation error as $\Delta\mathbf{h}_k(n) \triangleq \hat{\mathbf{h}}_k(n) - \mathbf{h}_k$. Then (7.6) can be represented as

$$\begin{aligned} \hat{\mathbf{x}}_k(n) &= \mathbf{C}_{\hat{\varepsilon}_k(n-1)}(n)\mathbf{D}_k(n)\mathbf{h}_k + \mathbf{C}_{\hat{\varepsilon}_k(n-1)}(n)\mathbf{D}_k(n)\Delta\mathbf{h}_k(n) \\ &= \mathbf{x}_k(n) + [\mathbf{C}_{\hat{\varepsilon}_k(n-1)}(n) - \mathbf{C}_{\varepsilon_k}(n)]\mathbf{D}_k(n)\mathbf{h}_k + \mathbf{C}_{\hat{\varepsilon}_k(n-1)}(n)\mathbf{D}_k(n)\Delta\mathbf{h}_k(n). \end{aligned} \tag{7.8}$$

Plugging (7.1) and (7.8) into the right hand side of (7.7), we obtain

$$\hat{\mathbf{y}}_k(n) = -\sum_{i=1,i\neq k}^{K} \mathbf{C}_{\hat{\varepsilon}_i(n-1)}(n)\mathbf{D}_i(n)\Delta\mathbf{h}_i(n) + \mathbf{C}_{\varepsilon_k}(n)\mathbf{D}_k(n)\mathbf{h}_k + \mathbf{w}_k(n), \tag{7.9}$$

where

$$\mathbf{w}_k(n) \triangleq -\sum_{i=1,i\neq k}^{K} [\mathbf{C}_{\hat{\varepsilon}_i(n-1)}(n) - \mathbf{C}_{\varepsilon_i}(n)]\mathbf{D}_i(n)\mathbf{h}_i + \mathbf{v}(n). \tag{7.10}$$

We observe from (7.9) that the kth user's measurement $\hat{\mathbf{y}}_k(n)$ depends not only on ε_k but also on $\boldsymbol{\zeta}_k(n) \triangleq [-\Delta\mathbf{h}_1^T(n), \ldots, -\Delta\mathbf{h}_{k-1}^T(n), \mathbf{h}_k^T, -\Delta\mathbf{h}_{k+1}^T(n), \ldots, -\Delta\mathbf{h}_K^T(n)]^T$.

By multiplying $\mathbf{C}_{\varepsilon_k}^H(n)$ on both sides of (7.9), we obtain

$$\begin{aligned}\mathbf{C}_{\varepsilon_k}^H(n)\hat{\mathbf{y}}_k(n) &= -\sum_{i=1,i\neq k}^{K}\mathbf{C}_{[\hat{\varepsilon}_i(n-1)-\varepsilon_k]}(n)\mathbf{D}_i(n)\Delta\mathbf{h}_i(n)+\mathbf{D}_k(n)\mathbf{h}_k+\mathbf{C}_{\varepsilon_k}^H(n)\mathbf{w}_k(n)\\ &= \tilde{\Upsilon}_k(n)\mathbf{D}(n)\boldsymbol{\zeta}_k(n)+\mathbf{C}_{\varepsilon_k}^H(n)\mathbf{w}_k(n),\end{aligned} \tag{7.11}$$

where $\tilde{\Upsilon}_k(n) \triangleq [\mathbf{C}_{[\hat{\varepsilon}_1(n-1)-\varepsilon_k]}(n),\ldots,\mathbf{C}_{[\hat{\varepsilon}_{k-1}(n-1)-\varepsilon_k]}(n),\ \mathbf{I}_{(n+1)},\mathbf{C}_{[\hat{\varepsilon}_{k+1}(n-1)-\varepsilon_k]}(n),\ldots,$ $\mathbf{C}_{[\hat{\varepsilon}_K(n-1)-\varepsilon_k]}(n)]$, and $\mathbf{I}_m$ is an $m\times m$ identity matrix. By defining

$$\begin{aligned}\Upsilon_k(n) \triangleq\ & [\mathbf{C}_{[\hat{\varepsilon}_1(n-1)-\hat{\varepsilon}_k(n-1)]}(n),\ldots,\mathbf{C}_{[\hat{\varepsilon}_{k-1}(n-1)-\hat{\varepsilon}_k(n-1)]}(n),\mathbf{I}_{(n+1)},\\ & \mathbf{C}_{[\hat{\varepsilon}_{k+1}(n-1)-\hat{\varepsilon}_k(n-1)]}(n),\ldots,\mathbf{C}_{[\hat{\varepsilon}_K(n-1)-\hat{\varepsilon}_k(n-1)]}(n)],\end{aligned}$$

(7.11) can be represented as

$$\mathbf{C}_{\varepsilon_k}^H(n)\hat{\mathbf{y}}_k(n)=\Upsilon_k(n)\mathbf{D}(n)\boldsymbol{\zeta}_k(n)+\mathbf{u}_k(n), \tag{7.12}$$

where

$$\mathbf{u}_k(n)=[\tilde{\Upsilon}_k(n)-\Upsilon_k(n)]\mathbf{D}(n)\boldsymbol{\zeta}_k(n)+\mathbf{C}_{\varepsilon_k}^H(n)\mathbf{w}_k(n). \tag{7.13}$$

Therefore, from (7.12), $\boldsymbol{\zeta}_k(n)$ can be represented by

$$\boldsymbol{\zeta}_k(n)=\left\{[\Upsilon_k(n)\mathbf{D}(n)]^H\Upsilon_k(n)\mathbf{D}(n)\right\}^{-1}[\Upsilon_k(n)\mathbf{D}(n)]^H[\mathbf{C}_{\varepsilon_k}^H(n)\hat{\mathbf{y}}_k(n)-\mathbf{u}_k(n)]. \tag{7.14}$$

In addition, from (7.12), the measurement $\hat{y}_k(n)$ can be represented as

$$\hat{y}_k(n)=e^{j2\pi\frac{n\varepsilon_k}{N}}\boldsymbol{\gamma}_k^T(n)\boldsymbol{\zeta}_k(n)+e^{j2\pi\frac{n\varepsilon_k}{N}}u_{k,n}(n), \tag{7.15}$$

where $\boldsymbol{\gamma}_k^T(n)$ and $u_{k,n}(n)$ denote the last row of $\Upsilon_k(n)\mathbf{D}(n)$ and $\mathbf{u}_k(n)$, respectively. By replacing $\boldsymbol{\zeta}_k(n)$ on the right hand side of (7.15) with the expression in (7.14), we

have that

$$\hat{y}_k(n) = e^{j\frac{2\pi n\varepsilon_k}{N}} \tilde{\mathbf{g}}_k^T(n)\mathbf{C}_{\varepsilon_k}^H(n)\hat{\mathbf{y}}_k(n) + \varpi_k(n), \tag{7.16}$$

where $\tilde{\mathbf{g}}_k^T(n)$ is a row vector defined as $\tilde{\mathbf{g}}_k^T(n) = \boldsymbol{\gamma}_k^T(n)\{[\Upsilon_k(n)\mathbf{D}(n)]^H \Upsilon_k(n)\mathbf{D}(n)\}^{-1}$ $\times [\Upsilon_k(n)\mathbf{D}(n)]^H$, and

$$\varpi_k(n) = -e^{j2\pi\frac{n\varepsilon_k}{N}} \tilde{\mathbf{g}}_k^T(n)\mathbf{u}_k(n) + e^{j2\pi\frac{n\varepsilon_k}{N}} u_{k,n}(n). \tag{7.17}$$

From (7.16), we notice that the measurement $\hat{y}_k(n)$ has been represented as a function of ε_k only. The observation noise term is given by $\varpi_k(n)$. To apply the EKF algorithm, the variance of $\varpi_k(n)$ is required to be known. It significantly affects the performance of the EKF as the Kalman gain is directly related to the observation noise power and indicates the confidence of the current innovation. The authors in [48] take an adaptive approach to estimate the observation noise power based on the weighted average of the sample noise powers. Here, we take another approach to approximate the observation noise power.

From (7.17), we observe that

$$\varpi_k(n) = -e^{j2\pi\frac{n\varepsilon_k}{N}} \mathbf{g}_k^T(n)\mathbf{u}_k(n), \tag{7.18}$$

where $\mathbf{g}_k^T(n) = \tilde{\mathbf{g}}_k^T(n) - [0, \ldots, 0, 1]$. From (7.13), we have the approximation that

$$\mathbf{u}_k(n) \approx \mathbf{C}_{\varepsilon_k}^H(n)\mathbf{w}_k(n). \tag{7.19}$$

This is because the first term in (7.13) consists of the multiplications of the elements from $\Delta\mathbf{h}_i^T(n)$ and the diagonal elements of $[\mathbf{C}_{\varepsilon_k}(n) - \mathbf{C}_{\hat{\varepsilon}_k(n-1)}(n)]^H$. The multiplication could be much smaller than the remaining term. Therefore, by plugging the

approximation in (7.19) and (7.10) into (7.18), we have

$$\begin{aligned}\varpi_k(n) &\approx e^{j2\pi\frac{n\epsilon_k}{N}}\mathbf{g}_k^T(n)\mathbf{C}_{\varepsilon_k}^H(n)\sum\nolimits_{i=1,i\neq k}^{K}[\mathbf{C}_{\hat{\varepsilon}_i(n-1)}(n)-\mathbf{C}_{\varepsilon_i}(n)] \\ &\quad\times\mathbf{D}_i(n)\mathbf{h}_i - e^{j2\pi\frac{n\epsilon_k}{N}}\mathbf{g}_k^T(n)\mathbf{C}_{\varepsilon_k}^H(n)\mathbf{v}(\mathbf{n}). \qquad (7.20)\end{aligned}$$

From (7.20), we observe that the observation noise consists of two terms. The first term comes from the multiuser interference and the second term comes from the channel noise. Let $\varpi_k^1(n)$ denote the first term. It can be represented as

$$\varpi_k^1(n) = e^{j2\pi\frac{n\epsilon_k}{N}}\sum\nolimits_{i=1,i\neq k}^{K}\mathbf{g}_k^T(n)\mathbf{C}_{\varepsilon_k}^H(n)\mathbf{C}_{\varepsilon_i}(n)[\mathbf{C}_{[\hat{\varepsilon}_i(n-1)-\varepsilon_i]}(n)-\mathbf{I}_{(n+1)}]\mathbf{D}_i(n)\mathbf{h}_i.$$

We notice that $2\pi n[\hat{\varepsilon}_i(n-1)-\varepsilon_i]/N$ is small when n is small. Furthermore, when n is large, $\hat{\varepsilon}_i(n-1)$ would be close to ε_i, which also makes $2\pi n[\hat{\varepsilon}_i(n-1)-\varepsilon_i]/N$ a very small value. Therefore, by using the approximation that $e^{j2\pi n[\hat{\varepsilon}_i(n-1)-\varepsilon_i]/N} \approx 1+j2\pi n[\hat{\varepsilon}_i(n-1)-\varepsilon_i]/N$, $\varpi_k^1(n)$ can be approximated by

$$\varpi_k^1(n) \approx \sum\nolimits_{i=1,i\neq k}^{K}[\hat{\varepsilon}_i(n-1)-\varepsilon_i]e^{j2\pi\frac{n\epsilon_k}{N}}\mathbf{g}_k^T(n)\mathbf{C}_{\varepsilon_k}^H(n)\mathbf{C}_{\varepsilon_i}(n)\tilde{\mathbf{B}}(n)\mathbf{D}_i(n)\mathbf{h}_i,$$

where $\tilde{\mathbf{B}}(n) \triangleq \frac{j2\pi}{N}\mathrm{diag}([0,1,\ldots,n])$.

Let us treat $\mathbf{h}_i$ and ε_i as unknown constants, and $\hat{\varepsilon}_i(n-1)$ as a realization of a random variable denoted by $\hat{\epsilon}_i(n-1)$ with mean equivalent to ε_i and variance denoted by $E\{[\hat{\epsilon}_i(n-1)-\varepsilon_i]^2\}$. Then the variance of $\varpi_k^1(n)$ can be approximated as

$$\mathrm{var}(\varpi_k^1(n)) \approx \sum\nolimits_{i=1,i\neq k}^{K} E\left\{[\hat{\varepsilon}_i(n-1)-\varepsilon_i]^2\right\}\left|\mathbf{g}_k^T(n)\mathbf{C}_{\varepsilon_k}^H(n)\mathbf{C}_{\varepsilon_i}(n)\tilde{\mathbf{B}}(n)\mathbf{D}_i(n)\mathbf{h}_i\right|^2. \qquad (7.21)$$

Therefore, the observation noise power is approximated by

$$\mathrm{var}(\varpi_k(n)) \approx \mathrm{var}(\varpi_k^1(n)) + \mathbf{g}_k^T(n)\mathbf{g}_k^*(n)\sigma_n^2. \qquad (7.22)$$

In calculating $\mathrm{var}(\varpi_k^1(n))$, the true values of $\mathbf{h}_i$ and ε_i are required. We could

replace them with $\hat{\mathbf{h}}_i(n)$ and $\hat{\varepsilon}_i(n-1)$, respectively, to obtain an approximated value of $\text{var}(\varpi_k^1(n))$. In addition, the variance of the CFO estimation at the previous recursion, i.e., $E\left\{[\hat{\varepsilon}_i(n-1)-\varepsilon_i]^2\right\}$ is also required in calculating $\text{var}(\varpi_k^1(n))$. It can be obtained as a by-product from the evolution of the EKF. In spite of its simplicity, the variance obtained in this way may not give the true variance. This is because the CFO is uniformly distributed and not Gaussian, which is against the Gaussian model required for the application of the Kalman filter. Although the variance given by the EKF does not represent the true variance, it does maintain the trend that the true variance is following, that is the true variance decreases with the recursions. Therefore, we could assume that the variance given by the EKF is a scaled version of the true variance by a constant.

We notice from (7.22) that the observation noise power is the summation of two components. The first component represents the multiuser interference power and depends on the variance of the CFO estimation. The second component depends on σ_n^2. We know that the evolution of the EKF does not depend on the absolute value of the observation noise power. Actually, it relies much more on the relative fluctuation of the observation noise power from one recursion to the other. By using the variance given by the EKF in calculating $\text{var}(\varpi_k^1(n))$, we actually scale the first component by a constant, so the second component should also be scaled by the same constant. However, this constant is unknown. In addition, the knowledge of σ_n^2 may also be unavailable. Therefore, we resort to simulations to try to find the proper value for σ_n^2 that should be used in evaluating (7.22). We will show via simulations that by setting σ_n^2 in (7.22) to 5×10^{-4} and the initial variance to 1000, the proposed scheme gives a satisfactory CFO estimation performance in the range of MSE of interest, i.e., from 10^{-3} to 10^{-5}.

7.3.2 Outline of the Estimation Algorithm

We can set the state equation and the measurement equation for the kth user as

$$\varepsilon_k(n) = \varepsilon_k(n-1)$$

and

$$\hat{y}_k(n) \approx a(\varepsilon_k(n)) + \varpi_k(n),$$

where $a(\varepsilon_k(n)) = e^{j\frac{2\pi n\varepsilon_k(n)}{N}} \tilde{\mathbf{g}}_k^T(n)\mathbf{C}^H_{\varepsilon_k(n)}(n)\hat{\mathbf{y}}_k(n)$, and then apply the EKF algorithm [71] for each user. Let us summarize the CFO estimation scheme as follows.

Initial condition: $\hat{\varepsilon}_k(n_0-1) = 0$, $P_k(n_0-1) = 1000$, with $n_0 \geq KL$.

Computation: $n = n_0, \ldots, N-1$

1. Estimate the channel coefficients $\hat{\boldsymbol{\xi}}(n)$ via (7.5).
2. Reconstruct each user's signal component $\hat{\mathbf{x}}_k(n)$ for $k = 1, 2, \ldots, K$, via (7.6).
3. Separate each user's received signal $\hat{\mathbf{y}}_k(n)$ for $k = 1, 2, \ldots, K$, via (7.7).
4. Calculate the observation noise power $\text{var}(\varpi_k(n))$ for $k = 1, 2, \ldots, K$, via (7.22) and (7.21).
5. Run the kth user's EKF one step forward as follows, for $k = 1, 2, \ldots, K$.

   (a) Kalman Gain:

$$G_k(n) = \frac{P_k(n-1)A_k^*(n)}{|A_k(n)|^2 P_k(n-1) + \text{var}(\varpi_k(n))},$$

   where

$$A_k(n) = \left.\frac{\partial a(\varepsilon_k(n))}{\partial \varepsilon_k(n)}\right|_{\varepsilon_k(n)=\hat{\varepsilon}_k(n-1)} = e^{j\frac{2\pi n\hat{\varepsilon}_k(n-1)}{N}} \tilde{\mathbf{g}}_k^T(n)\mathbf{B}(n)\mathbf{C}^H_{\hat{\varepsilon}_k(n-1)}(n)\hat{\mathbf{y}}_k(n),$$

   and $\mathbf{B}(n) = \frac{j2\pi}{N}\text{diag}([n, n-1, \ldots, 0])$.

(b) Correction: $\hat{\varepsilon}_k(n) = g\{\hat{\varepsilon}_k(n-1) + G_k(n)[\hat{y}_k(n) - a(\hat{\varepsilon}_k(n-1))]\}$, where

$$g(x) = \begin{cases} \tau, & \text{if } x > \tau \\ x, & \text{if } -\tau \leq x \leq \tau \\ -\tau, & \text{if } x < -\tau \end{cases} . \tag{7.23}$$

(c) Variance: $P_k(n) = [1 - G_k(n)A_k(n)]\, P_k(n-1)$.

7.3.3 Computational Complexity

For the proposed scheme, the number of complex multiplications performed at the recursion when up to the nth sample is received can be approximated by $C(n, K, L) = (K^2L^2 + KL^2 + 3KL + 2L + 4K + 2)K(n+1) + K^2L^2(K+1)(KL+1) + 2K^2 + 9K$. It shows that the complexity at each recursion increases linearly with n. If $n_0 = KL$, then the total number of complex multiplications of the proposed scheme is given by $(K^2L^2+KL^2+3KL+2L+4K+2)K(N+KL+1)(N-KL)/2+[K^2L^2(K+1)(KL+1) + 2K^2 + 9K](N - KL)$.

For APFE, the number of complex multiplications at each iteration is given by $K[2N(K-1)^2L^2+(K-1)^3L^3+N^2(K-1)L+N_s(2N^2L+2NL^2+L^3+N^2+N)+NL]$, whereas it is $K[2NL + 2L^2N + L^3 + N^2L + N_s(N + N^2) + N]$ for SAGE, where N_s is the number of CFO candidates in the searching range of $[-\tau, \tau]$. We will compare their computational complexity by using the simulation results.

7.4 Simulation Results

In this section, we examine the performance of the proposed scheme. The OFDM system has $N = 128$ subcarriers with length of CP $L = 16$. In each run of the simulation, every user is assigned N/K pilot subcarriers randomly and the pilot symbols are generated randomly from a 4−PSK constellation. The multipath fading channel has $L_k = 8$ paths and an exponential power delay profile for all users,

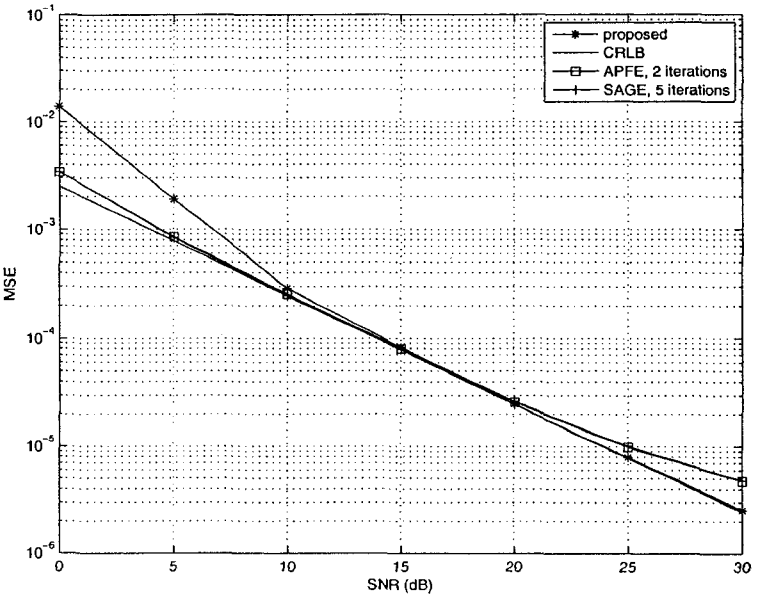

Figure 7.1: Performance comparison for system with $N = 128$, $L = 16$, $K = 2$.

i.e., $E\{|h_{k,l}|^2\} = \frac{1}{\sum_{i=0}^{7}\exp(-i)}\exp(-l)$, $l = 0, 1, ..., 7$. The timing offsets are integers uniformly distributed in the range of $[0, 8]$. The CFO is assumed to be uniformly distributed in the range of $[-0.5, 0.5]$. The SNR is defined as $\mathbf{s}_k^H\mathbf{s}_k/(N\sigma_n^2)$.

The CFO estimation performance is measured by the MSE. The MSE of the proposed scheme and the CRLB [47] are obtained by averaging $10,000$ runs of simulation over all active users in the system. We compare the proposed scheme with APFE [47] and SAGE [46]. For these two schemes, in the search range of $[-0.5, 0.5]$, 201 equally spaced CFO candidates are used to achieve a precision of 5×10^{-3}. For SAGE, its MSE is also obtained by averaging over $10,000$ runs of simulation whereas only $5,000$ runs are performed for APFE due to its computational complexity.

In Fig. 7.1, we consider the system with 2 users. We observe that the proposed EKF performs as well as the CRLB only with a divergence at low SNRs. Furthermore, at high SNR, the proposed scheme performs a little better than APFE with 2 iterations and SAGE with 5 iterations. We mention that the performance of APFE and SAGE can be further improved at high SNR by using a higher precision in the grid

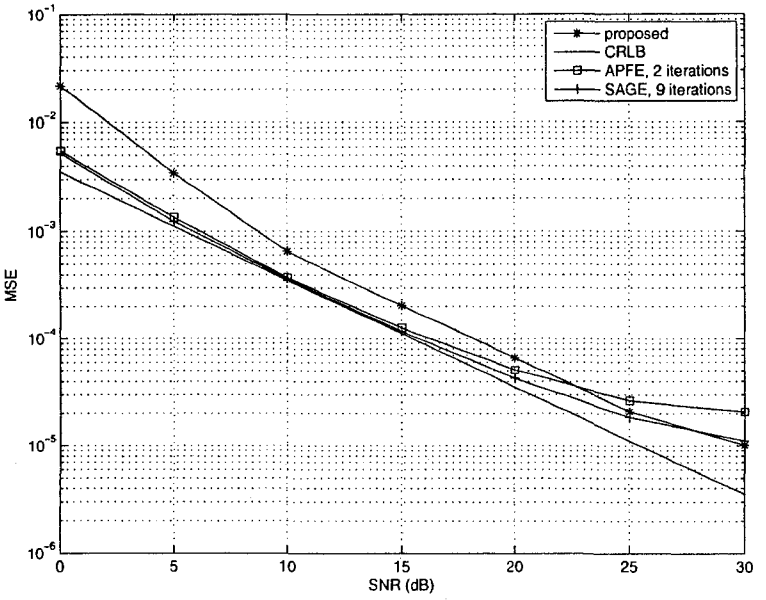

Figure 7.2: Performance comparison for system with $N = 128$, $L = 16$, $K = 4$.

search process or a few more iterations. However, this is at the cost of increased computational complexity which we will discuss later. We also mention that for SAGE, the number of iterations required for convergence increases with SNR, i.e., at low SNR, only 2 iterations are required whereas 5 iterations are required for high SNR.

As we know that the performance of the proposed scheme is somewhat dependent on the number of unknowns and the number of recursions. This is attributed to the fact that it refines the CFO estimates recursively. Consequently, when the number of unknowns is large, the proposed scheme may not be able to converge within a limited number of recursions. In Fig. 7.2, we consider a system with a relatively large number of unknowns, i.e., 4 users. We observe that the performance of the proposed scheme degrades as compared to the CRLB. From low to medium SNR, the proposed scheme is worse than APFE and SAGE. At high SNR, it performs a little better than APFE with 2 iterations and close to SAGE with 9 iterations. We also mention that SAGE can converge within 4 iterations at low SNR whereas 9 iterations are required for high SNR.

Table 7.1: Complexity comparison in terms of number of multiplications between the proposed scheme, APFE and SAGE.

# of users	proposed	APFE(iterations)	SAGE(iterations)
$K = 2$	3.5608×10^7	$4.8968 \times 10^8(2)$	$1.4554 \times 10^7(2), 3.6384 \times 10^7(5)$
$K = 4$	2.1766×10^8	$9.8860 \times 10^8(2)$	$5.8214 \times 10^7(4), 1.3098 \times 10^8(9)$

We compare the computational complexity of the proposed scheme with APFE [47] and SAGE [46] at a certain number of iterations in Table 7.1. The computational complexity is measured in terms of the number of complex multiplications. Comparing the proposed scheme with APFE, we observe that at high SNR, the proposed scheme has a little lower complexity than APFE while achieving a little better performance. We also observe that the computational complexity of SAGE is lower than the proposed scheme through low to medium SNRs and becomes close to the proposed scheme at high SNR.

7.5 Conclusions

In this chapter, we have proposed an EKF-based CFO estimation scheme for the uplink OFDM systems. The proposed scheme can be applied to the arbitrary CAS. The MAI cancellation based on the estimations obtained from a previous recursion is used for signal separation. The measurement equation is then represented as a function of CFO only by replacing the channel coefficients with a non-linear function of CFO. Finally, the observation noise power is approximated, and the scalar EKF is applied for each user to estimate its CFO. The proposed scheme can achieve the CRLB for small number of users whereas it degrades with increased number of users. Its computational complexity is a little lower than that of APFE and is close to SAGE at high SNR.

Chapter 8

Joint CFO and Channel Estimation for Uplink OFDM Systems: An Application of the Variable Projection Method

8.1 Introduction

The joint CFO and channel estimation problem based on one training symbol for the arbitrary CAS, which is also the concentration of this chapter, has been studied in [46], [47], [68], [72]. A common characteristic among these schemes is that they are iterative algorithms. As the SAGE [46], MSAGE [68] and APFE [47] algorithms require to perform grid search in the region where CFOs are known to be in minimizing or maximizing a number of one-dimensional objective functions, they have high computational complexity.

Recently, in [72], an iterative minimum mean square error (MMSE) method is proposed which stands out among all the others. The computational complexity is dramatically reduced while it maintains a good estimation performance. In this scheme, the objective is to minimize the mean-square distance between the received

signal and the reconstructed received signal. In each iteration, parameters are updated based on the MMSE criterion. We further notice that in this method, all the unknown parameters are treated together as a whole. Due to this characteristic, for the rest of this chapter, we refer to the scheme proposed in [72] as the non-separated MMSE method.

Their method motivates us to resort to another objective function that is the least-squares (LS) criterion. We notice that it results in a separable nonlinear LS (SNLLS) problem [73] where the unknown parameters can be separated into two sets, i.e., linear parameters corresponding to the channel coefficients, and nonlinear parameters corresponding to the CFOs. This motivates us to apply the variable-projection (VP) method in [73] which treats nonlinear and linear parameters separately to solve this SNLLS problem more efficiently.

A comprehensive review on the history and the applications of the VP method in the recent 30 years can be found in [73]. Textbook [74] also covers this topic. The idea behind the VP method is to eliminate the linear parameters from the objective function, such that the modified objective function involves only the nonlinear parameters [73]. This procedure results in a reduced dimensionality of the parameter space and a better-conditioned problem, which leads to convergence in a fewer number of iterations in comparison with the numerical method in which all the parameters are treated together as a whole. On the other hand, this procedure also results in a somewhat complicated modified objective function which in turn requires additional computations at each iteration. To this end, in [75] and [76], a simplified VP method is proposed which makes the computational complexity of the VP method at each iteration comparable to that of the non-separated numerical method. Ever since then, the VP method has been applied to many fields.

In this chapter, we propose a joint CFO and channel estimation method for uplink OFDM systems [77]. The proposed method consists of two steps. Motivated by the efficiency and wide applications of the VP method [76], the VP method is applied for CFO estimation in the first step. Following the VP method, the robust MMSE channel

estimation method is then applied in the second step. To measure the computational complexity of the proposed method, we analyze its required number of multiplications. We also examine its convergence speed in terms of CFO estimation as well as mean square error (MSE) performance. In our evaluation, we compare the proposed method to the non-separated MMSE method proposed in [72] since the latter achieves the best performance among existing methods. We show through several numerical examples that the proposed scheme is superior to the non-separated MMSE method in terms of convergence speed and MSE performance. The computational complexity of the proposed scheme is lower than that of the non-separated MMSE method at high signal-to-noise ratios (SNRs), and particularly so when the number of users is large. We also note here that one can also extend the proposed scheme in a straightforward manner to multiple antenna systems with similar favorable results.

The rest of the chapter is organized as follows. In Section 8.2, we describe the system model of the uplink OFDM channel. In Section 8.3, the iterative non-separated LS method is reviewed for the convenience of the introduction of the VP method. In Section 8.4, we propose a joint CFO and channel estimation method. Its computational complexity is analyzed in Section 8.5. In Section 8.6, we compare the proposed method with the non-separated MMSE method in [72] via computer simulations. Finally, conclusions are made in Section 8.7.

8.2 System Model

We consider an uplink OFDM system with N subcarriers and K users. The subcarriers are randomly assigned to users exclusively. Each user is assigned N_k subcarriers. Let $\mathbf{s}_k = [s_{k,0}, s_{k,1}, \ldots, s_{k,N-1}]^T$ denote the training symbols transmitted in the frequency domain by user k. The element $s_{k,i}$ is non-zero and takes its value from a constellation symbol only if the ith subcarrier is assigned to user k, and is zero otherwise. After the inverse discrete Fourier transform (IDFT), the N time-domain samples of the kth user's output signal denoted by $\mathbf{b}_k \triangleq [b_{k,0}, b_{k,1}, \ldots, b_{k,N-1}]^T$ are

then given by $\mathbf{b}_k = P_k \mathbf{W} \mathbf{s}_k$, where $\mathbf{W}$ is the normalized IDFT matrix with its element on the nth row and mth column defined as $\frac{1}{\sqrt{N}} e^{\frac{j2\pi mn}{N}}$ and P_k is the kth user's training signal power per pilot subcarrier. The IDFT output is then appended with a cyclic prefix (CP) to avoid inter-block-interference (IBI).

The kth user's training signal is then propagated through the multipath Rayleigh fading channel. Let us denote the number of the sample-spaced propagation paths between the kth user and the base station as L_k, and denote the fading coefficients by $h_{k,0}, h_{k,1}, \ldots, h_{k,(L_k-1)}$. The fading coefficients $h_{k,l}$'s with $l = 0, 1, \ldots, L_k - 1$, are modeled as complex Gaussian random variables with zero mean and variance $\sigma^2_{h,k,l}$, where $\sigma^2_{h,k,l} = E\{|h_{k,l}|^2\}$ is the average power of the lth propagation path of user k. Then the total average power of the kth user's channel impulse response is given by $\sigma^2_{h,k} = \sum_{l=1}^{L_k-1} \sigma^2_{h,k,l}$.

Assume the largest value of L_k among all the users as $L_{\max}$. Due to different distances to the base station, each user's signal also experiences an individual timing offset. The timing offset is normalized with respect to the sampling interval with the fractional part being absorbed into the channel impulse response [47]. Let us denote the kth user's timing offset by u_k. It is modeled as a discrete random variable uniformly distributed in the range [0, $u_{\max}$], where $u_{\max}$ is determined by the cell radius [47]. Therefore, in order to avoid the IBI, the length of CP, denoted by L, is required to be equal to or larger than $u_{\max} + L_{\max}$. In this sequel, the multipath fading channel between the kth user and the base station can be effectively modeled as having L paths with the fading coefficients denoted by $\mathbf{h}_k = [\mathbf{0}^T_{u_k}, h_{k,0}, h_{k,1}, \ldots, h_{k,(L_k-1)}, \mathbf{0}^T_{L-u_k-L_k}]^T$.

At the receiver, the CP is first removed. In the training symbol duration, the vector of the time-domain samples denoted by $\mathbf{y} \triangleq [y(0), y(1), \ldots, y(N-1)]^T$ can be represented as

$$\mathbf{y} = \sum_{k=1}^{K} \mathbf{x}_k + \mathbf{v}, \tag{8.1}$$

where $\mathbf{x}_k$ is user k's signal component, which is given by

$$\mathbf{x}_k \triangleq \mathbf{C}(\varepsilon_k)\mathbf{D}_k\mathbf{h}_k, \tag{8.2}$$

where ε_k denotes the kth user's CFO normalized with respect to the subcarrier interval and has a uniform distribution in the range $[-\tau, \tau]$. The diagonal matrix $\mathbf{C}(\varepsilon_k) \triangleq \text{diag}([1, e^{j2\pi\frac{\varepsilon_k}{N}}, \ldots, e^{j2\pi\frac{(N-1)\varepsilon_k}{N}}])$ represents the phase shift introduced by the CFO. The $N \times L$ matrix $\mathbf{D}_k$ is a Toeplitz matrix with its element on the mth row and nth column defined as $b_{k,[(m-n) \bmod N]}$. The channel noise samples, $\mathbf{v} = [v_0, v_1, \ldots, v_{N-1}]$, are modeled as independent complex Gaussian random variables with zero mean and variance σ_v^2.

Based on (8.2), (8.1) can also be represented as

$$\mathbf{y} = \Gamma(\boldsymbol{\varepsilon})\boldsymbol{\xi} + \mathbf{v}, \tag{8.3}$$

where $\boldsymbol{\xi} = \left[\mathbf{h}_1^T, \mathbf{h}_2^T, \ldots, \mathbf{h}_K^T\right]^T$, $\boldsymbol{\varepsilon} = [\varepsilon_1, \varepsilon_2, \ldots, \varepsilon_K]^T$ and $\Gamma(\boldsymbol{\varepsilon}) \triangleq [\mathbf{C}(\varepsilon_1)\mathbf{D}_1, \mathbf{C}(\varepsilon_2)\mathbf{D}_2, \ldots, \mathbf{C}(\varepsilon_k)\mathbf{D}_K]$.

8.3 A Review of the Iterative Non-separated LS Method

In this section, we review the iterative non-separated LS method for joint CFO and channel estimation. In this method, LS is used as the optimization criterion and all the parameters are treated together as a whole. Let us denote the vector of unknown parameters as $\boldsymbol{\theta} = [\boldsymbol{\xi}^T, \boldsymbol{\varepsilon}^T]^T$. Then (7.3) can be represented as

$$\mathbf{y} = \mathbf{f}(\boldsymbol{\theta}) + \mathbf{v}, \tag{8.4}$$

where $\mathbf{f}(\boldsymbol{\theta}) = \Gamma(\boldsymbol{\varepsilon})\boldsymbol{\xi}$. To estimate the unknown parameters, we try to find $\boldsymbol{\theta}$ that can minimize the LS cost function

$$J(\boldsymbol{\theta}) = \|\mathbf{y} - \mathbf{f}(\boldsymbol{\theta})\|^2 . \tag{8.5}$$

This nonlinear LS problem can be solved iteratively. By using the first order Taylor expansion in the neighborhood of a given point $\boldsymbol{\theta}^{(n)}$, $\mathbf{f}(\boldsymbol{\theta})$ can be approximated as

$$\mathbf{f}(\boldsymbol{\theta}) \approx \mathbf{f}(\boldsymbol{\theta}^{(n)}) + \mathbf{G}^{(n)}(\boldsymbol{\theta} - \boldsymbol{\theta}^{(n)}),$$

where $\mathbf{G}^{(n)}$ is the gradient of $\mathbf{f}(\boldsymbol{\theta})$ evaluated at $\boldsymbol{\theta} = \boldsymbol{\theta}^{(n)}$. The gradient $\mathbf{G} = \frac{\partial}{\partial \boldsymbol{\theta}^T}\mathbf{f}(\boldsymbol{\theta})$ is given by

$$\begin{aligned} \mathbf{G} \;=\; & [\mathbf{C}(\varepsilon_1)\mathbf{D}_1, \mathbf{C}(\varepsilon_2)\mathbf{D}_2, \ldots, \mathbf{C}(\varepsilon_K)\mathbf{D}_K, \\ & \Lambda\mathbf{C}(\varepsilon_1)\mathbf{D}_1\mathbf{h}_1, \Lambda\mathbf{C}(\varepsilon_2)\mathbf{D}_2\mathbf{h}_2, \ldots, \Lambda\mathbf{C}(\varepsilon_K)\mathbf{D}_K\mathbf{h}_K], \end{aligned} \tag{8.6}$$

where $\Lambda = j2\pi/N\mathrm{diag}([0, 1, \ldots, N-1])$. Therefore the cost function is approximated by

$$J(\boldsymbol{\theta}) \approx \| \mathbf{y} - \mathbf{f}(\boldsymbol{\theta}^{(n)}) - \mathbf{G}^{(n)}(\boldsymbol{\theta} - \boldsymbol{\theta}^{(n)}) \|^2 . \tag{8.7}$$

From (8.7), we observe that the nonlinear LS problem in (8.5) can now be solved iteratively by using a linear LS (LLS) approach at each iteration. Therefore, at the $(n+1)$th iteration, the unknown parameters are updated as $\boldsymbol{\theta}^{(n+1)} = \boldsymbol{\theta}^{(n)} + \boldsymbol{\delta}^{(n)}$, where

$$\boldsymbol{\delta}^{(n)} = [(\mathbf{G}^{(n)})^H\mathbf{G}^{(n)}]^{-1}(\mathbf{G}^{(n)})^H(\mathbf{y} - \mathbf{f}(\boldsymbol{\theta}^{(n)})). \tag{8.8}$$

8.4 Proposed Method

In this section, we propose a joint CFO and channel estimation method. The proposed method consists of two steps. In the first step, CFOs are estimated by using the VP method. We emphasize that the VP method is not new. However, to the authors' best knowledge, it has not been applied to the underlying estimation problem before. Then, in the second step, the channel coefficients are estimated by using the robust MMSE method.

8.4.1 VP Method for CFO Estimation

Following the approach in [76], we now present the VP method for CFO estimation by adapting the above result of the iterative non-separated LS method to the SNLLS problem in (8.5). We notice from (7.3) that the unknown parameters $\boldsymbol{\theta}$ can be separated into two sets, i.e., $\boldsymbol{\xi}$ and $\boldsymbol{\varepsilon}$, which consist of linear and nonlinear parameters, respectively. As that in [76], let us partition $\boldsymbol{\delta}^{(n)}$ as $\boldsymbol{\delta}^{(n)} = [(\boldsymbol{\delta}_{\boldsymbol{\xi}}^{(n)})^T, (\boldsymbol{\delta}_{\boldsymbol{\varepsilon}}^{(n)})^T]^T$, where $\boldsymbol{\delta}_{\boldsymbol{\xi}}^{(n)}$ and $\boldsymbol{\delta}_{\boldsymbol{\varepsilon}}^{(n)}$ consist of updates on the estimation of $\boldsymbol{\xi}$ and $\boldsymbol{\varepsilon}$, respectively. The idea of the VP method in [76] is that at the $(n+1)$th iteration, the nonlinear parameters are first updated by

$$\boldsymbol{\varepsilon}^{(n+1)} = \boldsymbol{\varepsilon}^{(n)} + \boldsymbol{\delta}_{\boldsymbol{\varepsilon}}^{(n)}. \tag{8.9}$$

Then, for a fixed $\boldsymbol{\varepsilon}^{(n+1)}$, the solution to the LLS problem $\min_{\boldsymbol{\xi}} ||\mathbf{y} - \Gamma(\boldsymbol{\varepsilon}^{(n+1)})\boldsymbol{\xi}||^2$ is used to update $\boldsymbol{\xi}$, that is

$$\boldsymbol{\xi}^{(n+1)} = [(\Gamma(\boldsymbol{\varepsilon}^{(n+1)}))^H \Gamma(\boldsymbol{\varepsilon}^{(n+1)})]^{-1} (\Gamma(\boldsymbol{\varepsilon}^{(n+1)}))^H \mathbf{y}. \tag{8.10}$$

To obtain an explicit expression for $\boldsymbol{\delta}_{\boldsymbol{\varepsilon}}^{(n)}$, let us partition $\mathbf{G}^{(n)}$ into two submatrices as $\mathbf{G}^{(n)} = [\mathbf{G}_{\boldsymbol{\xi}}^{(n)}\ \mathbf{G}_{\boldsymbol{\varepsilon}}^{(n)}]$, where $\mathbf{G}_{\boldsymbol{\xi}}^{(n)}$ and $\mathbf{G}_{\boldsymbol{\varepsilon}}^{(n)}$ consist of the first KL and the last K columns of $\mathbf{G}^{(n)}$, respectively. By using the block matrix inversion lemma [74, pp.

678], we have from (8.8) that

$$\boldsymbol{\delta}_{\varepsilon}^{(n)} = [\mathbf{A}\ \mathbf{B}^{-1}][\mathbf{G}_{\boldsymbol{\xi}}^{(n)}\ \mathbf{G}_{\varepsilon}^{(n)}]^H(\mathbf{y} - \mathbf{f}(\boldsymbol{\theta}^{(n)})),$$

where $\mathbf{B} = (\mathbf{G}_{\varepsilon}^{(n)})^H\mathbf{G}_{\varepsilon}^{(n)} - (\mathbf{G}_{\varepsilon}^{(n)})^H\mathbf{G}_{\boldsymbol{\xi}}^{(n)}[(\mathbf{G}_{\boldsymbol{\xi}}^{(n)})^H\mathbf{G}_{\boldsymbol{\xi}}^{(n)}]^{-1}\ (\mathbf{G}_{\boldsymbol{\xi}}^{(n)})^H\mathbf{G}_{\varepsilon}^{(n)}$. The submatrix $\mathbf{A}$ is not of interest as we have $(\mathbf{G}_{\boldsymbol{\xi}}^{(n)})^H(\mathbf{y} - \mathbf{f}(\boldsymbol{\theta}^{(n)})) = (\Gamma(\boldsymbol{\varepsilon}^{(n)}))^H(\mathbf{y} - \Gamma(\boldsymbol{\varepsilon}^{(n)})\boldsymbol{\xi}^{(n)}) = \mathbf{0}$, where the last equality comes from the way we obtain $\boldsymbol{\xi}^{(n)}$ in the nth iteration, i.e., (8.10) with $\boldsymbol{\xi}^{(n+1)}$ and $\boldsymbol{\varepsilon}^{(n+1)}$ replaced by $\boldsymbol{\xi}^{(n)}$ and $\boldsymbol{\varepsilon}^{(n)}$, respectively. Therefore, we obtain that

$$\begin{aligned}\boldsymbol{\delta}_{\varepsilon}^{(n)} &= \{(\mathbf{G}_{\varepsilon}^{(n)})^H\mathbf{G}_{\varepsilon}^{(n)} - (\mathbf{G}_{\varepsilon}^{(n)})^H\mathbf{G}_{\boldsymbol{\xi}}^{(n)}[(\mathbf{G}_{\boldsymbol{\xi}}^{(n)})^H\mathbf{G}_{\boldsymbol{\xi}}^{(n)}]^{-1}(\mathbf{G}_{\boldsymbol{\xi}}^{(n)})^H\mathbf{G}_{\varepsilon}^{(n)} + \eta^{(n)}\mathbf{I}_K\}^{-1} \\ &\quad \times(\mathbf{G}_{\varepsilon}^{(n)})^H(\mathbf{y} - \mathbf{f}(\boldsymbol{\theta}^{(n)})), \qquad (8.11)\end{aligned}$$

where $\eta^{(n)}$ is a positive value employed to stabilize the algorithm, which is known as the Levenberg-Marquardt technique [74, pp. 625].

Armed with the above discussion, we may now summarize the VP method as follows.

- Initially, set $\eta^{(0)}$ to a small value, i.e., $\eta^{(0)} = 0.01$ and $\boldsymbol{\varepsilon}^{(0)} = \mathbf{0}_K$.
- Obtain $\boldsymbol{\xi}^{(0)}$ by (8.10).
- At the $(n+1)$th iteration, with $n = 0, 1, \ldots,$
  - Calculate $\boldsymbol{\delta}_{\varepsilon}^{(n)}$, $\boldsymbol{\varepsilon}^{(n+1)}$ and $\boldsymbol{\xi}^{(n+1)}$ using (8.11), (8.9) and (8.10), respectively.
  - If $\boldsymbol{\theta}^{(n+1)}$ reduces the cost function such that $J(\boldsymbol{\theta}^{(n+1)})^{1/2} \leq J(\boldsymbol{\theta}^{(n)})^{1/2}$, then set $\eta^{(n+1)} = \eta^{(n)}/10$ and check the stopping criterion.
  - If within the $(n+1)$th iteration, $\boldsymbol{\theta}^{(n+1)}$ does not reduce the cost function, then $\eta^{(n)}$ is progressively increased by a factor, i.e., $\eta^{(n)} = 10\eta^{(n)}$, each time with $\boldsymbol{\delta}_{\varepsilon}^{(n)}, \boldsymbol{\varepsilon}^{(n+1)}$ and $\boldsymbol{\xi}^{(n+1)}$ recomputed until $J(\boldsymbol{\theta}^{(n+1)})^{1/2} \leq J(\boldsymbol{\theta}^{(n)})^{1/2}$ is achieved.

There are several recommended stopping criteria, such as the relative-change and relative-offset criterion [74, pp. 640]. For simplicity, we use the relative-change criterion proposed in [72] for this VP method. Therefore, after the $(n+1)$th iteration, if

$$J(\boldsymbol{\theta}^{(n)})^{1/2} - J(\boldsymbol{\theta}^{(n+1)})^{1/2} < \delta \tag{8.12}$$

is satisfied, then we stop the computation; otherwise, continue to the next iteration. This stopping criterion indicates how the algorithm is progressing and stops it when there is not much improvement. Therefore, δ is set to a small positive value.

8.4.2 Robust MMSE Channel Estimation

The above VP method provides estimation for both CFOs and channel coefficients based on the LS criterion, i.e., $\boldsymbol{\varepsilon}^{(n_0)}$ and $\boldsymbol{\xi}^{(n_0)}$, where n_0 denotes the index of the last iteration of the VP method. We observed from the simulation results, however, that the VP method provides a good CFO estimation performance, but it does not provide reliable channel estimation when the number of users is relatively large. This is because of the LS criterions, where optimality is not guaranteed. This motivates us to use the MMSE channel estimation method, that is

$$\hat{\boldsymbol{\xi}} = [(\Gamma(\boldsymbol{\varepsilon}^{(n_0)}))^H \Gamma(\boldsymbol{\varepsilon}^{(n_0)}) + \sigma_v^2 \mathbf{R}_{\boldsymbol{\xi}\boldsymbol{\xi}}^{-1}]^{-1} (\Gamma(\boldsymbol{\varepsilon}^{(n_0)}))^H \mathbf{y},$$

where $\mathbf{R}_{\boldsymbol{\xi}\boldsymbol{\xi}} = E\{\boldsymbol{\xi}\boldsymbol{\xi}^H\}$. As the channel power delay profile (PDP) as well as the timing offset are usually unknown, we do not have knowledge of $\mathbf{R}_{\boldsymbol{\xi}\boldsymbol{\xi}}$. So, we resort to the robust MMSE channel estimation method [78].

Let us define the received SNR as

$$\rho = \frac{\sum_{k=1}^{K} \sigma_{b,k}^2 \sigma_{h,k}^2}{\sigma_v^2},$$

where $\sigma_{b,k}^2 = E\{|b_{k,n}|^2\} = \frac{N_k P_k}{N}$ denotes the average power of the time-domain samples

of the kth user's training signal. We assume that the estimation of ρ is available at the receiver and is denoted by $\hat{\rho}$. Let us denote the received signal power of user k as $\sigma_k^2 = \sigma_{b,k}^2 \sigma_{h,k}^2$. We also assume that σ_k^2's are roughly equal for all users implying that some power control algorithm is used. Then, the robust MMSE channel estimator is given by [78]

$$\hat{\boldsymbol{\xi}} = [(\Gamma(\boldsymbol{\varepsilon}^{(n_0)}))^H \Gamma(\boldsymbol{\varepsilon}^{(n_0)}) + \hat{\rho}^{-1} KL\mathbf{A}]^{-1} (\Gamma(\boldsymbol{\varepsilon}^{(n_0)}))^H \mathbf{y}, \tag{8.13}$$

where $\mathbf{A}$ =diag$([\sigma_{b,1}^2, \sigma_{b,2}^2, \ldots, \sigma_{b,K}^2]) \otimes \mathbf{I}_L$.

8.5 Complexity Analysis

In this section, we analyze the required number of multiplications of the proposed method and compare it with that of the non-separated MMSE method in [72]. In what follows, several established facts are used. To obtain an inverse of an $m \times m$ matrix, a multiplication of an $m_1 \times m_2$ matrix with an $m_2 \times m_3$ matrix, a multiplication of an $m_1 \times m_1$ diagonal matrix with an $m_1 \times m_2$ matrix, the numbers of multiplications are m^3, $m_1 m_2 m_3$, and $m_1 m_2$, respectively.

Let us first consider the proposed method. For the initialization of the VP method, the number of multiplications required in calculating $\boldsymbol{\xi}^{(0)}$ and $J(\boldsymbol{\theta}^{(0)})$ is given by $c_{\text{VP},0} = (K^2L^2N + K^3L^3 + KLN + K^2L^2) + (KLN + N)$. At each iteration of the VP method, we need to evaluate $\mathbf{G}^{(n)}$, $\boldsymbol{\delta}_{\varepsilon}^{(n)}$, $\boldsymbol{\xi}^{(n+1)}$ and $J(\boldsymbol{\theta}^{(n+1)})$ for at least one time with the number of required multiplications given by $c_{\text{VP},1} = (KN) + (K^2N + K^2LN + K^3L^2 + K^3L + K + K^3 + KN + K^2) + (2KLN + K^2L^2N + K^3L^3 + K^2L^2) + (KLN + N)$, where we have assumed that $[(\mathbf{G}_{\boldsymbol{\xi}}^{(n)})^H \mathbf{G}_{\boldsymbol{\xi}}^{(n)}]^{-1}$ has already been evaluated in the last iteration and its value is stored for use in this iteration. If, within an iteration, $\eta^{(n)}$ is updated, then $\boldsymbol{\delta}_{\varepsilon}^{(n)}$, $\boldsymbol{\xi}^{(n+1)}$ and $J(\boldsymbol{\theta}^{(n+1)})$ are required to be evaluated again with the number of multiplications given by $c_{\text{VP},2} = (K + K^3 + K^2) + (2KLN + K^2L^2N + K^3L^3 + K^2L^2) + (KNL + N)$. Finally, the robust MMSE channel estimation method requires the number of multiplications given by $c_{\text{MMSE}} = K^3L^3 + K^2L^2$, where we have assumed

that $(\Gamma(\boldsymbol{\varepsilon}^{(n_0)}))^H\Gamma(\boldsymbol{\varepsilon}^{(n_0)})$ and $(\Gamma(\boldsymbol{\varepsilon}^{(n_0)}))^H\mathbf{y}$ have already been evaluated before by the VP method and are stored for use by the robust MMSE channel estimator. Therefore, the total number of multiplications is $c = c_{\text{VP},0} + n_1 c_{\text{VP},1} + n_2 c_{\text{VP},2} + c_{\text{MMSE}}$ where n_1 is the number of iterations, and n_2 is the number of times that η is updated.

Next, let us consider the non-separated MMSE method in [72]. In the initialization step, in calculating $\boldsymbol{\xi}^{(0)}$ and $J(\boldsymbol{\theta}^{(0)})$, the required number of multiplications is $c_{\text{non-separated},0} = (K(L^2N+L^3+LN+L^2))+(KNL+N)$. In each iteration, $\mathbf{G}^{(n)}$, $\boldsymbol{\theta}^{(n+1)}$ and $J(\boldsymbol{\theta}^{(n+1)})$ are required to be evaluated for at least one time with the number of multiplications given by $c_{\text{non-separated},1} = (KN)+(K^2(L+1)^2N+K^3(L+1)^3+K(L+1)N+K^2(L+1)^2+K(L+1))+(2KNL+N)$. If within an iteration, $\beta^{(n)}$ is updated, then $\boldsymbol{\theta}^{(n+1)}$ and $J(\boldsymbol{\theta}^{(n+1)})$ are required to be reevaluated with the number of multiplications given by $c_{\text{non-separated},2} = (K(L+1))+(2KNL+N)$. The total number of multiplications is similarly given by $c = c_{\text{non-separated},0} + n_1 c_{\text{non-separated},1} + n_3 c_{\text{non-separated},2}$, where n_3 denotes the number of times when β is updated. We will demonstrate the total number of multiplications of the two methods by using simulation results in the next section.

8.6 Simulation Results

In this section, we examine the performance of the proposed method. The OFDM system is assumed to have $N = 128$ subcarriers with length of CP $L = 16$. In each run of the simulations, every user is assigned $N_k = \lfloor N/K \rfloor$ interleaved pilot subcarriers and the pilot symbols are generated randomly from a binary phase-shift keying (BPSK) constellation. The power of the training symbol on each subcarrier is $P_k = 1$. The multipath fading channel has $L_k = 6$ paths and an exponential power delay profile for all users , i.e., $\sigma_{h,k,l}^2 = \frac{1}{\sum_{i=0}^{5} e^{-i}} e^{-l}$, $l = 0, 1, ..., 5$. The power of each user's channel impulse response is normalized to unity, i.e., $\sigma_{h,k}^2 = 1$, unless stated otherwise. The timing offsets are integers uniformly distributed in the range $[0, 10]$. The CFOs are uniformly distributed in the range $[-0.5, 0.5]$. The SNR is defined

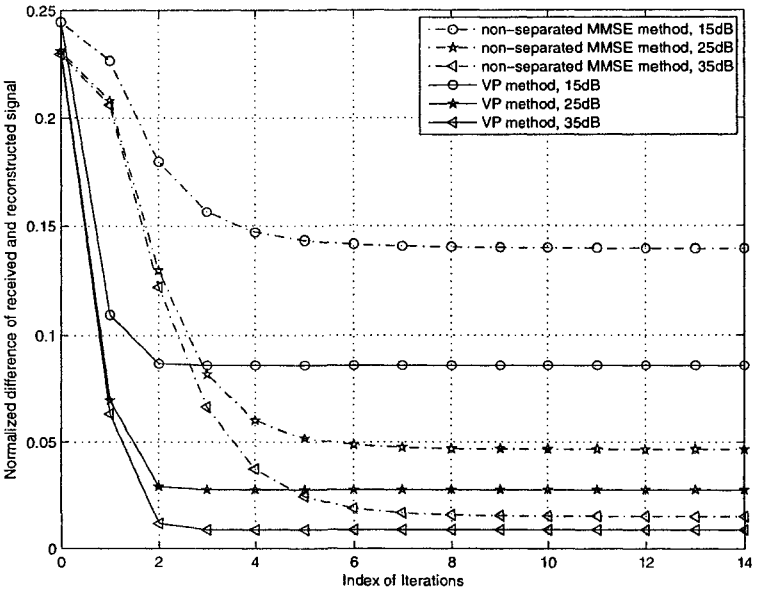

Figure 8.1: Comparison of the convergence speed in terms of $E\{\frac{\|\mathbf{y}-\mathbf{f}(\boldsymbol{\theta}^{(n)})\|}{\|\mathbf{y}\|}\}$ as a function of iteration of the VP method and the non-separated MMSE method with $K = 6$.

as $\frac{P_k}{\sigma_v^2}$. The figures shown in this section are obtained by averaging 10,000 runs of simulation. The MSE and CRLB [47] are obtained by averaging over all active users in the system unless stated otherwise.

We compare the proposed method and the non-separated MMSE method [72] in terms of the convergence speed, MSE performance, computational complexity and near-far effect. For the non-separated MMSE method, γ is fixed and β is reduced repeatedly if required, i.e., $\gamma = 1$ and $\beta = \frac{5}{6}\beta$. Unless stated otherwise, when $\beta < 10^{-15}$, β is set to 0 to terminate the line search process.

8.6.1 Convergence Speed

With the progress of the iterative VP method, we should observe convergence in two sequences, $\boldsymbol{\varepsilon}^{(n+1)} - \boldsymbol{\varepsilon}^{(n)} \rightarrow \mathbf{0}$, and $J(\boldsymbol{\theta}^{(n+1)}) - J(\boldsymbol{\theta}^{(n)}) \rightarrow 0$. In Figs. 8.1 and 8.2, we show $E\{\frac{\|\mathbf{y}-\mathbf{f}(\boldsymbol{\theta}^{(n)})\|}{\|\mathbf{y}\|}\}$ and MSE of CFO estimation as a function of iteration for the VP

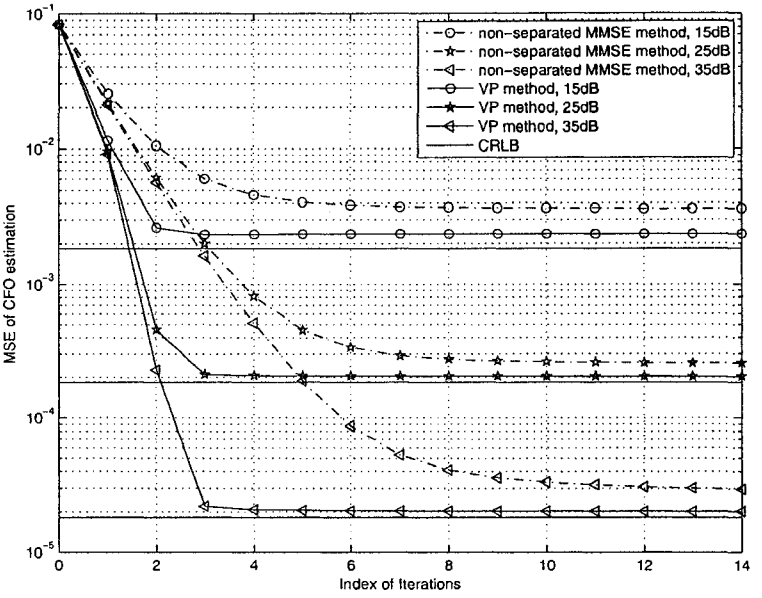

Figure 8.2: Comparison of the convergence speed in terms of the MSE of CFO estimation as a function of iteration of the VP method and the non-separated MMSE method with $K = 6$.

method and the non-separated MMSE method with $K = 6$ and at several SNRs. We observe that the VP method converges faster than the non-separated MMSE method.

8.6.2 MSE Performance

In Fig. 8.3, we show the MSE of CFO estimation for $K = 2, 4, 6$ users, respectively. The same stopping criterion, i.e., (8.12) with $\delta = 0.1\sigma_v$, is employed for the two methods. We observe that the VP method can achieve the CRLB while the non-separated MMSE method [72] diverges away from the CRLB at high SNR for $K = 6$. By employing the same stopping criterion for the two methods, the better performance achieved by the VP method also confirms that the VP method results in a better defined minimization problem. We also show in the figure that the performance of the non-separated MMSE method can be improved to get closer to the CRLB by using a more stringent stopping criterion, i.e., $\delta = 0.01\sigma_v$ for $K = 6$ users. But this

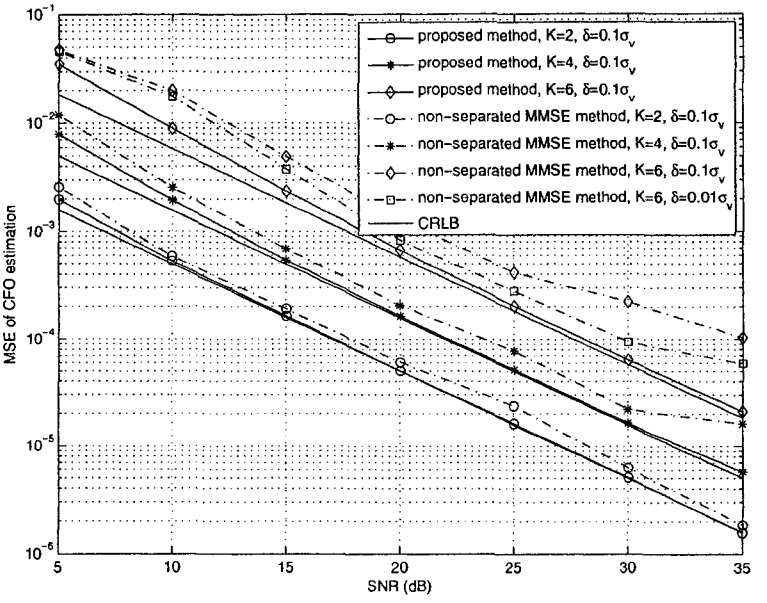

Figure 8.3: Comparison of the MSE of CFO estimation of the proposed method and the non-separated MMSE method with $K = 2$, 4, and 6.

is at the cost of an increased computational complexity. Furthermore, even with this additional complexity, the performance of the non-separated MMSE method is still inferior to that of the proposed method.

In Fig. 8.4, we show the normalized MSE (NMSE) performance of channel estimation of the two methods. The NMSE of channel estimation is defined as

$$\text{NMSE}_h = \frac{1}{N_s KL} \sum_{i=1}^{N_s} \sum_{k=1}^{K} \frac{||\hat{\mathbf{h}}_k^{(i)} - \mathbf{h}_k^{(i)}||^2}{||\mathbf{h}_k^{(i)}||^2},$$

where N_s is the number of simulation runs, $\hat{\mathbf{h}}_k^{(i)}$ and $\mathbf{h}_k^{(i)}$ are the estimated and the true effective channel, respectively. The true received SNR ρ is used in (8.13) by the proposed method. We observe that the proposed method can achieve better performance than that of the non-separated MMSE method. We further notice that the performance of the proposed method is better than the CRLB in some cases. This is because the proposed channel estimation method is based on the MMSE criterion

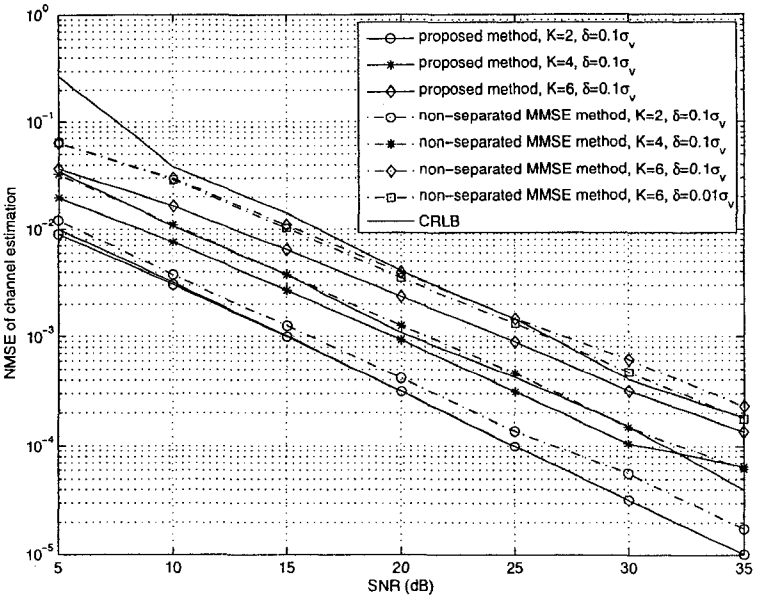

Figure 8.4: Comparison of the NMSE of channel estimation of the proposed method and the non-separated MMSE method with $K = 2$, 4, and 6.

where the second order statistics of the noise and channel are incorporated into the estimation process, whereas the CRLB is derived by treating CFO and channel coefficients as unknown constants. The CRLB is shown here only for the purpose of comparison.

8.6.3 Computational Complexity

In Fig. 8.5, we compare the computational complexity of the two methods in terms of the required average number of multiplications c. Firstly, the two methods are compared by using the same stopping criterion, i.e., (8.12) with $\delta = 0.1\sigma_v$. For the non-separated MMSE method, by setting $\beta = 0$ until $\beta < 10^{-15}$, we observe that its required average time by performing the method using Matlab is much greater than that of the proposed method. The reason for this is that in some cases the line search process only ends after updating β for about $\log_{(5/6)}^{10^{-13}} = 164$ or more times which is very time consuming. We also notice that by doing this, it only provides a

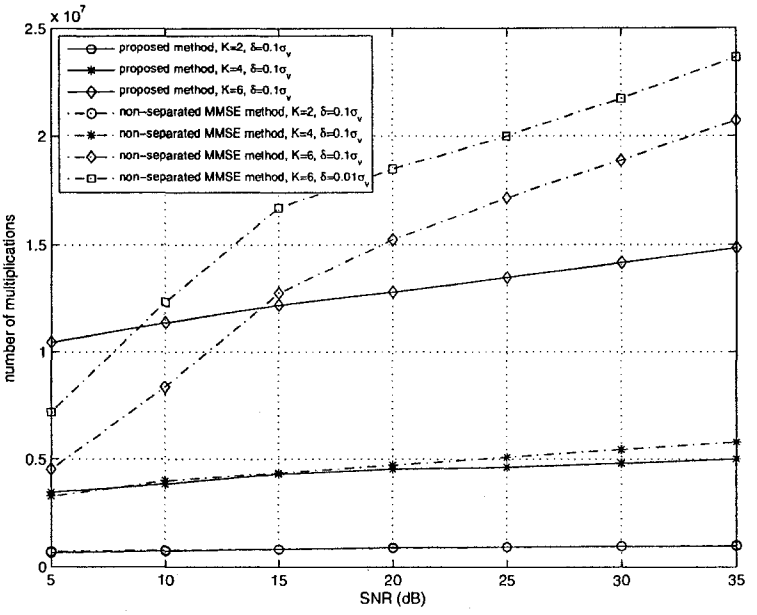

Figure 8.5: Comparison of the required number of multiplications of the proposed method and the non-separated MMSE method with $K = 2$, 4, and 6.

marginal performance improvement. Therefore, in order to obtain a fair comparison, for the non-separated MMSE method, β is set to 0 when $\beta < 0.4$ for $K = 2$ and 4; and β is set to 0 when $\beta < 0.04$ for $K = 6$ in obtaining the results in Fig. 8.5 for $\delta = 0.1\sigma_v$. This does not degrade their corresponding performance at all but saves lots of computations.

We observe from Fig. 8.5 that for $\delta = 0.1\sigma_v$, the computational burden of the proposed method is lower than that of the non-separated MMSE method at high SNRs particularly for large number of users. For $K = 6$ at 35dB, the non-separated MMSE method requires as many as 8.3 iterations on average to achieve convergence, whereas the proposed method only needs 3.7 iterations on average to achieve convergence. For this scenario, by using the proposed method, the computational burden can be saved by about 25%.

In Figs. 8.3 and 8.4, we have shown that by setting $\delta = 0.01\sigma_v$, the non-separated MMSE method can improve its performance a little. However, this comes at the cost

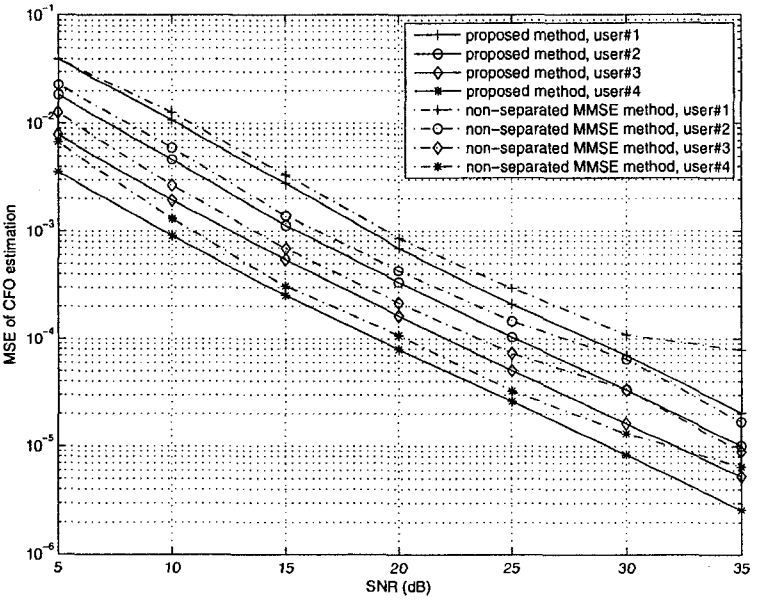

Figure 8.6: Comparison of the MSE of CFO estimation of the proposed method and the non-separated MMSE method with $K = 4$ and $\delta = 0.1\sigma_v$ in the presence of near-far effect.

of an increased complexity. In Fig. 8.5, we show the required number of multiplications of the non-separated MMSE method with $\delta = 0.01\sigma_v$, where β is set to 0 when $\beta < 0.1$ to save computations. As shown in the figure, the complexity of the non-separated MMSE method is higher than that of the proposed method at medium to high SNRs.

8.6.4 Impact of the Near-Far Problem

In practice, we may not have ideal power control. Next, we will show the impact of the near-far problem on the performance of the proposed method. Let us consider a system with $K = 4$ users. The power of each user's channel impulse response is set at $\sigma_{h,1}^2 = 1/4$, $\sigma_{h,2}^2 = 1/2$, $\sigma_{h,3}^2 = 1$ and $\sigma_{h,4}^2 = 2$, respectively. In Figs. 8.6 and 8.7, we show the CFO estimation and channel estimation performance of the two methods with respect to each user individually. Both methods use the same stopping

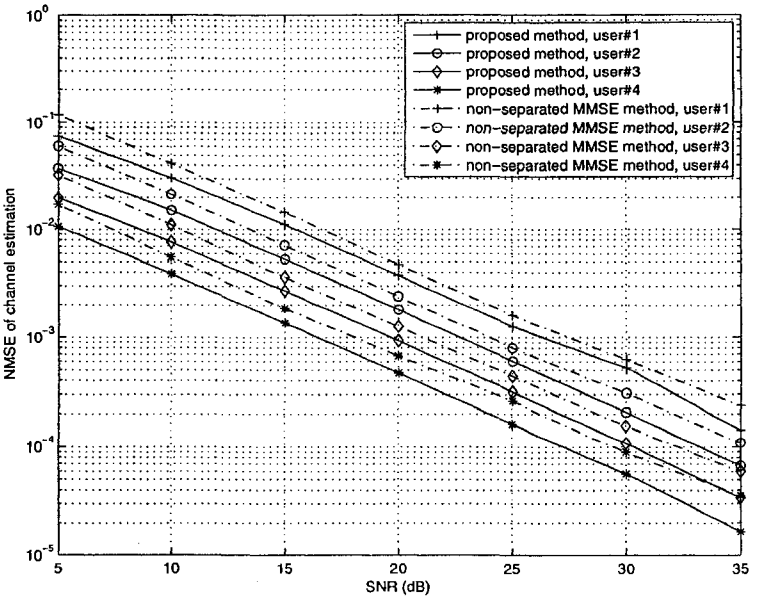

Figure 8.7: Comparison of the NMSE of channel estimation of the proposed method and the non-separated MMSE method with $K = 4$ and $\delta = 0.1\sigma_v$ in the presence of near-far effect.

criterion with $\delta = 0.1\sigma_v$. We observe that the proposed method performs better than the non-separated MMSE method in the presence of near-far problem in both CFO estimation and channel estimation.

8.7 Conclusions

In this chapter, we proposed a training-aided joint CFO and channel estimation method for the uplink channel of OFDM systems. The proposed scheme consists of two steps, where the VP method is used for CFO estimation and the robust MMSE method is used for channel estimation. We examined the proposed method in terms of the convergence speed, MSE performance, and computational complexity and compared it to those of the non-separated MMSE method. We demonstrated that the proposed method is superior to the non-separated MMSE method in terms

of convergence-speed and MSE performance. The computational burden of the proposed scheme is lower than that of the non-separated MMSE method for a large number of users at high SNRs.

Chapter 9

Conclusions and Future Work

9.1 Conclusions

We started with a literature review on the existing CFO estimation schemes. For the downlink channel, blind estimation schemes are classified based on the implicit properties that are exploited for estimation, e.g., CP-based, VSC-based, oversampling-based, CM-based, cyclostationarity-based and higer-order statistic based estimation schemes. Based on different intrinsic properties, different cost functions have been designed. To minimize the cost function, grid search method, Newton method, curve fitting method and root finding method can be used. For the uplink channel, estimation schemes are classified based on the CAS. As each user has its own CFO, CFO estimation for uplink channel is a more challenging problem. Some of these schemes directly extend the schemes for downlink channel to the uplink channel having block CAS. Some of these schemes exploit the characteristics introduced by the interleaved CAS in particular for estimation. Some other schemes take an approach to breakdown the multi-dimensional optimization problem into several one-dimensional optimization problems to reduce the complexity of CFOs estimation for the arbitrary CAS. While MSE is a major criterion to measure the performance of all kinds of estimation schemes, other criteria such as identifiability and computational complexity should also be taken into the consideration of the estimator design.

9.1.1 OFDM Downlink

For the downlink channel of OFDM systems, we designed three blind CFO estimation schemes.

By taking the UML approach, we proposed a VSC-based CFO estimation scheme for MIMO-OFDM systems in the presence of spatial correlation. The spatial correlation is introduced by closely placed antennas. The advantage of the UML approach is that it treats the nuisance parameters, i.e., channel and data, as random variables with known statistics. In this sequel, it enables us to incorporate spatial correlation into the CFO estimation naturally. In particular, we investigated the impact of receive spatial correlation on the CFO estimation. We show that, as compared to the CML estimator, the UML estimator can exploit the knowledge of receive spatial correlation as well as the existence of VSCs to make additional contribution for CFO estimation. But, this additional contribution is marginal as compared to the CML estimator. The implication of this result is that one need not take spatial correlation into account in developing VSC-based CFO estimation scheme for MIMO-OFDM systems. This should simplify such development process.

We also proposed a novel FFO estimation scheme with low complexity for OFDM systems employing CM signaling. We assume that the channel frequency response changes slowly in the frequency domain such that the channel frequency response on two consecutive subcarriers is approximately the same. Based on this assumption, we proposed a cost function which minimizes the difference of the signal power for each pair of consecutive subcarriers. Then, we proved that the proposed cost function is in a form of a cosine function and achieves its minimum at the true CFO. Furthermore, to minimize the cost function, the curve fitting method is used which only requires to evaluate the cost function at three points and makes the proposed estimation scheme very simple. We also extent the proposed scheme to MIMO-OFDM systems by exploiting the orthogonal structure of the employed OSTBCs. The proposed scheme significantly outperforms the kurtosis-type scheme in both SISO and MIMO systems at almost the same computational complexity. Compared with the

CM based subspace scheme, the proposed scheme has a lower computational complexity but it performs a little worse than the CM based subspace scheme over severe frequency selective fading channels.

Furthermore, we designed a FA based FFO estimator for DOFDM systems in which symbols are differentially modulated along the time direction on each subcarrier using an M-PSK modulation. The cost function is proposed under the assumption that channel keeps constant over two consecutive OFDM symbols. As the proposed scheme actually involves a symbol detection process implicitly within the estimation process, its cost function is very complicated such that it is almost prohibited to minimize the cost function by using the grid search method. Therefore, we modified the Newton method a little bit and applied it to minimize the proposed cost function efficiently. We also derived the constrained CRLB as a benchmark for blind CFO estimation method. The advantage of the proposed scheme is that it can achieve a better performance at high SNRs than that of the existing CM based subspace scheme. Furthermore, it has a wider application to systems having VSCs whereas the CM based subspace scheme can not. However, it requires to use two consecutive OFDM symbols and is sensitive to channel variations. Furthermore, it has a higher computational complexity than the CM based subspace scheme.

9.1.2 OFDM Uplink

As for the uplink channel of OFDM systems, we designed two training-aided CFO estimation schemes for the arbitrary CAS. One is based on a scalar EKF and the other one is on VP algorithm.

In the scalar EKF based scheme, at each recursion, the MAI cancellation is used to separate each user's measurement based on CFO and channel estimations obtained from a previous recursion. After that, we observe that the kth user's measurement depends not only on the kth user's CFO but also on a vector which consists of the kth user's channel coefficients and the other users' channel estimation errors. Therefore, in order to apply the scalar EKF, we replace this vector with a non-linear function

of CFO such that each user's measurement is now represented as a function of its CFO only. We also analyzed the observation noise power and use its approximation in the EKF algorithm. The simulation results show that the proposed scheme can achieve the CRLB at high SNR for two users with a complexity lower than that of the APFE and close to that of the SAGE. However, its performance degrades with increased number of users.

In the VP-based scheme, the CFOs are estimated by minimizing the LS cost function. By observing that this is a separable nonlinear LS problem, the VP method is applied to solve it iteratively. The idea behind the VP method is that at each iteration, the nonlinear parameters, i.e., the CFOs, are first updated, then the solution to the LLS problem is used to update the linear parameters, i.e., the channel coefficients. The advantage of the VP method is that it results in a better conditioned problem which indicates convergence in a fewer number of iterations in comparison with the non-separated method. Following the VP method, the channel estimation is obtained by using the robust MMSE method. We demonstrate through several numerical examples the superiority of the proposed scheme to the non-separated MMSE method in terms of convergence speed, computational complexity and estimation performance

9.2 Future Work

9.2.1 Optimum Training Sequence Design

In Chapters $4-6$, we propose blind CFO estimation schemes for the downlink channel of OFDM systems. The blind schemes are bandwidth efficient but rely on some inherent properties of the transmitted signal which implies some limits on their applications. Therefore, the pilot-aided and the training-aided estimation schemes are preferred in some scenarios. Many pilot-aided or training-aided estimation schemes have been proposed. But, most of the works in the literature focus on developing estimation methods and little attention has been devoted to the optimal training sequence design.

The training sequences used in the literature are usually generated randomly or chosen to take a particular structure in view of simplifying the estimation algorithm but not in aim to optimize the estimation performance. Actually, while the estimation methods target on how to achieve as better performance as possible, the characteristic of the training sequence answers what is the best estimation performance that exists to be achieved. Therefore, the training sequence is like a bottle neck. The only effort on developing efficient estimation method is far from enough. As a matter of fact, if the training sequence is not optimized, it may result in a poor estimation no matter how complex the estimation method is.

The optimal training sequence design involves selecting the training sequences which can give the best estimation performance among all the possible training sequences. It consists of selecting the pilot tone locations, the training sequence structures and the power allocation in both frequency and time domain. It is another approach that we can resort to obtain a simplified yet reliable estimator. In addition, a training sequence which is optimal for one scenario is not necessary optimal for the other. This indicates that the optimal training sequence design is much needed in practice where more constrains are present.

Firstly, the training sequence design for channel estimation in the presence of VSCs still constitutes an open problem. As a matter of fact, some optimal training sequences have been developed in the literature, but they are developed based on certain conditions, e.g., without the presence of VSCs, and not for the practical system configuration. However, by incorporating the presence of the VSCs into the development, it complicates the process in finding the solution to this optimization problem. Therefore, the optimal and robust training sequence design in more practical situations becomes an urgent issue needs to be addressed.

Secondly, the optimal training sequence design for both CFO and channel estimation is a long-standing problem. Training sequence design is usually studied separately for CFO estimation and channel estimation. The implication of this is that a training sequence that is optimal for CFO estimation may not necessarily be

optimal for the channel estimation. This implicates that individual training sequences which target on channel estimation and CFO estimation respectively have to be sent before the data transmission. This actually degrades the system bandwidth usage. In light of this, we believe the training sequence that can benefit both CFO and channel estimation to some extent is still lacking in the literature and deserves more research.

9.2.2 Channel Estimation and Synchronization for Cooperative Transmissions

MIMO systems and space-time coding techniques have demonstrated their advantages in increasing throughput and diversity gain by deploying multiple antennas. However, when the multiple antennas are collocated, there is a challenge in keeping these antennas far apart from each other so that they are not correlated. Furthermore, to keep the size small and the cost affordable, some wireless devices such as cellular phones can not afford having multiple antennas mounted on them. These challenges triggered the idea of cooperative transmissions.

Cooperative transmission is a new technology aiming at improving diversity for wireless communications. The ideal behind it is that the source node and the relays cooperatively accomplish the transmission to the destination such that a virtual multiple-transmit-antenna system is formed. The cooperative transmission has received lots of investigations recently. Most of works are based on the assumption of perfect channel estimation and synchronization. Channel estimation and synchronization for this configuration is still under investigation and can be considered as future work. We believe it is much harder and complicated than that for the centralized MIMO systems.

Bibliography

[1] ETSI EN 300 401 v1.3.3 (2001-05), *Radio broadcasting systems; Digital audio broadcasting (DAB) to mobile, portable and fixed receivers,* May 2001.

[2] ETSI, *Digital video broadcasting: Framing structure, channel coding and modulation for digital terrestrial television*, European Telecommunications Standard, EN 300−744, Aug. 1997.

[3] IEEE, *Part 11: Wireless LAN Medium Access Control (MAC) and Physical Layer (PHY) Specifications. High-speed Physical Layer in the* 5 *GHz Band*, IEEE Std 802.11a, 1999.

[4] IEEE, *Part 11: Wireless LAN Medium Access Control (MAC) and Physical Layer (PHY) Specifications. Amendment* 4*: Further Higher Data Rate Extension in the* 2.4 *GHz Band*, IEEE Std 802.11g, 2003.

[5] ETSI, *ETSI TS* 101 475. *Broadband Radio Access Networks (BRAN); HIPERLAN Type* 2*; Physical (PHY) layer*, Dec. 2001.

[6] *IEEE Standard for Local and Metropolitan Area Networks Part* 16: *Air Interface for Fixed Broadband Wireless Access Systems,* IEEE Std 802.16-2004 (Revision of IEEE Std 802.16-2001), pp. 1−857, 2004.

[7] Y. K. Kim and R. Prasad, 4*G roadmap and emerging communication technologies,* Boston : Artech House, 2006.

[8] UMTS: H. Holma and A. Toskala, *WCDMA for UMTS*, John Wiley and Sons, 2000.

[9] E. Telatar, "Capacity of multi-antenna Gaussian channels," *AT&T Bell Labs Internal Memo.*, Jun. 1995.

[10] G. Foschini and M. Gans, "On limits of wireless communications in a fading environment when using multiple antennas," *IEEE Wireless Pers. Commun.*, vol. 6, no. 3, pp. 311–335, Mar. 1998.

[11] V. Tarokh, H. Jafarkhani, and A. R. Calderbank, "Space-time block codes from orthogonal designs," *IEEE Trans. Inf. Theory,* vol. 45, no. 5, pp. 1456–1467, July 1999.

[12] V. Tarokh, N. Seshadri, and A. R. Calderbank, "Space-time codes for high data rate wireless communication: Performance criterion and code construction," *IEEE Trans. Inf. Theory*, vol. 44, pp. 744–765, Mar. 1998.

[13] G. J. Foschini, "Layered space-time architecture for wireless communication in a fading environment when using multi-element antennas," *Bell Laboratories Technical Journal*, vol. 2, pp. 41–59, Autumn 1996.

[14] H. EI Gamal and A. R. Hammons, "The layered space-time architecture: a new perspective," *IEEE Trans. Inf. Theory*, vol. 47, pp. 2321–2334, Sept. 2001.

[15] V. Tarokh, A. Naguib, N. Seshadri, and A. R. Calderbank, "Combined array processing and space-time coding," *IEEE Trans. Inf. Theory*, vol. 45, no. 4, pp. 1121–1128, May 1999.

[16] M. T. Zhong, A. B. Premkumar, and A. S. Madhukumar, "Performance investigation of STBC-OFDM systems with frequency offset and semi-blind approach for the correction," in *Proc. IEEE Veh. Technol. Conf.*, Vol.4, pp. 1836–1839, May 2004.

[17] H. A. Suraweera and J. Armstrong, "Performance of V-BLAST MIMO-OFDM systems with carrier frequency offset," in *Proc. IEEE Communications Theory Workshop*, pp. 73–78, Feb. 2005.

[18] J.-J. Van de Beek, M. Sandell, and P. O. Börjesson, "ML estimation of time and frequency offset in OFDM systems," *IEEE Trans. Signal Process.*, vol. 45, pp. 1800–1805, Jul. 1997.

[19] N. Lashkarian and S. Kiaei, "Class of cyclic-based estimators for frequency-offset estimation of OFDM systems," *IEEE Trans. Commun.*, vol. 48, pp. 2139–2149, Dec. 2000.

[20] M. Tanda, "Blind symbol-timing and frequency-offset estimation in OFDM systems with real data symbols," *IEEE Trans. Commun.*, vol. 52, pp. 1609–1612, Oct. 2004.

[21] H. Liu and U. Tureli, "A high-efficiency carrier estimator for OFDM communications," *IEEE Commun. Lett.*, vol. 2, pp. 104–106, Apr. 1998.

[22] S. Attallah, "Blind estimation of residual carrier offset in OFDM systems," *IEEE Signal Process. Lett.*, vol.11, pp. 216–219, Feb. 2004.

[23] B. Chen and H. Wang, "Maximum likelihood estimation of OFDM carrier frequency offset," in *Proc. IEEE Int. Conf. Commun.*, vol. 1, pp. 49–53, 2002.

[24] U. Tureli, H. Liu, and M. D. Zoltowski, "OFDM blind carrier offset estimation: ESPRIT," *IEEE Trans. Commun.*, vol. 48, pp. 1459–1461, Sept. 2000.

[25] P. Stoica and R. L. Moses, *Introduction to Spectral Analysis,* Prentice-Hall, 1997.

[26] X. Ma, C. Tepedelenlioğlu, G. B. Giannakis, and S. Barbarossa, "Non-data-aided carrier offset estimators for OFDM with null subcarriers: identifiability, algorithms, and performance," *IEEE J. Sel. Areas Commun.*, vol. 19, pp. 2504–2515, Dec. 2001.

[27] X. Ma, O. Mi-Kyung, G. B. Giannakis, and D. Park, "Hopping pilots for estimation of frequency-offset and multiantenna channels in MIMO-OFDM," *IEEE Trans. Commun.*, vol. 53, pp. 162–172, Jan. 2005.

[28] B. Chen and H. Wang, "Blind estimation of OFDM carrier frequency offset via oversampling," *IEEE Trans. Signal Process.*, vol. 52, pp. 2047–2057, Jul. 2004.

[29] M. Ghogho and A. Swami, "Blind frequency-offset estimator for OFDM systems transmitting constant-modulus symbols," *IEEE Commun. Lett.*, vol. 6, pp. 343–345, Aug. 2002.

[30] T. Roman and V. Koivunen, "Subspace method for blind CFO estimation for OFDM systems with constant modulus constellations," in *Proc. IEEE Veh. Technol. Conf.*, vol. 2, pp. 1253–1257, 2005.

[31] M. Lu, A. Nallanathan, and T. T. Tjhung, "Decoupled maximum likelihood blind carrier offset estimation for OFDM systems, " in *Proc. IEEE Veh. Technol. Conf.*, vol. 1, pp. 507–510, 2004.

[32] T. Roman and V. Koivunen, "Blind CFO estimation in OFDM systems using diagonality criterion," in *Proc. IEEE ICASSP*, vol. 4, pp. 369–372, May 2004.

[33] H. Bölcskei, "Blind estimation of symbol timing and carrier frequency offset in wireless OFDM systems," *IEEE Trans. Commun.*, vol. 49, pp. 988–999, Jun. 2001.

[34] B. Park, H. Cheon, E. Ko, C. Kang, and D. Hong, "A blind OFDM synchronization algorithm based on cyclic correlation," *IEEE Signal Process. Lett.*, vol. 11, pp. 83–85, 2004.

[35] M. Luise, M. Marselli, and R. Reggiannini, "Low-complexity blind carrier frequency recovery for OFDM signals over frequency-selective radio channels," *IEEE Trans. Commun.*, vol. 50, pp. 1182–1188, Jul. 2002.

[36] W. Chung and C. R. Johnson, "Blind carrier frequency offset synchronization for OFDM systems based on higher order statistics," in *Proc. of Conf. Inf. Sci. Syst.,* Princeton, NJ, Mar. 2002, pp. 624–629.

[37] Y. Yao and G. B. Giannakis, "Blind carrier frequency offset estimation in SISO, MIMO, and multiuser OFDM systems," *IEEE Trans. Commun.,* Vol. 53, pp. 173–183, 2005.

[38] J. Lee, H. Lou, D. Toumpakaris, and J. M. Cioffi, "A blind frequency tracking algorithm for OFDM transmission over frequency selective channels," in *Proc. IEEE Veh. Technol. Conf.,* vol. 1, pp. 578–582, 2004.

[39] J-J van de Beek, P. O. Börjesson, and et al., "A time and frequency synchronization scheme for multiuser OFDM," *IEEE J. Sel. Areas Commun.*, Vol. 17, pp. 1900–1914, Nov. 1999.

[40] S. Barbarossa, M. Pompili, and G.B. Giannakis, "Channel-independent synchronization of orthogonal frequency division multiple access systems," *IEEE J. Sel. Areas Commun.*, Vol. 20, pp. 474–486, Feb. 2002.

[41] D. Yoon and D. S. Han, "Robust frequency offset estimation with a single symbol for FH-OFDMA," *IEEE Wireless Telecommunications Symposium*, pp. 149–154, 2005.

[42] D. Niu and X. Dai, "Iterative carrier frequency offset estimation for OFDMA uplink based on null subcarriers," *IEEE 40th Annual Conference on Information Sciences and Systems,* pp. 295–299, Mar. 2006.

[43] H. Bolcskei, "Blind high-resolution uplink synchronization of OFDM-based multiple access schemes," *2nd IEEE Workshop on Signal Processing Advances in Wireless Communications*, pp. 166–169, May 1999.

[44] M. Hua and J. Zhu, "Blind estimation of frequency offset and time delay in uplink OFDMA," in *Proc. IEEE Veh. Technol. Conf.*, Vol. 3, pp.1768–1772, 2005.

[45] M. Morelli, "Timing and frequency synchronization for the uplink of an OFDMA system," *IEEE Trans. Commun.*, Vol. 52, pp. 296–306, 2004.

[46] M. Pun, S. Tsai, and C.-C. J. Kuo, "An EM-based joint maximum likelihood estimation of carrier frequency offset and channel for uplink OFDMA systems," in *Proc. IEEE Veh. Technol. Conf.,* Vol. 1, pp. 598–602, 2004.

[47] M. Pun, M. Morelli, and C.-C. J. Kuo, "Maximum-Likelihood synchronization and channel estimation for OFDMA uplink transmissions," *IEEE Trans. Commun.,* Vol. 54, pp. 726–736, Apr. 2006.

[48] P. Zhao, L. Kuang, and J. Lu, "Carrier frequency offset estimation using extended Kalman filter in uplink OFDMA systems," in *Proc. IEEE ICC,* vol. 6, pp. 2870–2874, Jun. 2006.

[49] Z. Cao, U. Tureli, and Y. Yao, "Deterministic multiuser carrier-frequency offset estimation for interleaved OFDMA uplink," *IEEE Trans. Commun.*, Vol. 52, no. 9, pp. 1585–1594, Sept. 2004.

[50] L. Zhao, J. Li, Z. Lu, and J. Pang, "Carrier-frequency offsets estimation based on ML and ESPRIT method for OFDMA uplink," in *Proc. IEEE AINA Conf.,* Vol. 2, Apr. 2006.

[51] X. Zeng and A. Ghrayeb, "Maximum likelihood carrier frequency offset estimation in correlated MIMO-OFDM systems," in *Proc. IEEE Workshop on Signal Processing Systems (SiPS 2006),* pp. 51–55, Oct. 2006.

[52] G. Vazquez and J. Riba, "Non-data-aided digital synchronization," in *Signal Processing Advances in Wireless and Mobile Communications: Trends in Sigle-User Systems,* G. B. Giannakis, Y. Hua, P. Stoica and L. Tong Eds., Prentice Hall, 2001, ch. 9.

[53] C.-N. Chuah, D. Tse, J. Kahn, and R. Valenzuela, "Capacity scaling in MIMO wireless systems under correlated fading," *IEEE Trans. Infor. Theory,* vol. 48, no. 3, pp. 637–650, Mar. 2002.

[54] S. M. Kay, *Fundamentals of Statistical Signal Processing: Estimation Theory,* Prentice Hall, 1993.

[55] X. Zeng and A. Ghrayeb, "A blind carrier frequency offset estimation scheme for OFDM systems with constant modulus signaling," *IEEE Trans. Commun.,* vol. 56, pp. 1032-1037, July 2008.

[56] T. S. Rappaport, *Wireless communications: Principles and Practice*, Prentice Hall, 1998.

[57] T. Roman, S. Visuri, and V. Koivunen, "Blind frequency synchronization in OFDM via diagonality criterion," *IEEE Trans. Signal Process.*, vol. 54, pp. 3125–3135, Aug. 2006.

[58] Z. Liu and B. Weng, "Finite-alphabet based blind carrier frequency offset estimation for differentially coded OFDM," *IEEE Globecom*, vol. 1, pp. 327–331, Dec. 2003.

[59] Z. Liu, B. Weng, and Q. Zhu, "Frequency offset estimation for differential OFDM," *IEEE Trans. Wireless Commun.,* vol. 4, no. 4, pp. 1737–1747, July 2005.

[60] C. Chen and J. Li, "Maximum likelihood method for integer frequency offset estimation of OFDM systems," *Electron. Lett.*, vol. 40, no. 13, pp. 813–814, June 2004.

[61] G. B. Kim, W. Lee, W. Jeong, D. Yoon, and S. K. Park, "An improved estimation of integer frequency offset in OFDM systems using ML method," in *Proc. IEEE ICCCAS,* June 2006, vol. 2, pp. 1120–1123.

[62] M. Morelli, A. N. D'Andrea, and U. Mengali, "Frequency ambiguity resolution in OFDM systems," *IEEE Commun. Lett.*, vol. 4, no. 4, pp. 134–136, April, 2000.

[63] X. Zeng and A. Ghrayeb, "A finite alphabet based frequency offset estimator for differential OFDM systems," submitted to *IEEE Trans. Wireless Commun.*.

[64] G. P. McCormick, *Nonlinear Programing, Theory, Algorithm and Applications*, John Wiley & Sons, Inc., 1983.

[65] P. Stoica and B. C. Ng, "On the Cramer-Rao bound under parametric constraints," *IEEE Signal Process. Lett.*, vol. 5, no. 7, pp. 177–179, July, 1998.

[66] B. M. Sadler, R. J. Kozick, and T. Moore, "Bounds on bearing and symbol estimation with side information," *IEEE Trans. Signal Process.*, vol. 49, no. 4, pp. 822–834, April, 2001.

[67] P. Dent, G. E. Bottomley, and T. Croft, "Jakes fading model revisited," *Electron. Lett.*, vol. 29, no. 13, pp. 1162–1163, June 1993.

[68] X. Fu, H. Minn, and C. Cantrell, "Two novel iterative joint frequency-offset and channel estimation methods for OFDMA uplink," in *Proc. IEEE GLOBECOM*, Nov. 2006, pp. 1–6.

[69] Y. Na and H. Minn, "Line search based iterative joint estimation of channels and frequency offsets for uplink OFDMA systems," in *Proc. IEEE GLOBECOM*, Nov. 2006, pp. 1–5.

[70] X. Zeng and A. Ghrayeb, "A carrier frequency offset estimation scheme based on a scalar extended Kalman filter for uplink OFDM systems," in *proc. IEEE ICC*, May 2008, pp. 568–572.

[71] S. Haykin, *Adaptive Filter Theory*, Prentice-Hall, 2002.

[72] Y. Na and H. Minn, "Line search based iterative joint estimation of channels and frequency offsets for uplink OFDMA systems," *IEEE Trans. Wireless Commun.*, vol. 6, no. 12, pp. 4374–4382, Dec. 2007.

[73] G. Golub and V. Pereyra, "Separable nonlinear least squares: the variable projection method and its applications" Inverse Problems, 19, pp R1–R26, 2002.

[74] G. A. F. Seber and C. J. Wild, *Nonlinear regression*, Wiley, New York, 1989.

[75] L. Kaufman, "A variable projection method for solving separable nonlinear least squares problem," *BIT*, 15, 49–57, 1975.

[76] R. H. Barham and W. Drane, "An algorithm for least squares estimation of nonlinear parameters when some of the parameters are linear," *Technometrics,* 14, 757–766, 1972.

[77] X. Zeng and A. Ghrayeb, "CFO estimation for uplink OFDM systems: an application of the variable projection method," accepted, *IEEE PIMRC 2008.*

[78] V. Srivastava, C. K. Ho, P. H. W. Fung and S. Sun "Robust MMSE channel estimation in OFDM systems with practical timing synchronization," *IEEE WCNC 2004*, vol. 2, pp. 711–716.